Università di Pisa

Facoltà di Ingegneria

Tesi di Laurea Specialistica In Ingegneria Elettronica

Curriculum Sistemi Elettronici

Digital Signal Processing and Generation for a DC Current Transformer for Particle Accelerators

Candidato: **Silvia Zorzetti**

Relatori:

Prof. Luca Fanucci

Ing. Manfred Wendt

ANNO ACCADEMICO 2011 - 2012

Contents

Introduction **1**

1 Introduction to the Accelerators **3**

1.1 Accelerators Overview 3

1.2 Circular Accelerators at the FNAL 7

2 Beam Diagnostics and Beam Current Measurements **9**

2.1 Beam Intensity and Beam Current 12

2.1.1 AC and DC Current in a Ring Accelerator 13

2.2 Beam Intensity measurement 14

2.2.1 Faraday Cup 14

2.2.2 Beam Current Transformer 15

2.2.2.1 Toroid 17

2.2.2.2 The AC Current Transformers 20

2.2.2.3 The Active Current Transformer 25

2.2.2.4 The DC Current Transformer 25

2.2.2.5 Single Core DCCT 26

2.2.2.6 Double Core DCCT 26

2.2.2.7 Combined AC and DC Current Transformer Systems . 29

2.2.3 Motivation of a DCCT based Beam Current Measurement 30

2.3 The Measurement of other Beam Parameters 31

2.3.1 Beam Profile Measurement 32

2.3.2 Beam Position Measurement 34

2.3.3 Beam Energy and Emittance 35

2.3.4 Beam Losses 36

3 DC Current Transformer at FNAL 37

3.1 System Overview 37

3.1.1 Nanocrystalline Toroids 40

3.1.1.1 Measurements on the toroids 43

3.1.2 Digitizer 45

3.1.3 Power Amplifier 46

3.1.4 Transition board 53

4 Digital Implementation 59

4.1 Sensor Model 61

4.2 DC Section 70

4.2.1 Numerically Controlled Oscillator 72

4.2.2 Cascade Integrator and Comb Filter 74

4.2.2.1 Simulink Implementation 77

4.2.3 Finite Impulse Response Filter 79
4.2.3.1 Simulink Implementation 80
4.2.4 Demodulator 81
4.3 Simulink Model 83

5 System Tests and Results 87

5.1 VHDL Implementation 87
5.1.1 NCO 87
5.1.1.1 Tests and measurements 89
5.1.2 CIC 91
5.1.2.1 Tests and Measurements 91
5.1.3 FIR Filter 94
5.1.3.1 Tests and measurements 94
5.1.4 AM demdulator 95
5.2 Open Loop response 97
5.3 Closed Loop 101

Conclusion 104

Acknowledgements 107

Introduction

At the Fermi National Accelerator Laboratory (Fermilab), a government funded national laboratory located near Chicago, IL, USA, particle accelerator based high-energy physics is explored.

This thesis activity was supported and entirely accomplished at Fermilab, in the Instrumentation Department of the Accelerator Division.

The thesis topic, digital signal processing and generation for a DC current transformer, focuses on the most fundamental beam diagnostics in the field of particle accelerators, the measurement of the beam intensity, or beam current. The technology of a DC current transformer (DCCT) is well known, and used in many areas, including particle accelerator beam instrumentation, as non-invasive (shunt-free) method to monitor the DC current in a conducting wire, or in our case, the current of charged particles travelling inside an evacuated metal pipe. So far, custom and commercial DCCTs are entirely based on analog technologies and signal processing, which makes them inflexible, sensitive to component aging, and difficult to maintain and calibrate.

The DCCT presented in this thesis is a new approach to minimize the use of analog technologies, and based the signal processing and generation of a DCCT system on digital technologies. This also was motivated by the fact, that the Fermilab in-house developed DCCT from 25 years ago (Bob Webber) now lacks in the availability of replacement electronics parts.

This DCCT is quite different from our previous analog-based system; it also differs from commercial DCCTs, e.g. made by Bergoz, as it adds an AC current transformer into the system to enhance the overall bandwidth. It soon will become the new standard for the beam intensity measurements at the ring accelerators at Fermilab.

Chapter 1

Introduction to the Accelerators

Particle accelerators are born as a unique tool for pure physics research. In order to look deep into the matter, very high energy are required. Electrostatic accelerators were already available at the end of the XIX century, but electric discharge limited the reachable voltage and therefore their interest for high energy physics. To overcome this limit repeated accelerations in linear structures (linacs) or in closed rings (circular accelerators) are now used. Particle accelerators cover big importance in the world of particle physics; they also represent the only way to produce antiparticles, like the positron or unstable particles. In addition particle accelerators found a wide range of applications, from industry to medicine. In this chapter an introduction to particle accelerators will be done, with particular attention to the accelerators at the Fermi National Laboratory.

1.1 Accelerators Overview

There is a wide range of accelerators. A classification can be done in different ways. The first one is a classification based on the mass of the particle to be accelerated, we can distinguish between the electron (e) and positron (e^+) accelerators, or the accelerator for protons (p) or for eavy particles (like the α particles). The second strategy is to distinguish basing on the operating mode. In particular between the fixed target accelerators, in which the beam is extracted and collides on targets of different materials, and colliders accelerators, in which two counter rotating particles beams collide in the experiment areas generating new particles.

The electrostatic accelerators were the first kind of accelerator realized in the history. One example is the Van de Graaff one which is able to generate from 10 to 15MeV .

Protons transported on a belt charge the surface of the spherical conductor (*Fig.* 1.1) . In this way a potential difference is built. When this instrument is used as accelerator an ion source is located inside the high voltage terminal, so that the ions are accelerated from the source to the target.

It is based on a vacuum pipe in which the protons are accelerated and on a belt, with materially transport the charge. The charge is controlled by changing the belt speed, in this way an hight potential difference is built. When this instrument is used as accelerator the ion source is located inside the hight voltage terminal, so that they are accelerated from the source to the target.

Electric discharge limited the reachable voltage and therefore the interest for high energy physics. Ising (Sweden, 1924) first proposed a scheme of linear accelerator by using hollow cylindrical electrodes in series. Wideroe (Germany, 1928) realized the first accelerator based on this idea. It consisted of three tubes, the first and third grounded to earth and the middle one powered with an oscillating voltage: acceleration occurs at both gaps providing that the voltage phase changes of 180 degrees during the time of flight along the middle tube. The high Radio Frequency power at high frequency required to get compact linac structures relies on a technology which became available only after the second world war with the development of the radar. While we have to wait till that for the first powerful linacs, circular accelerators were developed in the 30s (the cyclotron by Lawrence and Livingston) and 40s (the betatron by Kerst and Serber who applied an original idea by Wideroe).

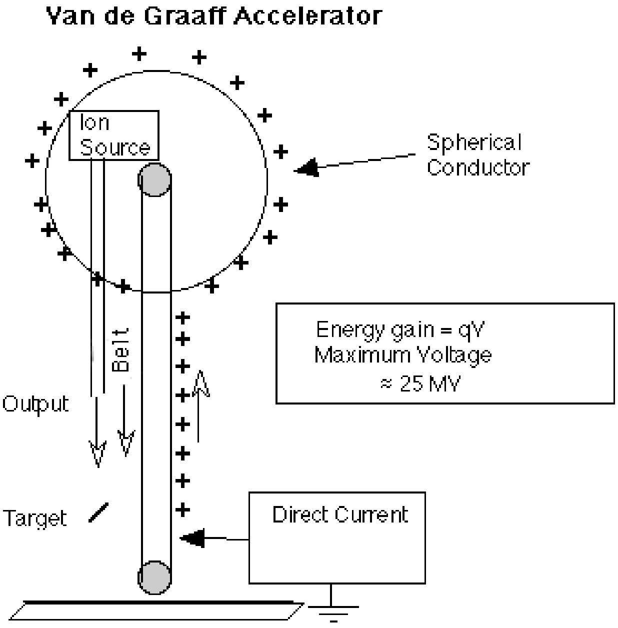

Figure 1.1: Van de Graaf accelerator

All these first circular accelerators used a unique large magnet for bending the particle trajectory. In the cyclotron the acceleration takes place every time the particles cross the gap between the two D of *Fig.* 1.2 in a similar way as in the Wideroe device, while the betatron (*Fig.* 1.3) uses the variation of the guiding magnetic field (Faraday law).

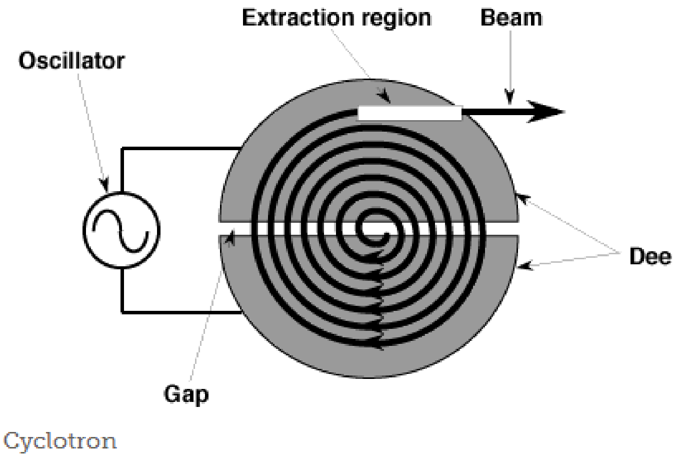

Figure 1.2: cyclotron

The major problem of cyclotrons and betatrons is the need for large magnets.

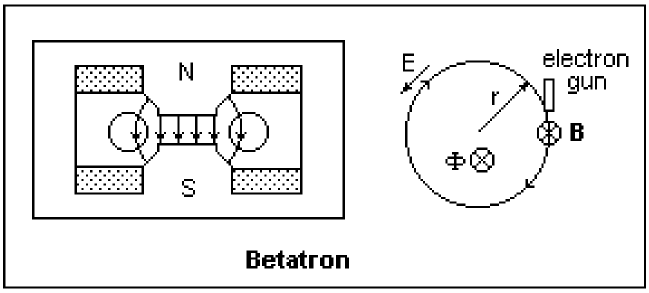

Figure 1.3: Betatron

In 1943 the australian Oliphant suggested to replace the single magnet by a chain of small magnets arranged in circle and to accelerate the particles by an alternating electric field applied between hollow electrodes (now it would be a "RF cavity") located at some position along the ring. Bending field and accelerating frequency must follow the energy in order to keep the orbit within the magnet aperture and to provide the correct electric field. This is why this kind of machine was called synchrotron.

In the first circular accelerators the transverse focusing was missed: while there is some "natural" focusing in the horizontal plane, particles with a speed component in the vertical plane spiral away from the middle plane and are lost. Accidentally it was discovered that by making the outer side of the magnet gap wider one would get a radial field component and thus some vertical focusing ("weak focusing"). Yet the real breakthrough came with the discovery of the the "strong focusing" principle by Christofilos who patented it in 1950. He found that by alternating magnets with wider aperture on the inner side with magnets with wider aperture on the outer side an overall focusing in both planes could be obtained. In their case the same magnet provides curvature and focusing. More flexibility is obtained by separating the two functions as done now in large accelerators. At the end of the 50's, the AGS (Brookhaven) and the PS (CERN) were built based on the new principle. These machines are still in operation.

Fig. 1.4 shows schematically a modern synchrotron.

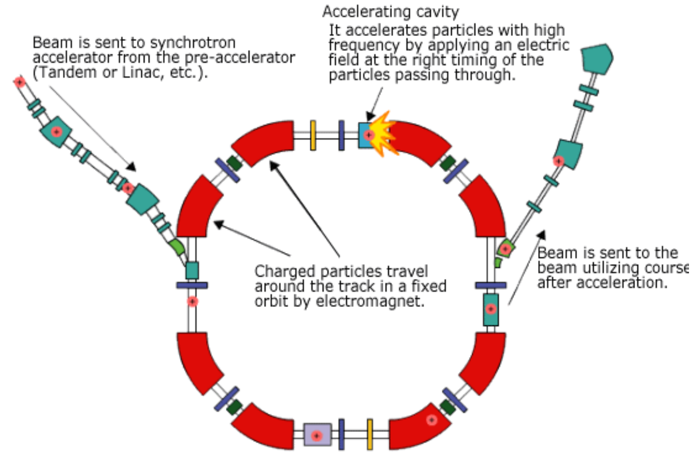

Figure 1.4: *Synchrotron*

1.2 Circular Accelerators at the FNAL

At the Fermilab there are different kinds of accelerators. There are linear accelerators, like the Preaccelerator, the Linac and the Booster, and there are circular accelerator, like the main Injector, the Tevatron and the Recycler. An Overview of those acclerators is in Fig. 1.5. The Main Injector (MI) is a synchrotron. It has 6 sections, 18 accelerating cavities and the maximum energy is 120GeV. It reached 150 GeV when used as injector for the Tevatron. The in September 2011 shut down Tevatron was the biggest accelerator at the Fermilab. The circumference is about 4 miles. There are eight accelerating cavities. It accelerated protons and antiprotons from 150Gev to 980GeV in 83 seconds. When the top energy was reached the two beams were brought into collision at the CDF and D0 experiment location. An Overview of those acclerators is in *Fig.* 1.5.

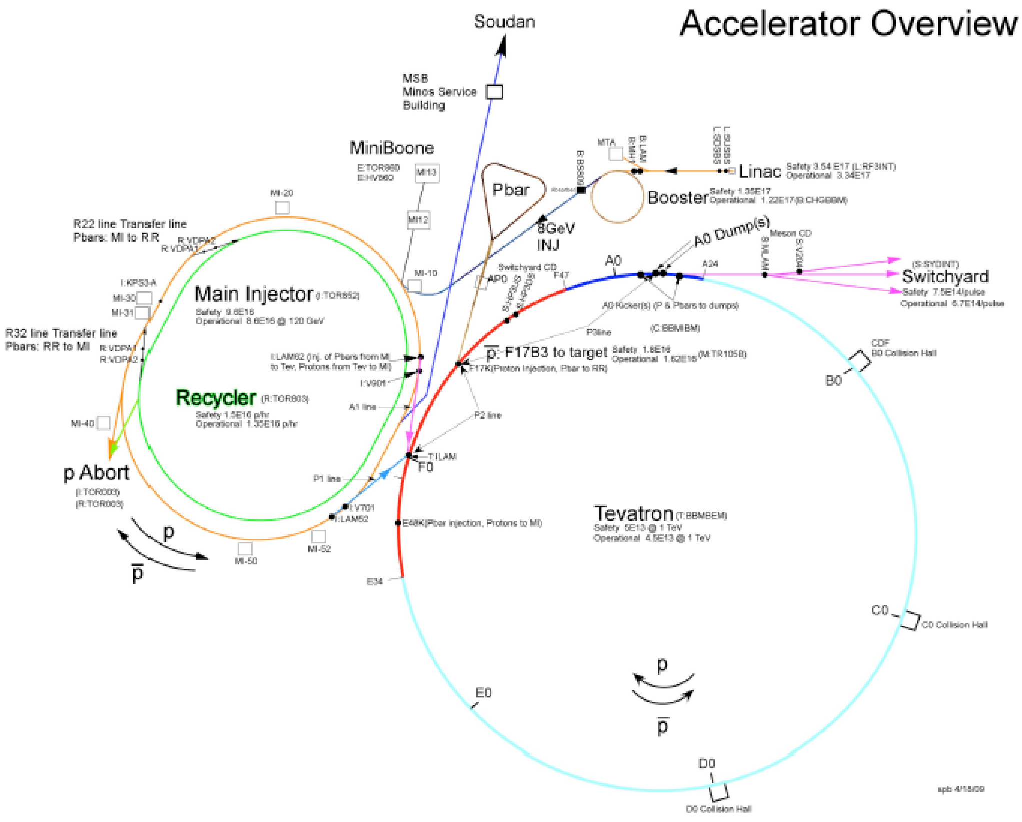

Figure 1.5: *Accelerator Overview at the Fermilab*

Chapter 2

Beam Diagnostics and Beam Current Measurements

Beam diagnostics are essential tools for any charged particle accelerator. The diagnostics instruments allow a systematic characterization of the properties of the beam, the beam parameters, essential to observe, qualify, and quantify accelerator functionality and beam quality. Without beam diagnostics the operation of the accelerator would basically be “blind”, i.e. neither it would be possible to analyze and understand issues and imperfections of the real world accelerator installation, nor improvements based, on systematic beam measurements and studies, could be implemented.

The beam diagnostics utilizes various instrumentation devices to measure the beam parameters, typically by signal detection (pick-up), processing the associated signals, and extracting the data, i.e. beam parameter of interest. Fundamental beam parameters to be directly measured are:
Beam current (I_{beam}); beam position ($\overline{x}$); beam profile (x_{width}); beam losses (r_{loss}).
Other beam parameters, such as beam energy, beam orbit, transverse emittance (ϵ), chromaticity (ξ), betatron and synchrotron tune, etc., can be derived indirectly.

Various method are applied to acquire these parameters, the most popular take advantage of scattering or *Columb* interactions, detection of electromagnetic fields induced by the beam, or the emission of photons by accelerated charges (synchrotron light).

Fig. 2.1 shows the schematics of a typical beam diagnostics system, here a beam position monitor. An electrical signal, dependent from the transverse displacement of the beam with respect to the vacuum chamber is obtained by an electromagnetic pick-up, which is part of the accelerator vacuum system. Because of the high ionization radiation dose during operation of the accelerator, most of the sensitive read-out electronics has to be located outside the accelerator tunnel. Therefore the beam signal may need to be amplified, e.g. with low noise amplifiers, before being transmitted via shielded cables to a central electronics room, where its waveform is digitized and and further processed as required. Beam diagnostics data and control of the instrument is handled by digital bus systems (e.g. CAN), or crate based systems (e.g. VME). Finally, the processed beam position data is transmitted to the control system, added with time stamps and other valuable information. In the accelerator control room (*Fig.* 2.2) the beam position data is visualized on workstation or PC screens for further investigation, observed, studied and analyzed by accelerator operators and scientists.

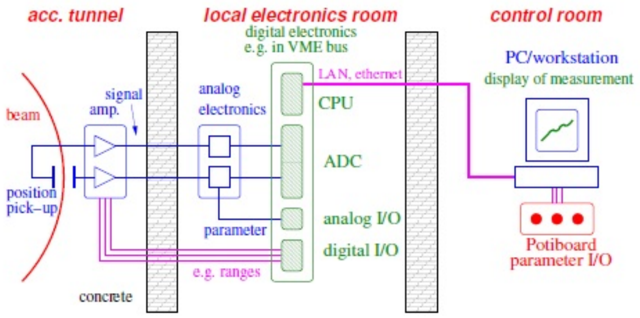

Figure 2.1: *Scheme of a typical beam instrument, from the detector (in this figure it is a beam position pick-up) to the data visualisation in the control room.*

The *Tab.*2.1 lists some typical instruments used for beam diagnostic, including the measured beam parameter(s), the physical effect utilized, and the effect on the beam.

In the following sections I will give a short overview on the various beam instruments,

Figure 2.2: *Fermilab Main Control Room.*

Instrument	**Physical effect**	**Measured beam parameter(s)**	**effect on the beam**
Faraday cup	charge collection	beam intensity	destructive
Current transformer (CT)	magnetic field	beam intensity	non destructive
Wall Current Monitor	Image Current	Beam Intensity and density distribution	Non destructive
Beam position monitor (BPM)	Electro-magnetic field	beam position and orbit	non destructive
Wire scanner	secondary emission	transverse profile and beam emittance	invasive
scintillator screen	photon emission	beam position and profile	invasive / destructive

Table 2.1: *Typical beam instrument, measured parameter and physical effect utilized.*

typically used for the measurement of the beam parameters, and diagnosis of accelerator systems. While this work is focussed on the beam current measurement, this general introduction gives an idea on the complexity and variety of accelerator instrumentation technologies.

2.1 Beam Intensity and Beam Current

For any type of charged particle it is possible to define the beam intensity [10, p1] as the number of charged particles per unit of time.

$$beam\ intensity = \frac{number\ of\ charged\ particles}{unit\ of\ time} \tag{2.1}$$

A flow of charged particles inside the vacuum chamber of an accelerator, passing perpendicular a (virtual) surface within Δt is equivalent to an electrical current, i.e. the beam current:

$$I_{beam} = \frac{ne}{\Delta t} = \frac{Q_{beam}}{\Delta t} \tag{2.2}$$

where $e = 1.6 \cdot 10^{-19}$ is the elementary charge, and *n* is the number of particles. In case of ion beams, the ionic charge state has to be considered in (2.2) [7, p10].

Another way to define the beam current is to consider the velocity $v = \beta c_0$ of the beam, i.e. the time it takes the particles to travel a given distance $\Delta\ell$:

$$I_{beam} = \frac{ne}{\Delta\ell}\beta c_0 = \frac{Q_{beam}}{\Delta\ell}\beta c_0 \tag{2.3}$$

Where $\beta = v/c_0$, v is the velocity of the beam, c_0 is the light speed, $\Delta\ell$ is the distance travelled along the accelerator's vacuum chamber, and Q_{beam} is the total charge of the beam.

In the circular accelerators, the same particles circulate many times, in some machines for many hours, in the vacuum chamber of a given circumference L.

We can define the beam intensity or current (2.3) for linear and circular accelerators, an equivalent average current (DC current) makes only sense to be defined and measured for a ring accelerator.

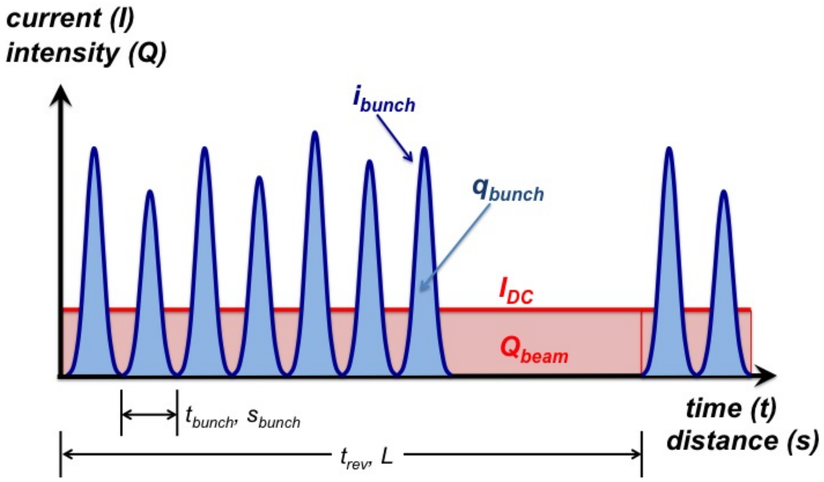

Figure 2.3: *Bunch and DC beam currents.*

2.1.1 AC and DC Current in a Ring Accelerator

The charged particles Q_{beam}=ne circulating with the velocity v in a ring accelerator are not uniformly distributed along the circumference L. Fig.2.3 illustrates the distribution of particles in a batch of 7 "bunches" (blue) along the circumference L. The particle bunches are formed by the RF acceleration process, which allows only particular "buckets" (areas along the circumfence) to be populated with particles (q_{bunch}). The number of particles in a bunch is quite large ($> 10^9$), we can only observe the envelopes of longitudinal, and transverse particle distributions in a bunch. Often bunches have not exactly the same intensity, furthermore a particle-free gap is left to allow injection and ejection into the ring accelerator.

The Bunch current (blue Fig.2.3) is the AC beam current measured by a beam current monitor with sufficient bandwidth to resolve t_{bunch}.

$$i_{bunch} = \frac{q_{bunch}}{t_{bunch}} \tag{2.4}$$

The DC beam current (red Fig.2.3) is the average current measured by a beam current monitor capable to monitor the DC *Fourier* component.

$$I_{DC} = \Sigma i_{bunch} = \Sigma \frac{q_{bunch}}{t_{bunch}} = \frac{ne}{L}\beta c_0 \tag{2.5}$$

Fig.2.3 illustrates the simplified time domain beam current signal (blue), observed at a measurement point, which repeats with the revolution time t_{rev}=L/v. The light-blue area below each bunch indicates the charge of the individual bunches q_{bunch}. In red the equivalent DC beam current is shown, as light-red area based on Q_{beam}=Σq_{bunch}, equally distributed along the circumfence L.

A particularity of ring accelerators occurs for if v=βc_0 changes during the acceleration cycle. While the beam intensity Q_{beam} stays constant, the observed beam current I_{beam} changes (2.3). This effect occurs only at non-relativistic beam energies, i.e. $\beta \ll 1$.

2.2 Beam Intensity measurement

The measurement of the beam intensity, or beam current is the most elementary and fundamental monitoring of a beam property, usually to optimise and enhance the number of particles in the accelerator.[10, p11], [11, p1]. The method applied for this beam diagnostics depends from the characteristic of the beam, and from the effect it has on the beam.

2.2.1 Faraday Cup

The *Faraday* Cup is the simplest way to measure the beam current, for that reason it was the first method applied for beam intensity monitoring. [5, p.2.04] [10, p.2.1]. It is based on a insulated conducting plate that collects the particles, here electrons, to measure the total equivalent current passing an ampere meter or a shunt resistor to ground (beam pipe).

Using a simple collector plate (*Fig.* 2.4(a)) electrons of higher energy have the possibility to liberate them self, or secondaries from the collector surface, escaping the collector, which results in a measurement error.

A good solution has been found using the *Faraday* Cup (*Fig.* 2.4(b)). The collector is now surrounded by an isolated metal cup with a hole, which allows the electrons to pass to the collector plate. The metal cup is brought to a negative potential to suppress the secondary emission, allowing a well calibrated measurement of the beam current over a wide range of beam intensities.

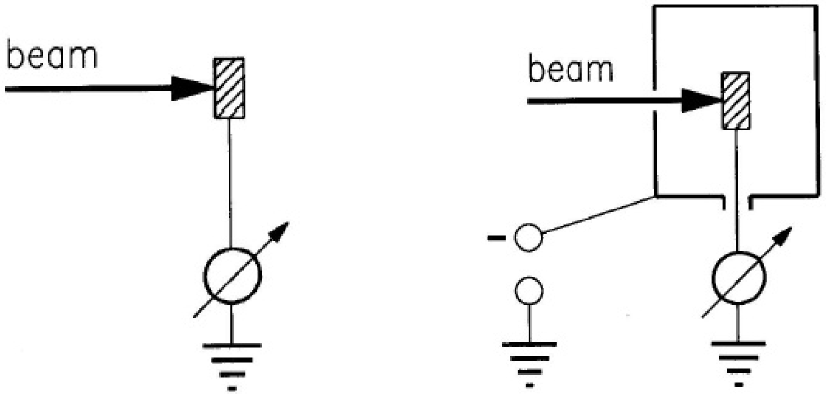

(a) (b)

Figure 2.4: *(a) Beam Simple Collector, (b) Faraday Cup*

Fig.2.5(a) and 2.5(b) show a more elaborated *Faraday* cup, which also includes a magnetic focussing system. Fig.2.6 shows the effect of the secondary emission suppressor voltage.

Being a destructive method, the Faraday Cup is used only in applications, where it is not interesting to monitor the beam intensity further downstream, the system is also limited in handling high beam powers. It is typically used in the low-energy sections of accelerators, so-called injectors, sometimes in beam transport systems, or as beam stopper, stopping the beam in case of emergency.

2.2.2 Beam Current Transformer

The beam current transformer is based on the principle, in which a charged particle beam (2.2) induces a magnetic field on a secondary winding. Passing through a toroidal

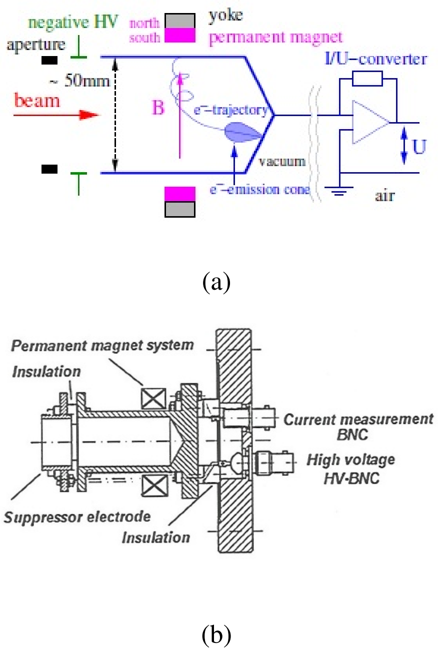

Figure 2.5: *(a) Faraday Cup Scheme, (b) Faraday Cup Construction Drawing*

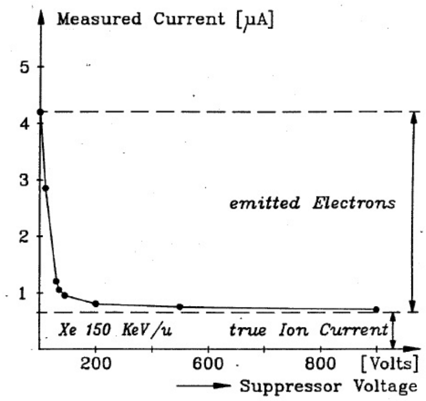

Figure 2.6: *Suppression of secondary electrons in Faraday Cup as function of the applied voltage*

transformer, the beam acts like a single turn winding, while the current induced on the secondary winding is proportional to the primary beam current *Fig.* 2.7.

As illustrated, the beam current transformer is an non-intercepting instrument, the particle beam passes almost without interference. Therefore this type of beam current monitor is widely used in accelerator instrumentation, including circular machines.

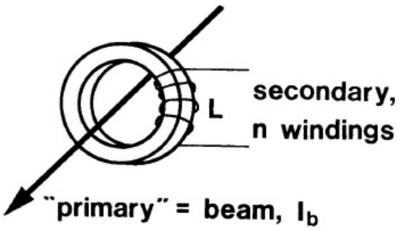

Figure 2.7: *Principle of the Beam Current Transformer*

Before discussing the details of the beam current transformer, it is helpful to describe some geometric and magnetic properties of the toroid as beam current pickup.

2.2.2.1 Toroid

A toroid consists out of a toroidal core of a material with high magnetic permeability μ, on which n wire turns of the secondary winding are distributed (*Fig.* 2.8).

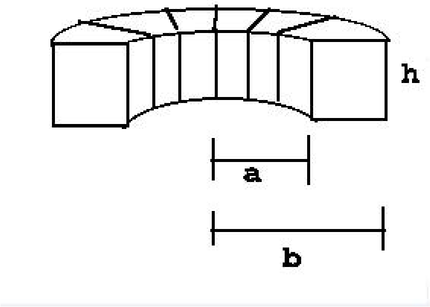

Figure 2.8: *Generic picture of a toroid, with the dimensions.*

The magnetic field, $\overrightarrow{B}$, induced by the current I_{Beam} (2.2) is calculated applying the *Biot-Savart's* law:

$$d\overrightarrow{B} = \mu_0 I_{Beam} \frac{d\overrightarrow{l} \times \overrightarrow{r}}{4\pi r^3} \tag{2.6}$$

where $\mu_0 = 4\pi \cdot 10^{-7} Vs/Am$ is the permeability of the vacuum, $d\overrightarrow{l}$ is the length in direction of the beam, and $\overrightarrow{r}$ is the distance between the center of the beam and the point where the field is measured. Assuming that the B-field doesn't depend on the transverse dimension of the beam, only the azimuthal component of the magnetic field B_ϕ has to be considered (*Fig.* 2.9).

$$\overrightarrow{B}_\phi = \mu_0 \frac{I_{Beam}}{2\pi r} \cdot \overrightarrow{e}_\phi \tag{2.7}$$

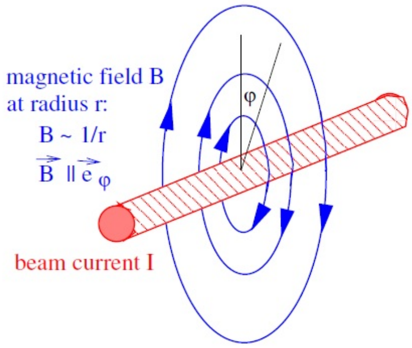

Figure 2.9: *Magnetic Field of the Beam Current*

A winding of N_k turns on the toroid induces a magnetic flux density (B_k). In general, the flux due to a wire current in a winding k is:

$$\Phi_k = \int_S \overrightarrow{B_k} \cdot d\overrightarrow{S} \tag{2.8}$$

With the previous considerations (2.7), the total flux is calculated only on the azimuthal surface.

$$\Phi_k = \int_a^b \overrightarrow{B_k} dr = \int_a^b \mu \frac{N_k i_k}{2\pi r} l = \mu \frac{N_k i_k l}{2\pi} \ln \frac{b}{a} \tag{2.9}$$

where b is the external radius and a is the internal radius and h the width, as shown in *Fig.* 2.8. While $\mu = \mu_r \mu_0$ is the total magnetic permeability, μ_r depends on the material.

The self inductance for each winding is defined as:

$$L_k = \mu \frac{N_k^2 h}{2\pi} \ln \frac{b}{a} \tag{2.10}$$

The single turn self inductance is:

$$L_0 = \mu \frac{h}{2\pi} \ln \frac{b}{a} \tag{2.11}$$

It is easy to note from (2.11), that L_0 depends only from the geometry (the internal and the external radii), as well as from the material (the magnetic permeability μ). Often it is also defined by the two geometric quantities, the cross sectional area A, and the magnetic path length P.

$$A = h(b - a) \tag{2.12a}$$

$$P = \pi(b + a) \tag{2.12b}$$

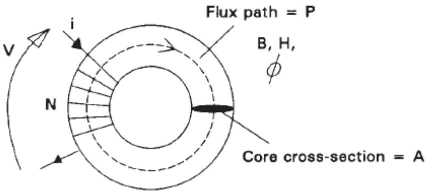

Figure 2.10: *Parameters for a generic toroid*

It is possible to demonstrate that L_0 (2.11) can be written in functions of A and P (2.12a and 2.12b):

$$L \simeq \mu \frac{N_k^2 A}{P} \tag{2.13}$$

Substituting the L_0 (2.11) in the 2.9, the flux for a winding becomes:

$$\Phi_k = \frac{L_k}{N_k} L_k \tag{2.14}$$

In case of more than one winding on the toroidal core, the total flux is the sum of the contribution from each winding:

$$\Phi_T = \sum_{m=1}^{k} \Phi_m = \sum_{m=1}^{k} \frac{L_m i_m}{N_m} \tag{2.15}$$

For each winding, the voltage is given by the Faraday's Law:

$$V_k = -N_k \frac{d\Phi_k}{dt} \tag{2.16}$$

Based on the toroidal transformer principle the measurement of AC and DC components of the beam current can be realized. Utilizing different design principles and technologies allow the optimization of these current transformers, to be applied to beam current measurements in particle accelerators, as well as monitoring the electric current in physical wires.

2.2.2.2 The AC Current Transformers

The classical AC current transformer is also called passive beam transformer, because it is made up by only passive elements. It basically consists out of a toroid with two set of windings. The primary winding is a single turn formed by the beam current passing through the toroid. The second winding is the pickup winding, connected to a burden resistor.

Fig. 2.11(a) shows the scheme of a classical current transformer, *Fig.* 2.11(b) the simplified equivalent circuit, in which L is the transformer inductance; R the load resistance; C_s the sum of parasitic capacitances between the components (cables and windings). An improved equivalent circuit would add a resistor, taking the resistance of the cable into account, and an inductance, to account for the equivalent cable inductance. Those adjunctive parasitic effects will be considered later in this paragraph.

For an ideal current transformer the induced current on the secondary winding is pro-

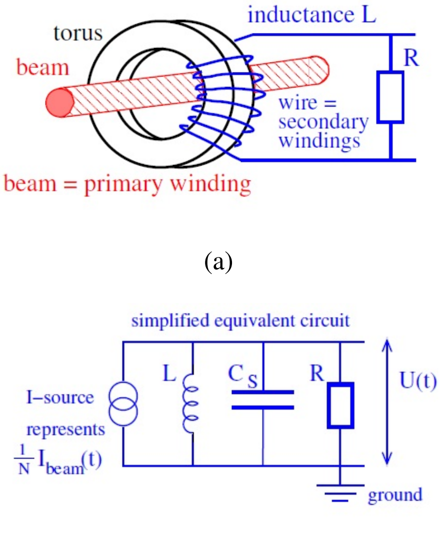

(a)

(b)

Figure 2.11: *(a) Scheme of a passive current transformer, (b) Simplified equivalent Circuit for a passive Current Transformer*

portional to the primary current:

$$I_{sec} = \frac{N_{prim}}{N_{sec}} I_{prim} \tag{2.17}$$

In our case N_{prim} is equivalent to a single turn of the I_{beam}, therefore N_{prim}=1, which simplifies (2.17):

$$I_{sec} = \frac{I_{beam}}{N_{sec}} \tag{2.18}$$

In the practical case, we measure the voltage $v(t)$, induced by the current $i_{sec}(t)$ in the secondary winding, passing the burden resistance R.

$$v(t) = Ri_{sec}(t) = \frac{R}{N} i_{beam}(t) = Zi_{beam}(t) \tag{2.19}$$

with N equals N_{sec}, and Z is the transfer impedance, sometimes called sensitivity (S).

For the complete picture, the reactive components in (2.19) have to be considered, i.e. the transfer impedance $Z = Z(\omega) = V(\omega)/R$ is frequency depending.

Let's calculate the transfer impedance in the *Laplace* domain:

$$Z(s) = sL \parallel \frac{1}{sC_s} \parallel R \tag{2.20}$$

After some algebra:

$$Z(s) = \frac{sL}{1 + s\frac{L}{R} + s^2 LC_s} \tag{2.21}$$

with $\tau = L/R$ as time constant.

We can simplify the response function of (2.21), by analysing for three different frequency regions:

- $\omega \ll R/L$, $Z(\omega) \to j\omega L$

  At low frequencies the transfer impedance is dominated by the inductance. At $\omega = 0$ the current in the secondary winding equals zero. This is the known characteristic of a transformer, which doesn't transfer a DC-current.

- $\omega \gg 1/(RC_s)$, $Z(\omega) \to 1/(j\omega C_s)$

  At high frequencies the parasitic capacitances dominate, the load resistance is not considered.

- $\frac{R}{L} \ll \omega \ll 1/(RC_s)$, $Z(\omega) \to R$

  In the desirable working region the transformer behaves like a highly damped parallel resonator with a lower frequency limit $\omega_{low} = 1R/L$, and an higher limit $\omega_{high} = RC_s$.

In the time domain it is worth to characterize the response of the current transformer to a rectangular, or step pulse. The rise time (τ_{rise}) is defined as response time for a step function, with 10% and 90% thresholds of the waveform amplitude. The rise time is defined by the high frequency characteristics of the system:

$$\tau_{rise} = \frac{\ln 0.9 - \ln 0.1}{\omega_{high}} = \frac{\ln 9}{2\pi f_{high}} \simeq \frac{1}{3 f_{high}} \tag{2.22}$$

The droop time (or droop rate) describes the discharge time, in which the exponential response signal drops to the $1/e$ of the initial value. The droop time is defined by the low frequency characteristics of the system, a transfer system with DC response would have a drop rate $\tau_{drop} \to \infty$.

$$\tau_{droop} = \frac{\ln 0.9 - \ln 0.1}{\omega_{low}} = \frac{\ln 9}{2\pi f_{low}} \simeq \frac{1}{3 f_{low}} \tag{2.23}$$

The above mentioned time constants have a general meaning, for the passive current transformer we can simply define the two time constants:

$$\tau_{rise} = \frac{1}{f_{high}} = RC_s \tag{2.24a}$$

$$\tau_{droop} = \frac{1}{f_{low}} = \frac{L}{R} \tag{2.24b}$$

Fig. 2.12 shows the effect of the finite bandwidth, i.e. the time constants on the response to a rectangular pulse signal, and, more realistic, on a *Gaussian* beam signal.

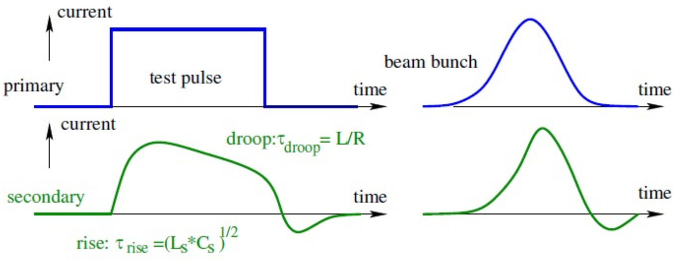

Figure 2.12: *Effect of the transformer time constants*

Other parasitic effects are:

- The relative magnetic permeability μ_r is frequency dependent, typically decreases with increasing frequency $\mu_r(\omega) \propto 1/\omega$.
- So far we considered only the parasitic capacitances C_s between the turns, and between wire and ground. If we include the properties of the cable between secondary winding and burden resistor R, the equivalent capacitance of the cable can be simply added to this parasitic capacitance $C_s = C_{sToroid} + C_{sCable}$. Furthermore we have to add the parasitic inductance L_s and the DC resistance R_L of the cable. *Fig.* 2.13 shows the equivalent circuit including the parasitics of the cable.

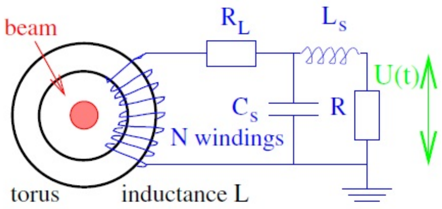

Figure 2.13: *Equivalent circuit of the current transformer, including parasitic effects of the cable*

Including these effects, we now find the time constants to be [7]:

$$\tau_{rise} = \sqrt{L_s C_s} \tag{2.25a}$$

$$\tau_{droop} = \frac{L}{R + R_L} \tag{2.25b}$$

Considering all the mentioned parasitic effects, it becomes clear, some design compromises have to be made, e.g. we cannot simply ask for a high sensitivity and a good low frequency performance simultaneously. A high sensitivity (large Z) requires a low turn ratio, i.e. a small number of N, as $v(t) \propto 1/N$. A high droop time $\tau_{droop} \propto L$ on the other hand requires a large inductance $L \propto N^2$, which then is into contradiction, and ask for a high relative permeability μ_r. In practice, we find us limited by the available core materials, giving typically $\mu_r \approx 10^5$ for low frequencies.

2.2.2.3 The Active Current Transformer

An active feedback circuit, based on an operational amplifier,see *Fig.* 2.14, can substantially improve some of the limitations of the passive beam current transformer.

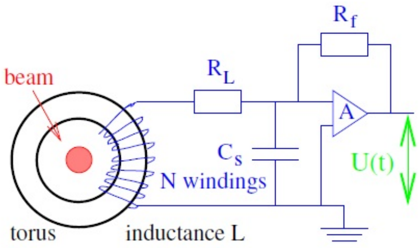

Figure 2.14: *AC Active Current Transformer*

The burden resistor is basically eliminated by the feedback circuit, which results in an improvement of the drop time

$$\tau_{drop} = \frac{L}{\frac{R_f}{A} + R_L} \simeq \frac{L}{R_L} \tag{2.26}$$

Using a typical operational amplifier with high gain A, the drop time is now limited by the cable DC resistance of a few ohms, which results in an extended low frequency response of the beam transformer. This reduced the baseline shift effect, when measuring long batches (pulses) of beam bunches. As positive side effect, there transfer impedance increases $Z \propto R_f/R_L$, the active circuit is more sensitive. This may allow to reduce the number of turns N, which reduces the high frequency parasitics, thus extend the upper frequency range.

In practice however, the active beam current transformer is of limited use, as it requires radiation hard operational amplifiers, and a well though through power supply.

2.2.2.4 The DC Current Transformer

As discussed, the classic transformer blocks the transfer of the DC component. To be able to measure the DC current component of the beam, a different, more complicated approach has to be followed.

2.2.2.5 Single Core DCCT

Lets consider a single core toroid with three windings, see (*Fig.* 2.15):

- The primary winding supplies the DC current $i_0 = i_{beam}$, which is equivalent to the beam current.
- The output signal of secondary winding is passed through a detection circuit.
- A modulation winding supplies $i_1 \cos(\omega t)$.

Different form the AC transformer, this single core DC current transformer (DCCT) operates in the non-linear regime of the core. The high level sine-wave modulation signal i_1 drives the toroidal core completely in saturation, causing higher order harmonics in the flux (*Fig.* 2.16). Without DC signal ($i_0 = 0$), only odd harmonics appear in the output signal. The 2^{nd}-order harmonic (twice the modulation frequency ω) appears with $i_0 \neq 0$, and is proportional to the DC current i_0 in the primary winding. A detection system for the 2^{nd}-order harmonic (indicated as rectifier in *Fig.* 2.15) senses the level of that harmonic, and therefore the primary DC current.

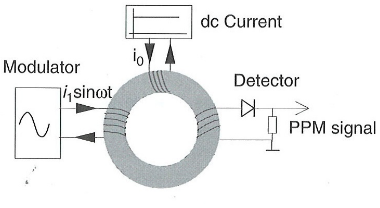

Figure 2.15: *Single core DC current transformer*

2.2.2.6 Double Core DCCT

The single core DCCT has numerous disadvantages, mostly, the modulation plus DC signals causes an asymmetric saturation with a large, unwanted 1^{st}-order harmonic. A

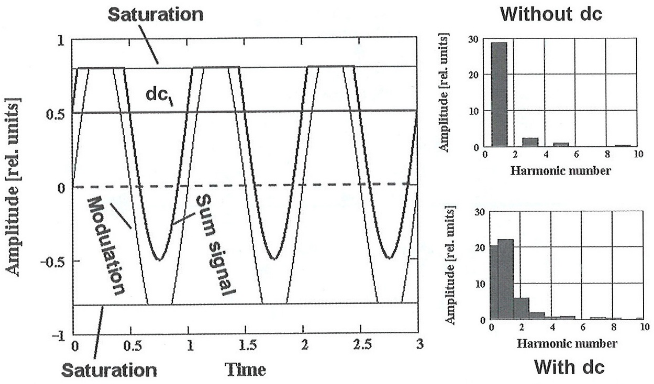

Figure 2.16: Time- and frequency domain signals of the single core DCCT

symmetric arrangement of two identical toroids results in an improved, now standard DCCT schema (*Fig.* 2.17). Both cores are driven by the same modulator signal $i_1 \cos(\omega t)$, as of the antisymmretic windings, in opposite phase, which causes a cancellation of the even harmonics in the flux (*Fig.* 2.18).

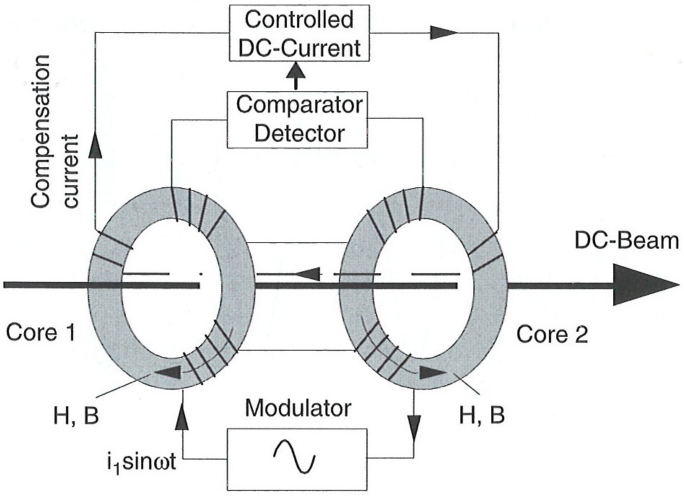

Figure 2.17: Double core DC current transformer

To further improve the symmetry, the measurement circuit is based on a feedback loop. The DC beam current is measured by analysing the amplitude of the 2^{nd} harmonic of the modulator frequency, similar to the single core DCCT. A common feedback winding passes a the measured DC current as compensation current, through both cores, which cancels the primary DC beam current, thus keeping the system in perfect symmetry.

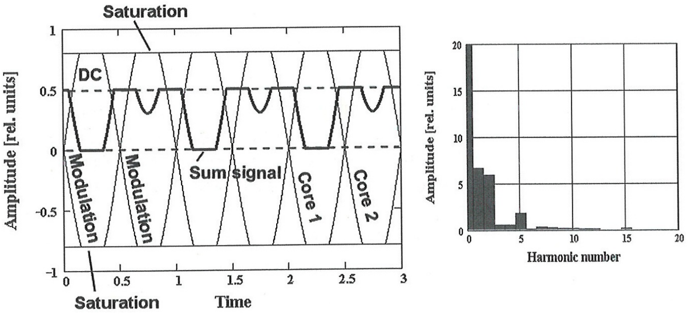

Figure 2.18: *Time- and frequency domain signals of the double core DCCT*

Lets analyse the double core DCCT by separating the identical cores. Each core is first analysed in the linear regime, no saturation assumed. In this analysis we suppress the compensation current, which later could simply be included as $I_{DCtotal} = I_{DCbeam} + I_{DCcomp}$.

From (2.15) the total flux in each of the cores sums to:

$$\Phi_T = L_0 i_0 + \frac{L_1 i_1}{N_1} + \frac{L_2 i_2}{N_2} \tag{2.27}$$

in which $i_1 = Acos(\omega_1 t)$, and the indices are: 0 → beam signal, 1 → modulation signal, 2 → detected signal.

From Faraday's Law (2.16) follows:

$$\frac{\Phi_T}{dt} = -\frac{v_2}{N_2} \tag{2.28}$$

For the detected current in the burden resistor $i_2 = v_2/R$, (2.28) becomes:

$$\frac{d\Phi_T}{dt} = -\frac{i_2 R_s}{N_2} \tag{2.29}$$

Now we continue the analysis in the frequency domain, by applying the *Laplace* variable $s = j\omega$:

$$s\Phi_T = -\frac{I_2(j\omega)R_s}{N_2} \tag{2.30}$$

Substituting (2.30) in (2.27) will result in an equation for the detected output current:

$$I_2(s) = -\frac{\tau s}{1+\tau s}\frac{I_0 + N_1 I_1(s)}{N_2} \tag{2.31}$$

with the time constant $\tau = L/R$ as described in (2.21). Substituting (2.31) into (2.27) we now find an equation for the total flux only based on modulator and beam currents:

$$\Phi_T = L_0 I_0 + \frac{L_1 I_1(s)}{N_1} + \frac{L_2}{N_2^2}\frac{\tau s}{1+\tau s}(I_0 + N_1 I_1(s)) \tag{2.32}$$

As we apply a high amplitude on the modulation current i_1, we always drive the high-μ_r DCCT cores deep into saturation, i.e. operating the cores in a very non-linear regime. As consequence, (2.32) holds only during the short “switching” periods, in which the detected voltage is non-zero:

$$v_2(t) = \begin{cases} 0 & \text{if } \Phi(t) \geq \Phi_{Tmax} \\ -N_2 \frac{d\Phi_T(t)}{dt} & \text{if } \Phi(t) < \Phi_{Tmax} \end{cases} \tag{2.33}$$

Summing the results of both cores and implementing the non-linear behaviour according to (2.33). In a Simulation model (using MatLab and Simulink), we can analyse the behaviour of the double core DCCT in detail. This model will be explained in the *Chapter 4*.

2.2.2.7 Combined AC and DC Current Transformer Systems

The upper frequency limit of the DCCT is well below the modulation frequency, typically a few $100Hz$. To measure a bunched beam signal (2.3), a bandwidth from the DC to some MHz is required, which calls to combine AC and DC current transformers into a single system.

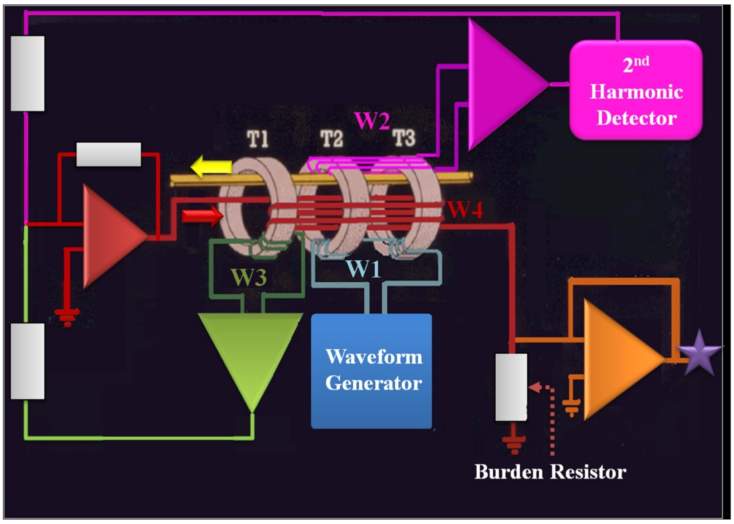

Figure 2.19: *Schematic diagram block of a combined system*

Fig. 2.19 shows the schema of a combined AC and DC current transformer, as it is further elaborated in this thesis. We find here the symmetric double core DCCT (T2 and T3), plus a 3^{rd} core for the AC current transformer (T1). The beam current is compensated by the overall feedback up using winding W4, continuously establishing a zero net flux in the toroids. The current in winding W4 is monitored by a burden resistor, which returns the broadband beam current signal.

2.2.3 Motivation of a DCCT based Beam Current Measurement

As mentioned earlier in this chapter, measurement, and continuous monitoring of the beam current is the most essential beam diagnostic in any particle accelerator. While a passive AC transformer fulfills some basic requirement for the beam current monitoring, the far more complex DCCT based system has several important advantages, particular if combined with an AC current transformer:

- A precise absolute calibration of the beam current instrument is mandatory. This is difficult, almost impossible in case of an AC transformer, as it requires a pulse signal as calibration standard. A DC current as calibration standard is quite feasible, such that the absolute calibration error is $< 10^{-4}$.

- The capture of particles in the RF buckets is not always perfect, in case of problems $I_{DC} \neq \Sigma i_{bunch}$. In case of a proton storage ring, the uncaptured protons may coast in the ring as "extra" DC current, which can only be detected with a DC current transformer. The detection of coasting DC beam current is of particular importance in accelerators with superconducting magnets, like the Tevatron (Fermilab) or LHC (CERN).
- The dynamic intensity range of the flux compensated DCCT is large compared to a simple passive AC current transformer, no gain switching and re-calibration required.
- A combined AC / DC current transformer is the most complex beam current instrumentation, but has many advantages, capable to monitor the beam current over a wide dynamic range, well calibrated, over a large frequency range starting at DC.

While there a numerous of other reasons a DCCT is the essential beam current diagnostics in a ring accelerator, the system is complex and requires attention to the details.

2.3 The Measurement of other Beam Parameters

While this thesis is dedicated to the measurement of the beam intensity, the monitoring of other important beam parameters is also essential, and requires different technologies. The following section tries to give a very brief overview.

2.3.1 Beam Profile Measurement

The particles in the beam are distributed in three dimensions, see *Fig.* 2.20. The beam profile is the intensity distribution of the particles along each spatial coordinate. The longitudinal coordinate is indicated with s, and defines the beam profile the direction of motion of the beam; the transverse plane is orthogonal to the longitudinal coordinate, and is identified with two axis, x (horizontal) and y (vertical). Usually the beam profile measurement refers to the transverse plane, the longitudinal beam profile measurement is called bunch length measurement.

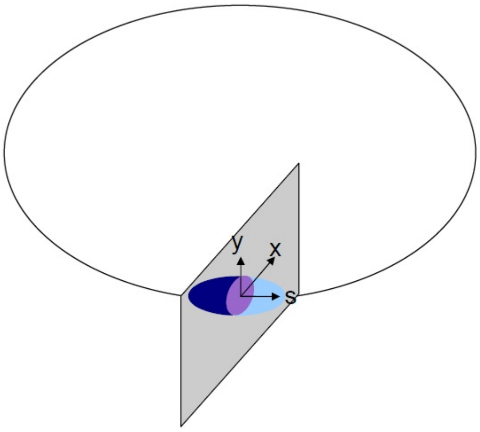

Figure 2.20: *Beam Profile*

The transverse beam profile measurement consist in quantifying the beam intensity profile at a particular location along the accelerator. The continuous monitoring of the beam profile is important to optimize various parameters of the accelerator, to study the distribution of the charge, and to match different parts of the accelerator facility in the transverse plane. To simplify and compare the beam profiles from several locations, a beam width information is extracted from the beam profile, which often is assumed to have *Gaussian* shape. The analysis of the beam sizes help to understand beam blow-up effects, instabilities, matching of the accelerator optics, and many other beam dynamics effects.

The measurement of the transverse beam profile can simply be realised by using a scintillation screen. A scintillation material is applied on a flat surface (screen), for which the emission of light doesn't depend from heat, but from a chemical reaction or electron interactions. When a charged particle passes a scintillator screen, it absorbs parts of its energy. After a short time the energy is emitted as photon radiation, as the electrons in the scintillating material fall back to their initial low energy state. This radiation, which is proportional to the number of beam particles per unit area, is amplified and elaborated by electronic light sensors, e.g. photomultipliers, photodiodes or, most commonly in the modern instruments, CCDs (charge coupled device).

In practice, the scintillator screen is mounted inside the beam pipe, inclined by 45° to the beam. A window under 90° is used to image the profile of the beam, which is captured by a sensor (e.g. TV-camera), as shown in *Fig.* 2.21. The final result appears as 2-D image of the beam cross section. A second window is often used to pass light on the screen for calibration and adjustment purposes.

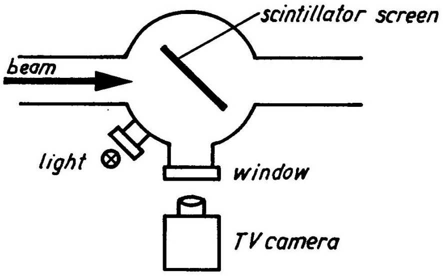

Figure 2.21: *Beam Profile*

Other beam profile monitor techniques take advantage from the secondary emission effect, here a wire grid arrangement with a fine pitch measures the beam profile for a single transverse plane. Each wire operates like a current-to-voltage converter, in the following signal processing the 1-D beam profile is rebuild. Other beam profile measurement methods utilizes photon effects (compton scattering, photo detachment), or coulomb scattering.

2.3.2 Beam Position Measurement

The beam position refers to the transverse plane and is related to the beam profile, it is the center of gravity (or center of charge) of the transverse particle distribution. *Fig.* 2.22 shows a typical particle distribution in the transverse plane, in which the beam position in both transverse coordinates is zero.

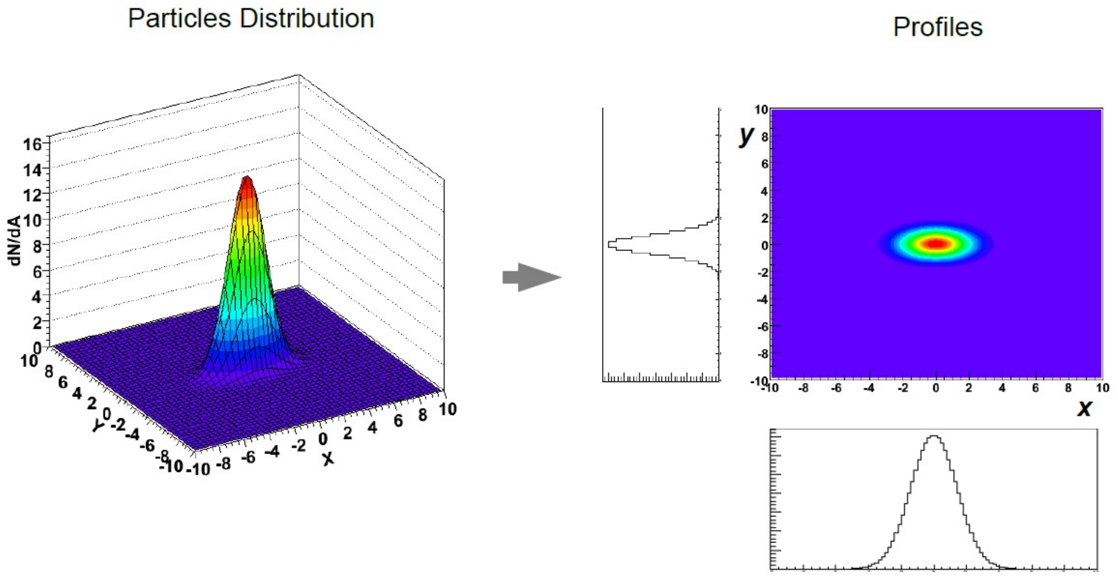

Figure 2.22: *Beam Profile on the Transverse Plane*

A beam position monitor (BPM) is a non-invasive detector to measure the center of charge of a bunched beam, i.e. the beam position. The BPM detector typically is a RF antenna device, e.g. an insulated metal plate capturing the electromagnetic field of the passing beam bunches.

A capacitive pick-up is a simple type of BPM detector, able to monitor the beam position. A typical pick-up configuration (*Fig.*) uses a tube with radius a and length l inside a grounded beam pipe. It can be demonstrated, as the transverse beam displacement varies with respect to the central beam orbit, the total charge induced by I_{beam} on the tube surface is proportional to the beam position [9] [8]. The charge on a surface of the cylinder is:

$$Q_{im} = -Q_{beam} l(1 + \frac{x}{a}) \tag{2.34}$$

where Q_{beam} is the total charge of the beam (2.3) and x is the horizontal beam position to be measured. The same relation is also valid for an orthogonal arrangement to measure the vertical beam position y.

2.3.3 Beam Energy and Emittance

- **Beam energy**

  As the beam passes a magnetic dipole field, the particles will be deflected, proportional to the H-field strength of the magnet and the beam energy. A spectrometer magnet arrangement is used to measure the beam energy, in which a BPM located downstream the deflection magnet monitors the position of the deflected beam. Based on the known geometry and the exact measurement of the deflecting field, the beam energy can be determined. Other methods to measure the beam energy are based on compton scattering, or a time-of-flight measurement in case of non-relativistic beams.

- **Emittance**

  The transverse beam emittance is related to the transverse beam profile measurement. The beam emittance is defined as surface of an envelope, described by the beam particles in an orthogonal phase-space, with displacement (position) and angle coordinates. The emittance information is extracted from the beam profile measurement at several locations, or by a special emittance scan procedure, and is an important value that describes the beam quality.

2.3.4 Beam Losses

Every particle accelerator looses some of the primary beam particles during acceleration, transfer or storage of the beam. This usually is unwanted, and the beam loss has to be minimized, as the radiation or heat of lost particles can cause nuclear reactions and may destroy components of the accelerator, or cause malfunctions. The instruments to detect beam losses are called beam loss monitors (BLM), and are installed near crucial points, usually outside of the vacuum pipe.

The detector type used depends on the loss mechanism, primary and secondary particle energy and type, e.g. protons, electrons, γ-rays, neutrons, etc. Charged particles are easier to be detected, also within a short distance. Instead, e.g. neutrons are difficult to be detected, and even more difficult are the neutrinos, which will travel a large distance before interacting with any material.[2]

Chapter 3

DC Current Transformer at FNAL

At the Fermilab there are different kinds of DCCT Systems. One type was designed and built at FNAL in the 80's. It was first installed in the Tevatron and later in the Main Ring when the Tevatron was commissioned. Currently it is installed in all machines except the Recycler. The DCCT was built with two sections. The toroids' material was supermalloy. The overall system bandwidth was 2MHz.[3] In the Recycler there is a commercial DCCT, designed from Bergoz Instrumentation. The Bergoz Parametric Current Transformer, PTC-113-0100-MA is a complete system, including sensor, electronics and cables. There are only toroids for the DC section, the material is Vitrovec. In 2004 the system failed, due to an asymmetry of permeability between the toroids for the detection of the DC component. The system was replaced with the Bergoz NPTC 115-C100. It will be replaced with the new DCCT System developed at the Fermilab, the implementation of this new system is the goal of this thesis activity.

3.1 System Overview

The sensor of the DCCT system consists of three nanocrystalline toroids mounted inside a double shield of μMetal. The DC section consists in two toroids connected in series but oppositely wound. There are power amplifiers to furnish the correct power to drive the toroids in saturation. The system is completed by three VME boards: two transition boards, and one digitizer. The transitions board are boards between the digitizer and the power amplifier. In them, there are filters and gain stages, to better drive the signal to or from the digitizer. One transition board is for the driving loop at $400Hz$. The other one for the feedback loop. The digitizer provides the digital control of the system. All these boards are housed in a VME create. The controller of the crate is in the front end that interfaces with the Accelerator Control Network. *Fig.* 3.1 shows the connections and the function of every single part.

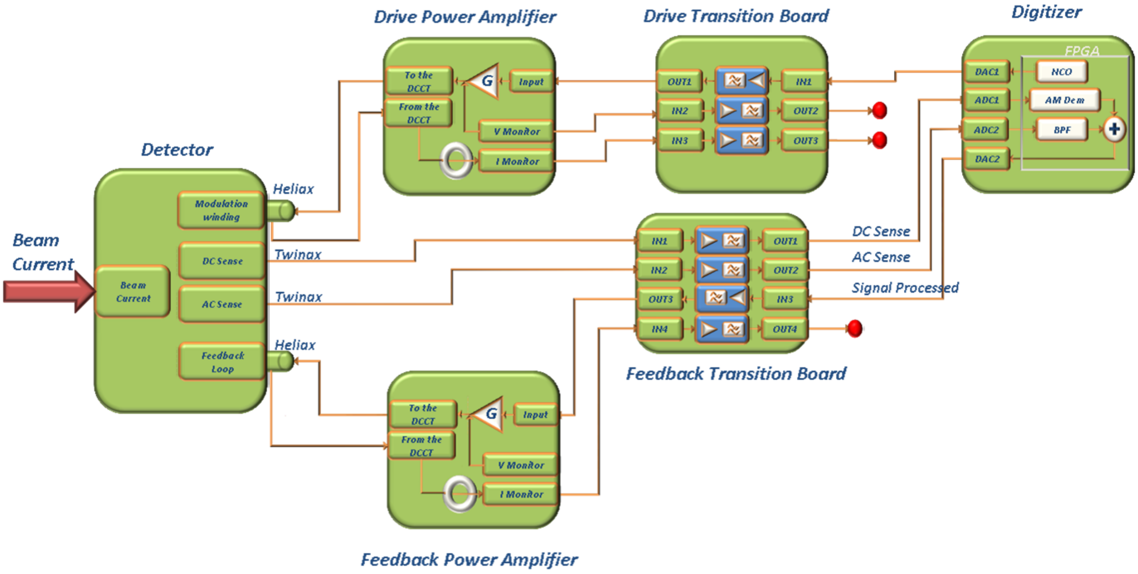

Figure 3.1: *System Block Diagram. Connection between the digitizer, the power amplifier and the transition boards, the red points are the monitoring points. The output of the system will be the Current Monitor on the feedback loop power amplifier, but it is not yet implemented*

The modulating signal, a sinewave at $400Hz$, is digitally generated by a Numerically Controlled Oscillator (NCO), inside the digitizer. It passes through the drive loop transition board and the drive loop power amplifier. Then it goes to the forward wire of the modulator winding and come back with the return wire to the power amplifier. This signal can also be monitored.

Once the modulating signal saturate toroids, a beam current is picked up using the AC sense and the DC sense windings. Each has different bandwidths, determined by the number of turns. Both pickup windings go to the digitizer through transition board. In the digitizer, the signals are processed and elaborated. The result is passed back to the transition board and then the feedback loop power amplifier. This amplifier is connected to the pick up with one wire, and the return wire goes back again to the power amplifier where it is terminated on 5Ω.

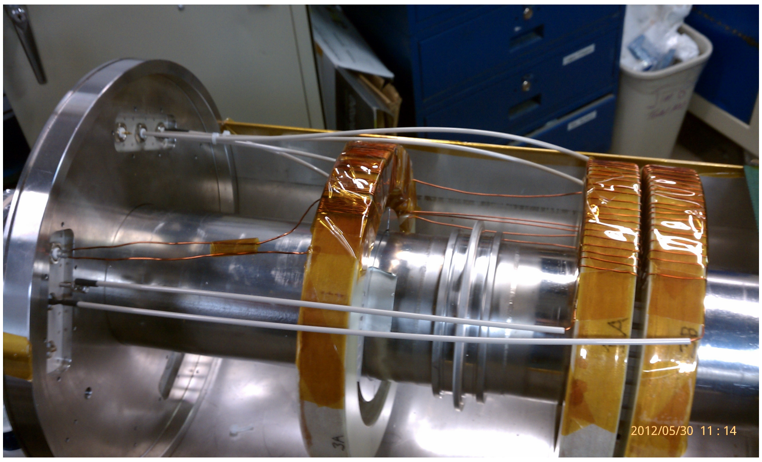

Figure 3.2: *Picture of the 3 toroids in the shield*

3.1.1 Nanocrystalline Toroids

In the past the best product available with the high permeability was the supermalloy (80% *Ni* , 20% *Fe*). Nanocrystalline is now what the industry offers as improvement. The permeability is higher compared with cores of similar sizes. Also the commercial products are using the nanocrystalline cores.

The toroids for this DCCT are made of nanocrystalline material (*Fig.* 3.3), produced by MK Magnetics, instead of ferrite or supermalloy.

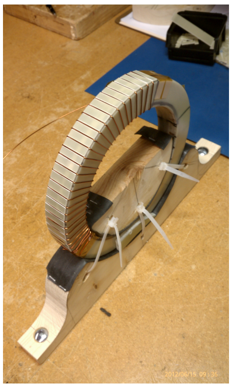

Figure 3.3: *Picture of one toroid in nanocristalline material*

It is possible to have higher performances because the permeability of the nanocrystalline is up to 50% higher then the supermalloy material and up to ten times higher then ferrite material. The core losses are lower, the maximum magnetic field $Bmax$ is higher, and the switching losses are lower.

Six toroids STC1728M1S-A were order from MKK Magnetics Inc. with the following specifications:

Parameter	**Symbol**	**Value**	**Units**
Outer Diameter	OD	8.5	in
		0.216	m
Inner Diameter	ID	6.5	in
		0.165	m
Height	h	0.984	in
		0.025	m

Such parameters ad $\mu_r = 100000$ and $B_{sat} = 12300G = 1.230T$ are fixed. The parameters of the toroid are calculated as follow:

Parameter	**Symbol**	**Value**	**Units**
Length (Circumference)	P	23.562	in
		0.598	m
Cross Sectional Area	A	0.817	in^2
		$526.9e-6$	m^2
Volume	V	24.502	in^3
		$401.5e-6$	m^3

By knowing the physical parameters of the toroid it is possible to establish the specification of the system.

- **Current and voltage to drive the toroids into the saturation**

  The power furnished to drive the toroids into the saturation can be established using the table in *Fig.* 3.4.

  A compromise between the drive frequency selection and power requirement is need. At $400Hz$ and $N = 22$, $I_{sat} = 2.66A$ and $V_{sat} = 35.84V$ is needed. Considering that the DCCT has two toroids, the number of turns for each modulating winding is $N_{mod} = 11$.

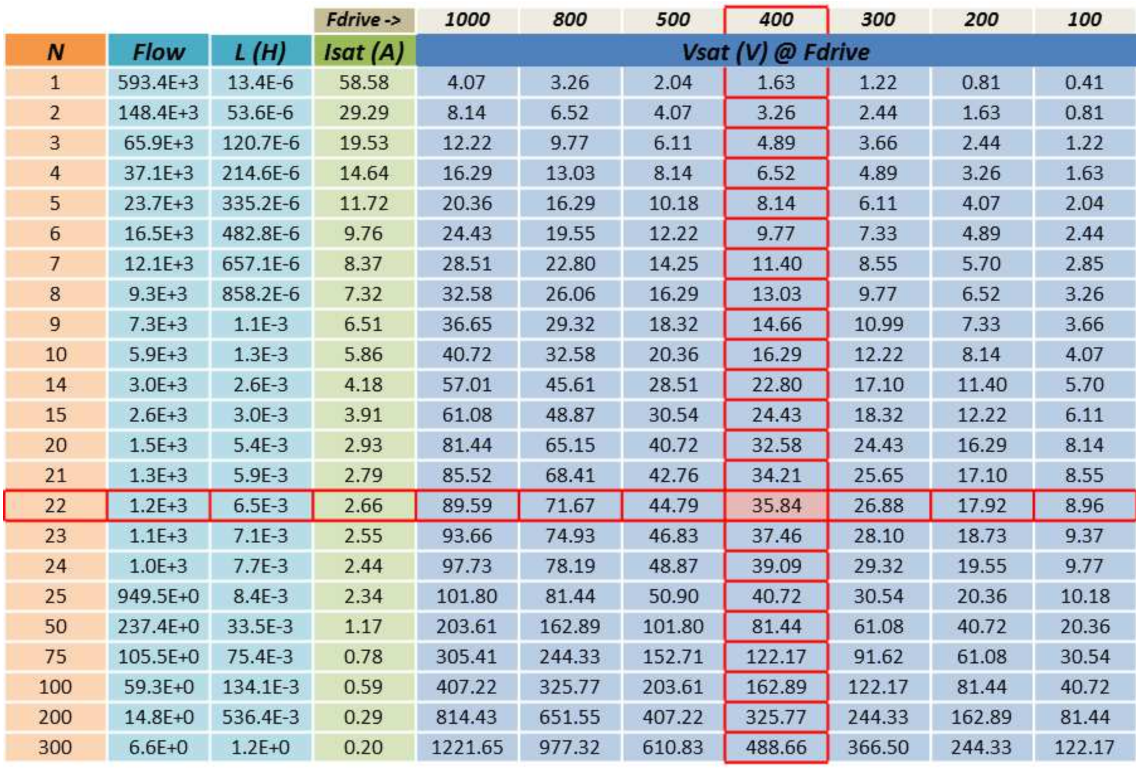

			Fdrive ->	1000	800	500	400	300	200	100
N	Flow	L (H)	Isat (A)	Vsat (V) @ Fdrive						
1	593.4E+3	13.4E-6	58.58	4.07	3.26	2.04	1.63	1.22	0.81	0.41
2	148.4E+3	53.6E-6	29.29	8.14	6.52	4.07	3.26	2.44	1.63	0.81
3	65.9E+3	120.7E-6	19.53	12.22	9.77	6.11	4.89	3.66	2.44	1.22
4	37.1E+3	214.6E-6	14.64	16.29	13.03	8.14	6.52	4.89	3.26	1.63
5	23.7E+3	335.2E-6	11.72	20.36	16.29	10.18	8.14	6.11	4.07	2.04
6	16.5E+3	482.8E-6	9.76	24.43	19.55	12.22	9.77	7.33	4.89	2.44
7	12.1E+3	657.1E-6	8.37	28.51	22.80	14.25	11.40	8.55	5.70	2.85
8	9.3E+3	858.2E-6	7.32	32.58	26.06	16.29	13.03	9.77	6.52	3.26
9	7.3E+3	1.1E-3	6.51	36.65	29.32	18.32	14.66	10.99	7.33	3.66
10	5.9E+3	1.3E-3	5.86	40.72	32.58	20.36	16.29	12.22	8.14	4.07
14	3.0E+3	2.6E-3	4.18	57.01	45.61	28.51	22.80	17.10	11.40	5.70
15	2.6E+3	3.0E-3	3.91	61.08	48.87	30.54	24.43	18.32	12.22	6.11
20	1.5E+3	5.4E-3	2.93	81.44	65.15	40.72	32.58	24.43	16.29	8.14
21	1.3E+3	5.9E-3	2.79	85.52	68.41	42.76	34.21	25.65	17.10	8.55
22	1.2E+3	6.5E-3	2.66	89.59	71.67	44.79	35.84	26.88	17.92	8.96
23	1.1E+3	7.1E-3	2.55	93.66	74.93	46.83	37.46	28.10	18.73	9.37
24	1.0E+3	7.7E-3	2.44	97.73	78.19	48.87	39.09	29.32	19.55	9.77
25	949.5E+0	8.4E-3	2.34	101.80	81.44	50.90	40.72	30.54	20.36	10.18
50	237.4E+0	33.5E-3	1.17	203.61	162.89	101.80	81.44	61.08	40.72	20.36
75	105.5E+0	75.4E-3	0.78	305.41	244.33	152.71	122.17	91.62	61.08	30.54
100	59.3E+0	134.1E-3	0.59	407.22	325.77	203.61	162.89	122.17	81.44	40.72
200	14.8E+0	536.4E-3	0.29	814.43	651.55	407.22	325.77	244.33	162.89	81.44
300	6.6E+0	1.2E+0	0.20	1221.65	977.32	610.83	488.66	366.50	244.33	122.17

Figure 3.4: *Correspondence between the number of turns, the saturation current and voltage and the driving frequency*

The correct level of current and voltage are provided by the power amplifier. Since maximum voltage output from the DAC on the digitizer is $1Vpp$, the gain of the power amplifier has to be al least $A_v = 36$, providing also the correct current.

- **Sense winding Bandwidths**

  It is necessary to check the bandwidth of each section for a certain number of turns in the sense windings. The second harmonic must fall inside the passband of the DC Sense. For the AC section, the passband should be wide.

  Using the measurement setup shown in *Fig.* 3.5, the bandwidth for a toroid with $N = 20$, $N = 100$ and $N = 200$ has been calculated and it is shown in *Fig.* 3.6. With a lower number of turns, the component at $800Hz$ doesn't fall into the bandpass. $N = 100$ was chosen for the DC Sense and $N = 200$ for the AC Sense.

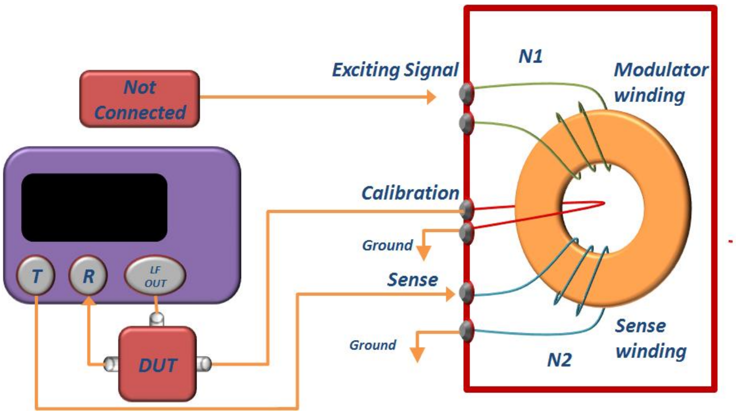

Figure 3.5: *Setup to measure the toroids bandwidth for different number of turns; N2 is variable.*

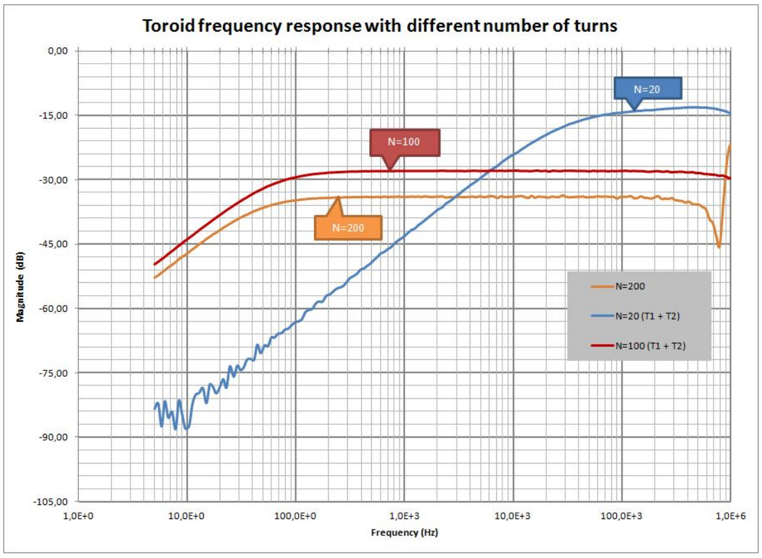

Figure 3.6: *Toroids bandwidth measurement for different number of turns.*

3.1.1.1 Measurements on the toroids

Each toroid has a different magnetization curve. The pair for the DCCT has to have matched magnetization curves.

Several measurements have been done to observe how the toroids responds when working as DCCT.

The measure setup is shown in *Fig.* 3.7.

The waveform generator generates an input signal is at $400Hz$, and $360mVpp$ of amplitude. It is then amplified from the power amplifier to provide the correct value of voltage and current to saturate the toroids.

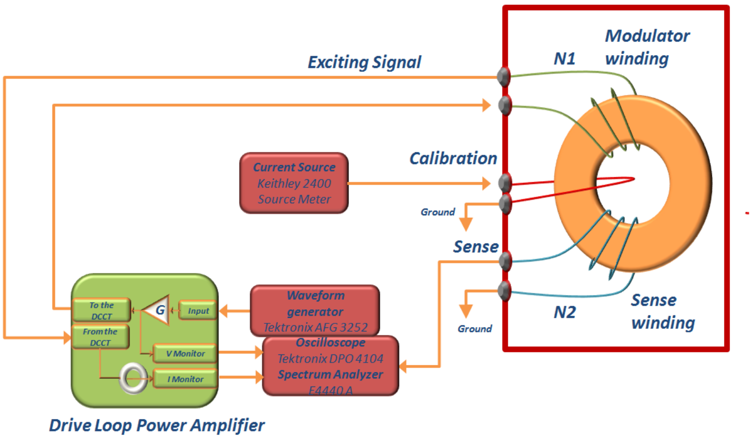

Figure 3.7: *Measurement setup for a single toroid*

The two induced voltage signals are not exactly the same. Moreover the difference between them is not zero, as aspected from the theoretical point of view. This result is shown in *Fig.* 3.8. The second harmonic is not cancelled. There is a mismatch between the toroids that has to be add in the digital implementation.

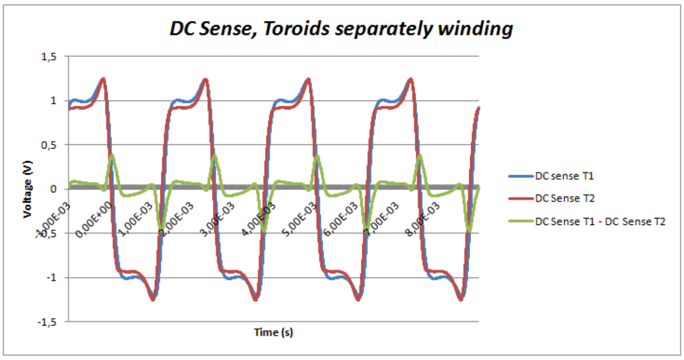

Figure 3.8: *Difference between the DC Sense measurements of the two toroids.*

3.1.2 Digitizer

The digitizer is the core of the system. The signal picked up from the sensors is processed and then sent back to the system.

Fig. 3.9 shows a block diagram of the digitizer and the most important components on it. There are 2 DAC chips (Texas Instrument DAC3283). Each DAC has a double output, so that the total DAC outputs are 4, each on 16 bits. The signal come in through 4 ADC chips (Texas Instrument ADS62P49), operating on 14 bits that are digitally converted to 16 bits.

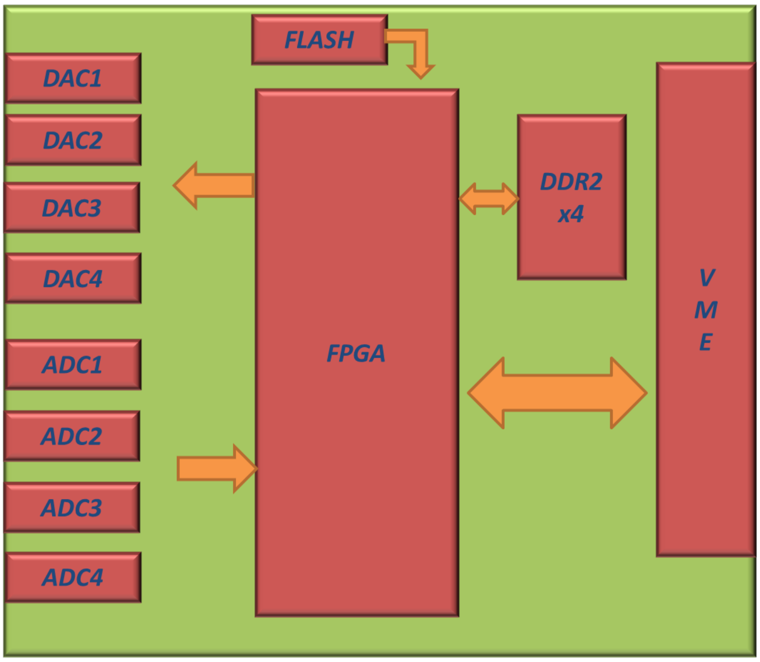

Figure 3.9: *Digitizer and most important devices for the signal processing*

With 4 ADCs and DACs one digitizer can control 2 DCCT systems. The DAC outputs are used one to drive the toroids into the saturation, providing the signal at $400Hz$. The amplitude is variable from 0 to 1Vpp. The other one is used to output the processed signal. The ADC inputs are used for the DC and the AC sense windings.

The FPGA is an Altera Cyclon IV E (EP4CE115P29C8LN) with which the signal is processed. All the interfaces with the DAC and the ADC chips are realized in VHDL.

The system is completed by a flash memory, that programs the FPGA with the firmware when powered on. There are also 4 banks of memories DDR2, in case such data has to be saved. In addition, there is the VME interface, that allow to control to access to the digitizer's memory registers.

To control the such internal registers inside of the DAC, the ADC and the memories, or some signals internal to the FPGA, a LabView Interface as been implemented. It communicates with the FPGA and the other components through the VME.

In *Fig.* 3.10 an example of the Labview interface used to control such registers in the FPGA.

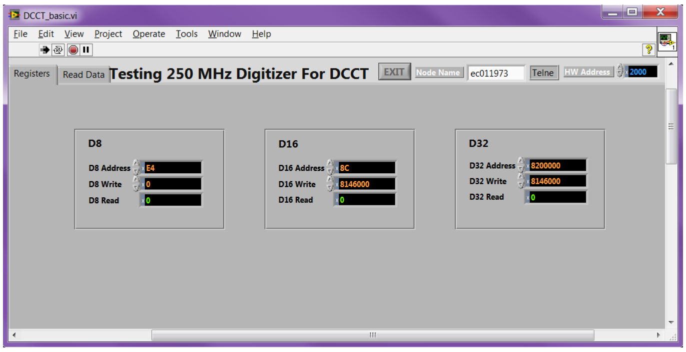

Node Name ec011973

HW Address 2000

D8 Address E4
D8 Write 0
D8 Read 0

D16 Address 8C
D16 Write 8146000
D16 Read 0

D32 Address 8200000
D32 Write 8146000
D32 Read 0

Figure 3.10: *LabView interface to control the internal registers on the FPGA*

3.1.3 Power Amplifier

The power amplifier is necessary to provide the power that the toroids need to saturate. An Acopian W48LT940 is used to supply $\pm 48V$ to the power amplifier.

In the system, there are two power amplifiers. One is for the drive loop, and the other is for the feedback loop.

- **Drive Loop Power Amplifier**

  A block diagram is shown in *Fig.* 3.11.

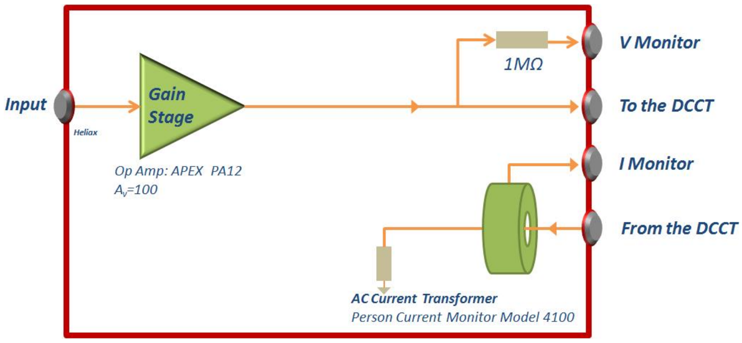

Figure 3.11: *Drive Loop Power Amplifier Block Diagram*

Inputs:

Input : Signal from the drive loop transition board, to be amplified and to drive the modulator winding of the DCCT.

From the DCCT : Return wire from the modulator winding of the DCCT, to terminate connections.

Outputs:

Voltage Monitor: To monitor the voltage of the signal sent to the DCCT.

Current Monitor: To monitor the current of the signal sent to the DCCT.

To the DCCT: Signal at $400Hz$ sent to the modulator winding.

The input is a sinewave with a variable amplitude to have in output the necessary voltage to saturate the toroids. It is amplified by an operational amplifier with a gain $A_v \sim 100$. The DC Component is blocked with a capacitor in series, in order to minimize the offset. The signal so obtained must have an amplitude of about $40V$, and a current of about $3A$, it is sent to the modulator winding to saturate the toroid.

The test setup in *Fig.* 3.12 has been used to check that the current and the voltage that have to saturate the toroids.

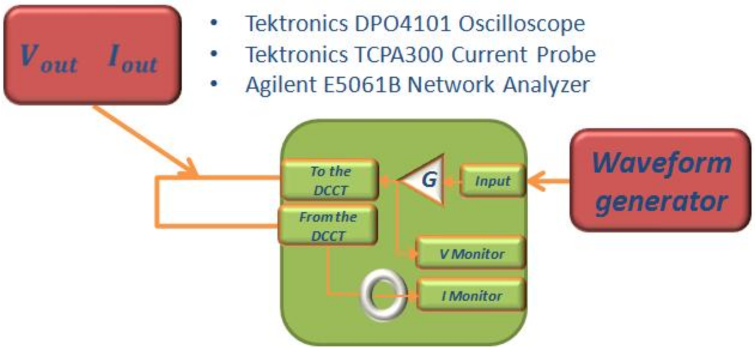

Figure 3.12: *Block diagram to measure the driving current and voltage from the drive loop power amplifier to the toroids.*

If *Fig.* 3.13 the voltage outside the power amplifier is shown. The input signal is $400mVpp$, the output is about $48.38Vpp$, that means that $G = 100.79$. The output current is shown in *Fig.* 3.14, it is more then $3A$. With these parameters the toroids are well saturated.

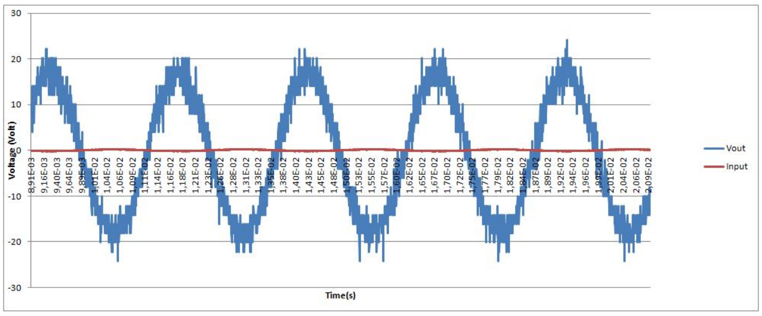

Figure 3.13: *Voltage in input and in output at the drive loop power amplifier.*

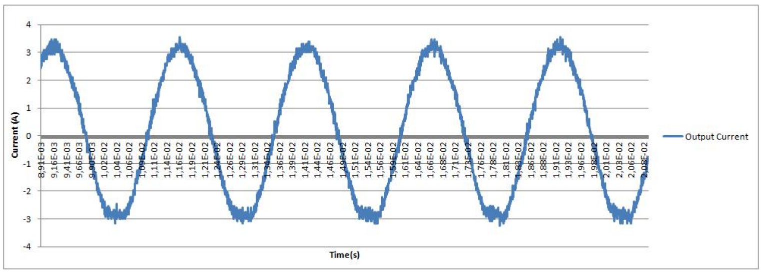

Figure 3.14: *Output current from the power amplifier.*

Inside the power amplifier, there is a little AC current transformer (Pearson Current

Monitor Model4100). The return wire passes through this toroid and induce a signal that can be used to monitor current.

Using the signal from the voltage monitor and the current monitor pins, it is possible to measure and monitor also the hysteresis of the toroids.

There are also some leds to check the power supply regulators.

To test the power amplifier the test setup in *Fig.* 3.15 has been used.

The frequency response from the input to the output has been measured, with the setup in *Fig.* 3.15.

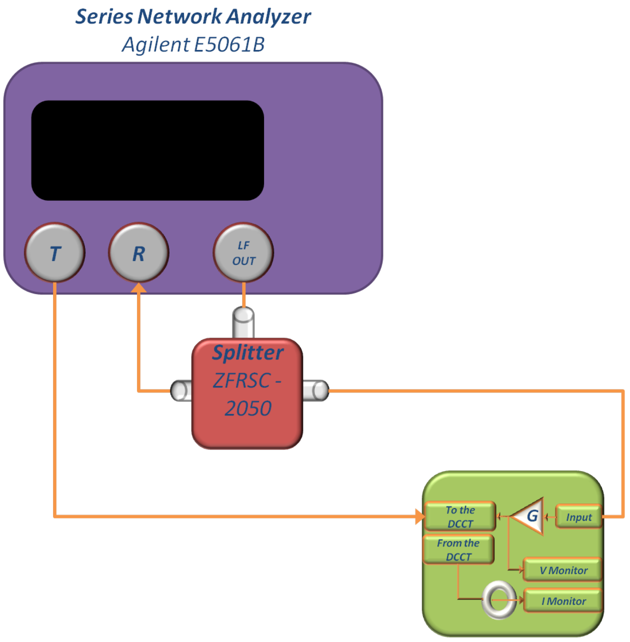

Figure 3.15: *Measure setup for the frequency response for the power amplifier*

In this way we see that the frequency components of interest fall in the passband. The result is in *Fig.* 3.16.

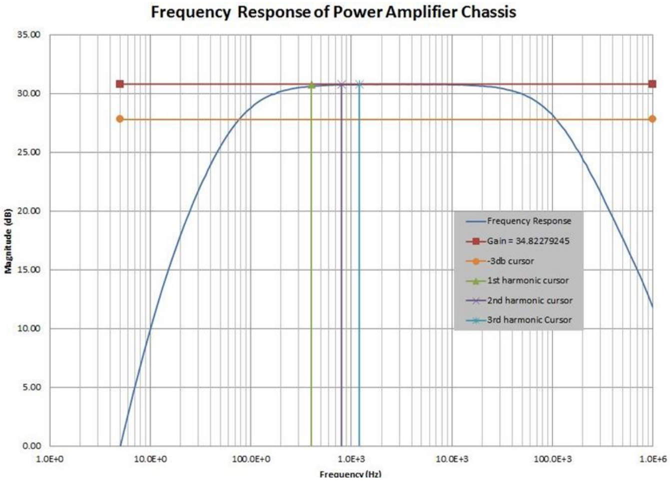

Figure 3.16: *Drive Loop Power Amplifier Block Diagram*

- **Feedback Loop Power Amplifier**

  The block diagram of the feedback loop power amplifier is similar to the block diagram of the drive loop power amplifier. Some differences will due to the different function of the two power amplifier. In fact the feedback loop power amplifier has to amplify also the DC component.

  Inputs:

  Input : Signal from the Feedback Loop Transition Board, to be amplified to drive the feedback wire.

  From the DCCT : Return wire from the feedback.

  Outputs:

  Voltage Monitor: Not Connected

  Current Monitor: Not yet Connected, will be the output of the system.

  To the DCCT: Signal from the transition board, processed by the FPGA and amplified.

  The input is an AC and DC signal, whose the maximum amplitude is $1Vpp$. It is amplified and then sent to the return feedback winding. It will be then possible to monitor the current with the Current Monitor Output, that is not yet available. The same AC current transformer used previously is not useful because blocks the DC component.

  As in the drive loop power amplifier there are some leds to check the power supply.

  For the feedback power amplifier, the same measurements of the drive loop power amplifier has been done. The gain is the same The only difference is in the frequency response. Since this amplifier has no DC blocking capacitor, the bandwidth is wider.

  This result is underlined in the frequency response, between the input and the output, the measure setup is the same used for the drive loop power amplifier and the response is in *Fig.* 3.17.

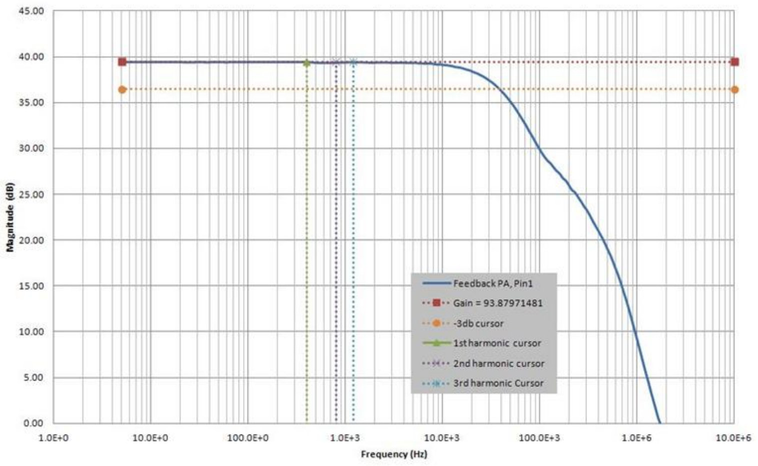

Figure 3.17: *Frequency response for the feedback loop power amplifier*

3.1.4 Transition board

There are two transition boards, used to connect the digitizer to the power amplifiers, with some gain and filter stages.

- **Drive Loop Transition Board**

  This transition board is between the digitizer and the drive loop power amplifier. A channel drives the sinevawe at $400Hz$ (digitally generated) to the modulation winding on the detector. The voltage and current monitor from the power amplifier are used as inputs to the other two channels.

  Inputs:

  IN1: Excitation signal at $400Hz$ from the digitizer;

  IN2: Drive Voltage Monitor, from the drive loop power amplifier;

  IN3: Drive Current Monitor, from the drive loop power amplifier;

  Outputs:

  OUT1: The Input on $IN1$ passes through 3 10th order low pass filters. They are made by the Linear Technology (LTC1569CS8) and the passive components have values to make $f_c = 800Hz$ (the second harmonic). There is also the a notch filter made with an operational amplifier and passive components, to remove $f_c = 1200Hz$ (the third harmonic). So that this output signal is a sinewave at $400Hz$.

  OUT2: Dive Voltage Monitor. Connected to the $IN2$ with a buffer.

  OUT3: Drive Current Monitor. Connected to the $IN3$, as the previous case there is a buffer in the middle.

  Such measurement has been done also on the Drive Loop Transition board, the test setup will be similar to the one used to measure the frequency response for the power amplifier.

The frequency response for each channel has been measured.

The first channel, connects the digitizer to the modulating winding of the DCCT, the second and third harmonic are very attenuated(*Fig.* 3.18).

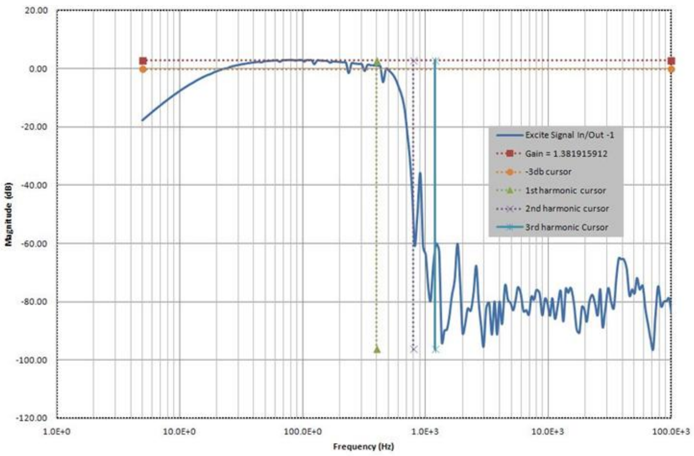

Figure 3.18: *Drive loop transition board, Channel 1 frequency response*

For the other channels, that is only to monitor the attenuation in 0dB (*Fig.* 3.19, *Fig.* 3.20).

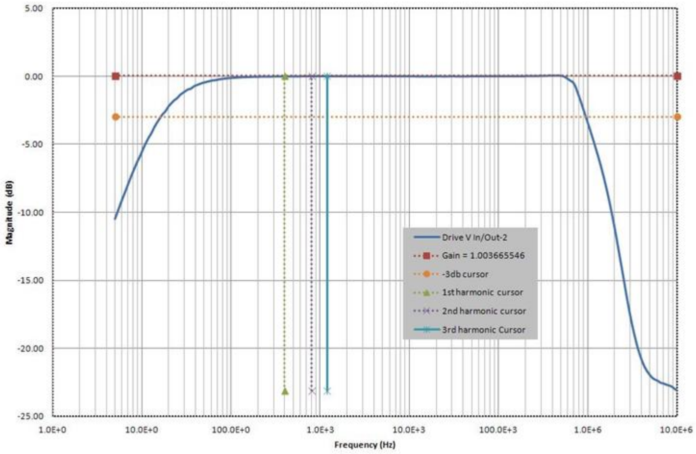

Figure 3.19: *Drive loop transition board, Channel 2 frequency response*

- **Feedback Loop Transition Board**

  This transition board is between the digitizer and the drive feedback power amplifier. It drives the signal from the AC Sense and DC Sense windings on the detector

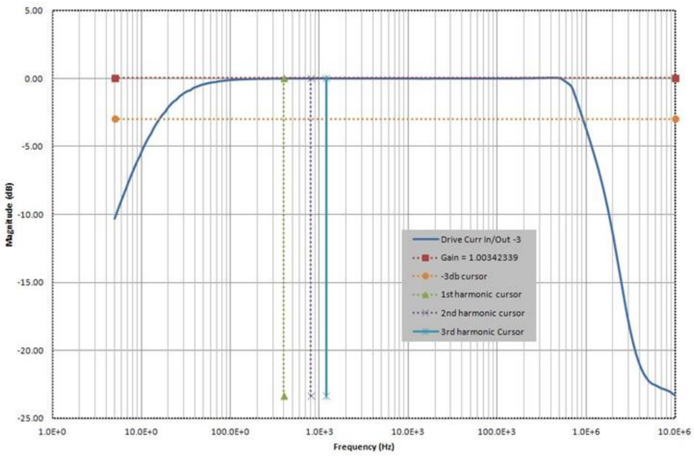

Figure 3.20: Drive loop transition board, Channel 3 frequency response

to the digitizer to be elaborated, as well as from the digitizer to the feedback loop. The block diagram is in *Fig.* 3.21

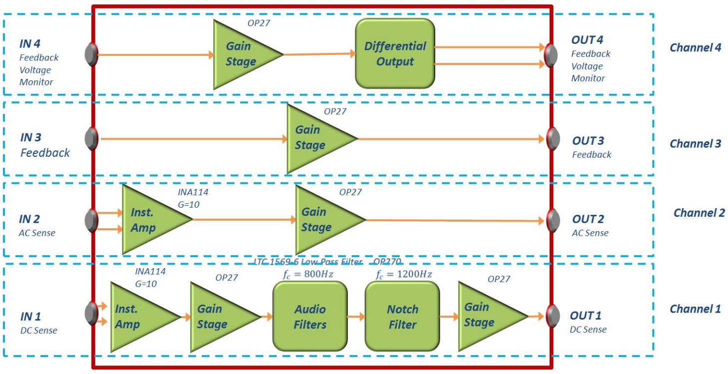

Figure 3.21: Feedback loop Transition Board Block Diagram

Inputs:

IN1: Induced signal from the DC Sense winding on the DCCT;

IN2: Induced signal from the AC Sense winding on the DCCT;

IN3: Feedback, from the digitizer.

IN4: Feedback Monitor, from the power amplifier.

Outputs:

OUT1: DC Sense. The Input on $IN1$ comes from the DC Sense. The second harmonic of the signal from this winding is proportional to the beam current. It is important to detect this second harmonic and to cut possible components of $400Hz$. For this reason there is a notch filter with $f_c = 400Hz$ and 3 stages of low pass filters with $f_c = 1200Hz$.

OUT2:AC Sense. From the AC sense, we are interested to detect the beam current from $100Hz$ to $1MHz$. Such gain stages and buffers are on this route.

OUT3: Feedback. The signal on $IN3$ comes from the digitizer. It is elaborated to rebuild the AC and DC components of the beam current. To make a feedback control loop, this current needs to come back into the digitizer. This output is then connected to the feedback loop power amplifier and come back to the detector.

OUT4: Feedback Current Monitor. Return wire from the feedback winding, to monitor the feedback current.

To make the measurement the test setup is the same that the drive loop transition board.

The channel 1 is the DC sense, it is basically a signal in a bandwidth from 0 to 100 Hz modulated at $800Hz$. As we can see from the *Fig.* 3.22, the second harmonic (800Hz) is less attenuated then the first and the third, while the DC Sense bandwidth is respected.

Also the AC Bandwidth is respected. The band pass is flat until $1MHz$, which is the upper limit of the AC Sense bandwidth. The same is for the channel 3 and the channel 4.

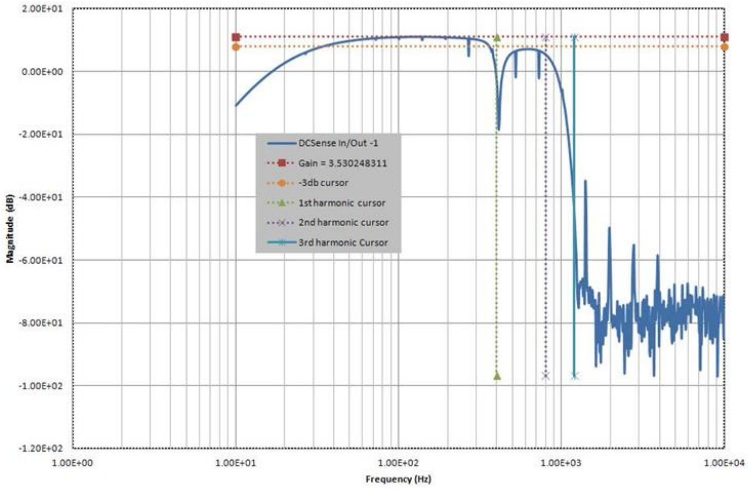

Figure 3.22: *Feedback loop transition board, $Channel1$ frequency response*

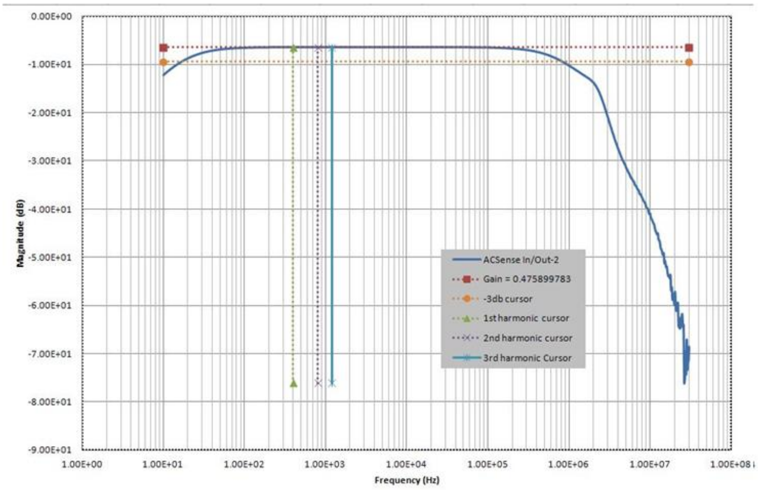

Figure 3.23: *Feedback loop transition board, $Channel2$ frequency response*

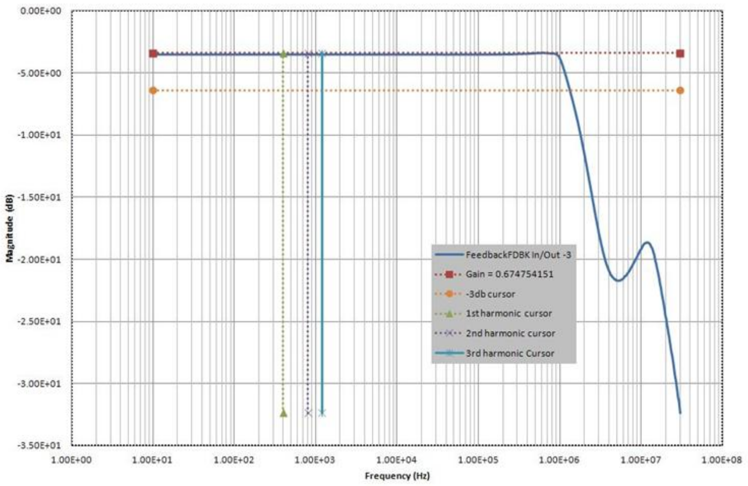

Figure 3.24: *Feedback loop transition board,* $Channel3$ *frequency response*

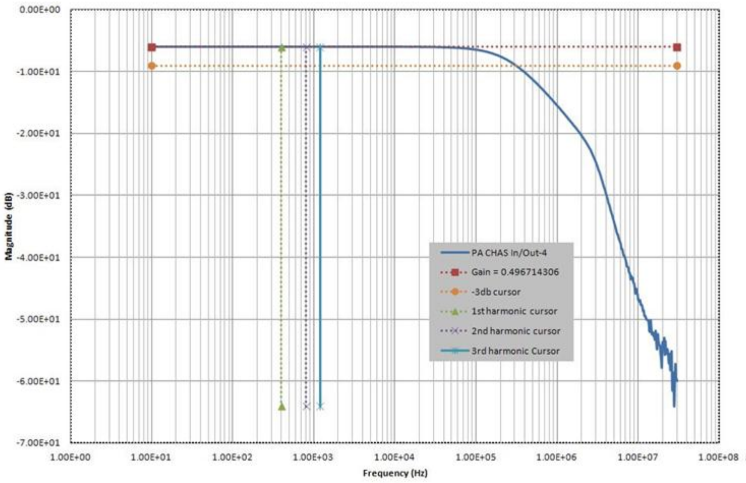

Figure 3.25: *Feedback loop transition board,* $Channel4$ *frequency response*

Chapter 4

Digital Implementation

In this chapter, the VHDL algorithm that has been implemented to detect the DC component of the beam current will be explained. Also, the model made in Simulink to simulate the system will be presented. The block diagram of the FPGA's primary functions to realize is in *Fig.* 4.1.

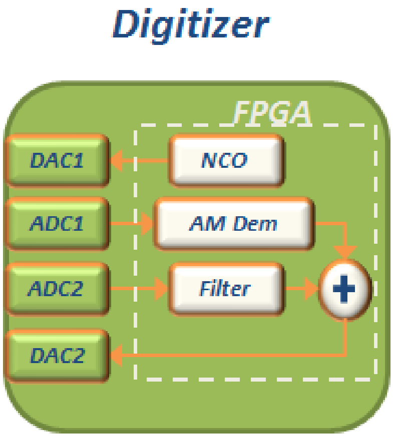

Figure 4.1: *Block Diagram of the function to realize in VHDL with the respective output on the physical board*

The signal coming from the DC section is at low frequency, modulated at $800Hz$. To be demodulated it has to be multiplied by a sinewave at $800Hz$, this is also digitally generate with the NCO. There is a digitally implemented AM demodulator, to detect the second harmonic coming from the DC section in the sensor. A filter to discriminate the AC band will be implemented in future. Finally those signals are summed and put in output.

Another DAC output send a sinewave at $400Hz$ to modulate two cores in the sensor. It is digitally generated by an NCO. One reason why the modulator signal is generated using the FPGA is to avoid unlocked phase alignment. In this way the two NCOs, one that provide the source, one that elaborate the signal, are locked in phase.

The VME interface completes the system. The VME can work using three data modes: D8, D16 and D32. Different registers, of a the different bit length can be controlled using an appropriate data mapping (i.e. to control the gain of the feedback signal, or the offset, or the internal registers of the DACs and ADCs). In *Fig.* 4.2 an example of the data mapping for this firmware.

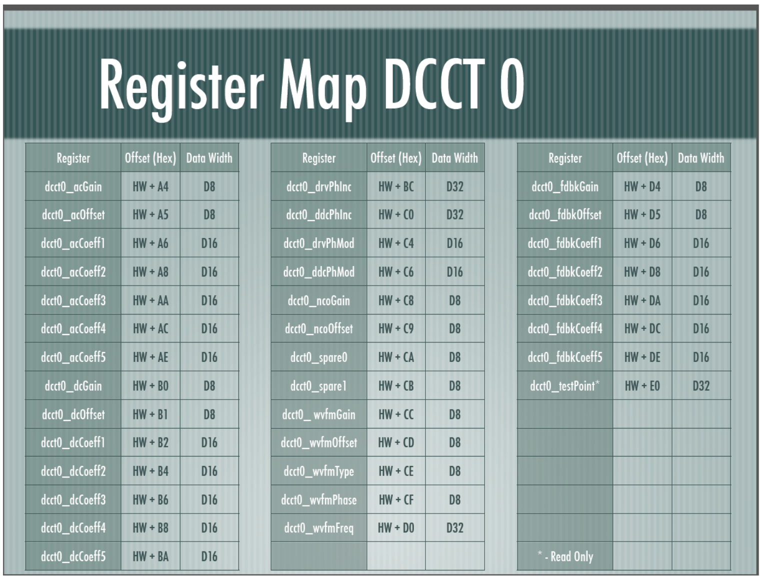

Register Map DCCT 0

Register	Offset (Hex)	Data Width	Register	Offset (Hex)	Data Width	Register	Offset (Hex)	Data Width
dcct0_acGain	HW + A4	D8	dcct0_drvPhInc	HW + BC	D32	dcct0_fdbkGain	HW + D4	D8
dcct0_acOffset	HW + A5	D8	dcct0_ddcPhInc	HW + C0	D32	dcct0_fdbkOffset	HW + D5	D8
dcct0_acCoeff1	HW + A6	D16	dcct0_drvPhMod	HW + C4	D16	dcct0_fdbkCoeff1	HW + D6	D16
dcct0_acCoeff2	HW + A8	D16	dcct0_ddcPhMod	HW + C6	D16	dcct0_fdbkCoeff2	HW + D8	D16
dcct0_acCoeff3	HW + AA	D16	dcct0_ncoGain	HW + C8	D8	dcct0_fdbkCoeff3	HW + DA	D16
dcct0_acCoeff4	HW + AC	D16	dcct0_ncoOffset	HW + C9	D8	dcct0_fdbkCoeff4	HW + DC	D16
dcct0_acCoeff5	HW + AE	D16	dcct0_spare0	HW + CA	D8	dcct0_fdbkCoeff5	HW + DE	D16
dcct0_dcGain	HW + B0	D8	dcct0_spare1	HW + CB	D8	dcct0_testPoint*	HW + E0	D32
dcct0_dcOffset	HW + B1	D8	dcct0_ wvfmGain	HW + CC	D8			
dcct0_dcCoeff1	HW + B2	D16	dcct0_wvfmOffset	HW + CD	D8			
dcct0_dcCoeff2	HW + B4	D16	dcct0_wvfmType	HW + CE	D8			
dcct0_dcCoeff3	HW + B6	D16	dcct0_wvfmPhase	HW + CF	D8			
dcct0_dcCoeff4	HW + B8	D16	dcct0_wvfmFreq	HW + D0	D32			
dcct0_dcCoeff5	HW + BA	D16				* - Read Only		

Figure 4.2: *VME Data Mapping*

4.1 Sensor Model

To make a digital model of the DCCT system it is necessary to describe the behaviour of the sensor and to relate the amplitude of the second harmonic to the intensity of the dc component of beam current. It is important to note that this is a simplified model, based on ideal physics parameters. The Simulink model is in *Fig.* 4.3, while the main block in *Fig.* 4.4.

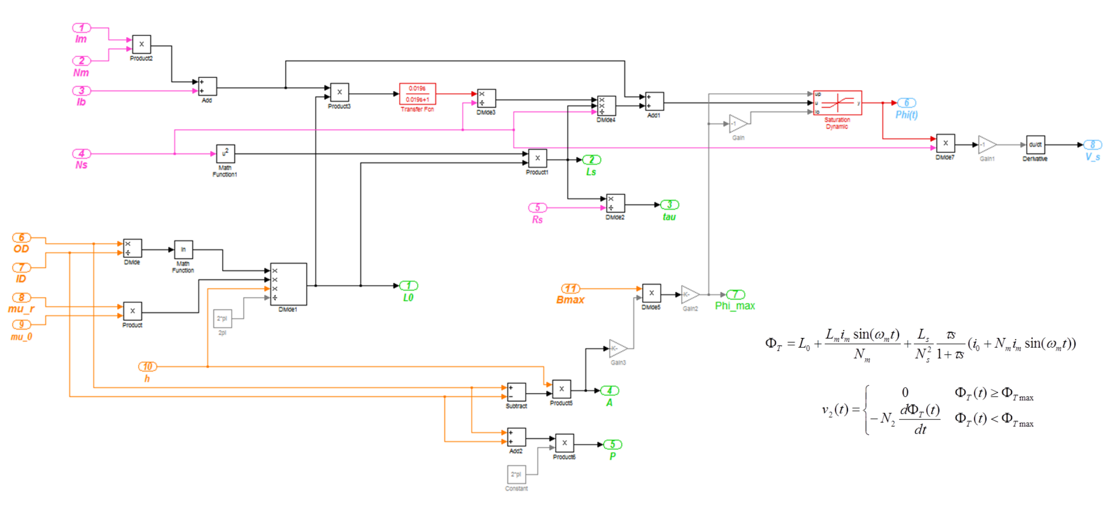

Figure 4.3: *Model of the toroids behaviour , implemented in Simulink*

As explained in the *Chapter 2*, the second harmonic is due to the mismatch of flux between the two toroids when they saturate, this distortion is proportional to the DC current applied. To simulate this behaviour such physical equations (2.32, 2.33) were applied, to calculate the flux, the voltage on the secondary winding, and other parameters of the toroid such as the inductance, and the time constant.

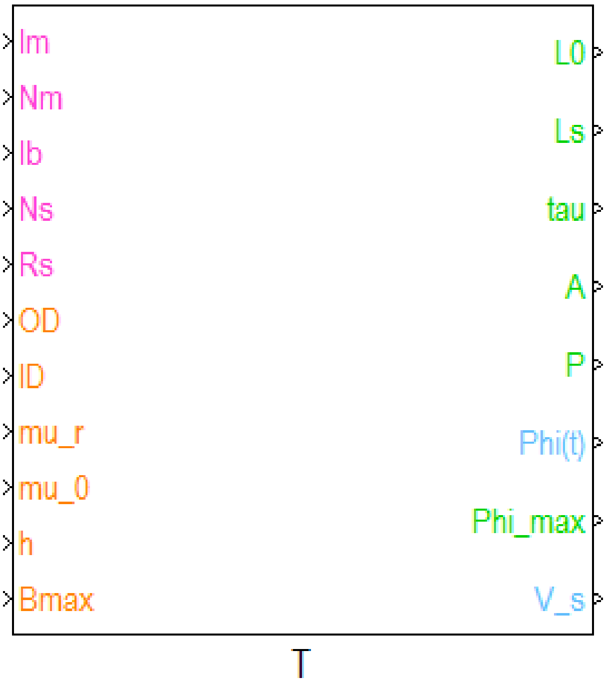

Figure 4.4: *Main block for the simulation of the toroid's behaviour.*

- **Inputs**

  1. I_m: modulating current, $I_m = A_m \cos \omega t$;
  2. N_m: number of turns on the modulator winding;
  3. I_b: current to be detected, the bandwidth goes from $0Hz$ to $100Hz$;
  4. N_s: number of turns on the sense winding;
  5. R_s: burden resistor on the sense winding;

6. OD: output diameter of the toroid;
7. ID: inner diameter of the toroid;
8. μ_r: relative permeability;
9. μ_0: permeability n free space;
10. h: height of the toroid;
11. B_{max}: maximum magnetic field;

- **Outputs**

  1. L_0: self inductance for one turn winding;
  2. L_s: self inductance for the sense winding;
  3. τ: time constant;
  4. A: cross sectional area;
  5. P: path length;
  6. $\Phi(t)$: Flux in time domain;
  7. Φ_{max}: maximum flux;
  8. V_s: output voltage on the sense winding;

In order to have a complete model two toroids have to be considerated. They are driven with two sinewaves in opposite phase. The final configuration is the one in *Fig.* 4.5.

With this model the flux and the voltage can be monitored. The first test is done for $i_b = 0$. As aspected the output is zero. In fact, the fluxes and the output voltages, separately considered, match between the toroids. The total output is zero. In the picture *Fig.* 4.6, the flux is shown, separately for each toroid. The same for the voltage in *Fig.* 4.7. Finally, the sum of the two signal, it is fixed at zero. There is a zoom of this result, in *Fig.* 4.8.

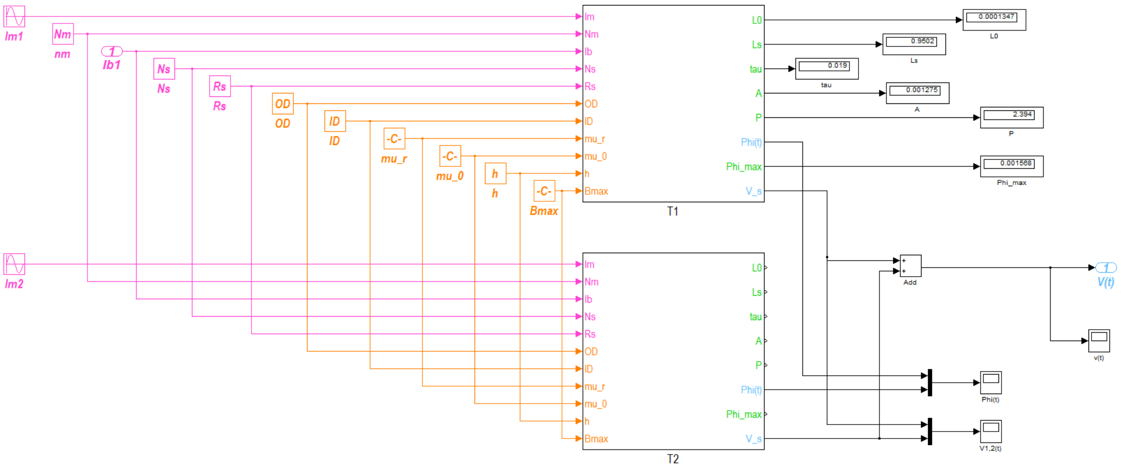

Figure 4.5: *Model of the toroids behaviour, concerning the two toroids*

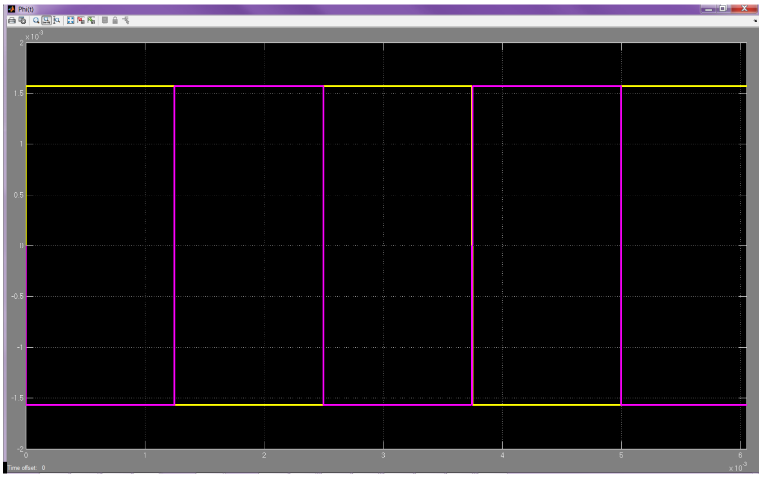

Figure 4.6: *Flux calculated from each toroid, with no input. The yellow trace is referred to the first toroid and the pink trace to the second toroid*

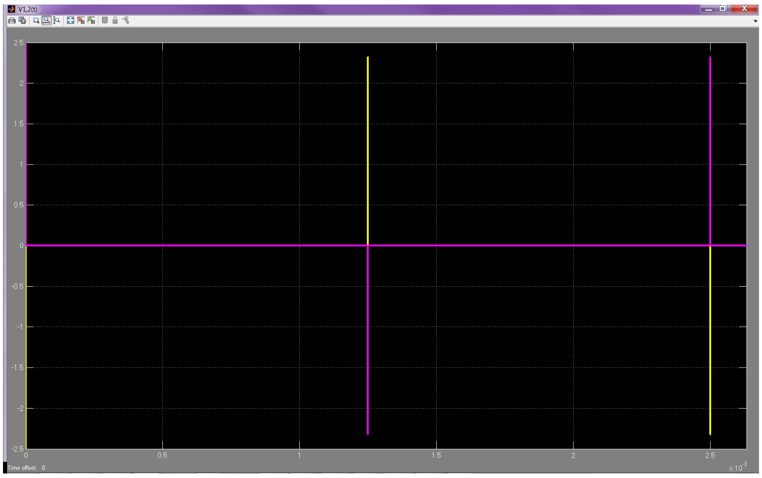

Figure 4.7: *Voltage output calculated from each toroid, the yellow trace is referred to the first toroid and the pink trace to the second toroid.*

Figure 4.8: *Zoom voltage output calculated from each toroid, the yellow trace is referred to the first toroid and the pink trace to the second toroid, in this way it is easier to see that they match and that the sum will be zero.*

If a current is applied in input (i.e. $i_b = 1$), there is a mismatch for the flux and the voltage (*Fig.* 4.9 for the separately toroids). So the output voltage of the combined system is not zero. But a frequency component of interest is at $800Hz$ and its multiples. In *Fig.* 4.10, the voltage output from the toroids separately is shown. The spectrum is in *Fig.* 4.11. A zoom is available in *Fig.* 4.12). In *Fig.* 4.13 the combined output and the spectrum *Fig.* 4.14, (a zoom is available in *Fig.* 4.15).

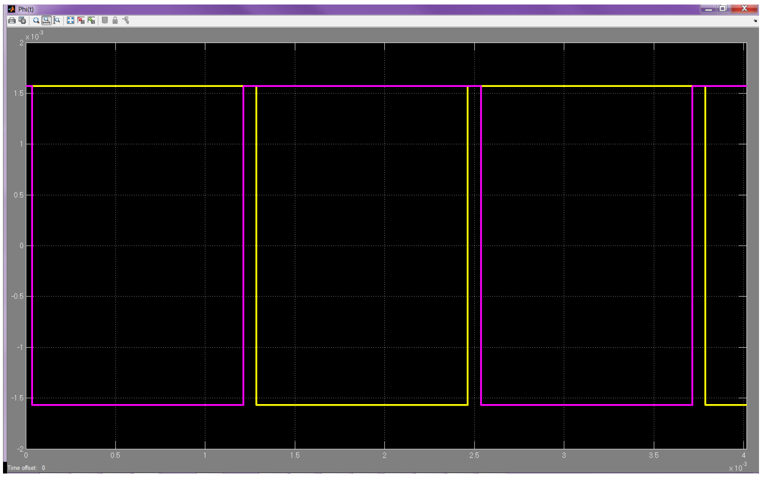

Figure 4.9: *Flux calculated from each toroid, with a constant signal in input. The yellow trace is referred to the first toroid and the pink trace to the second toroid*

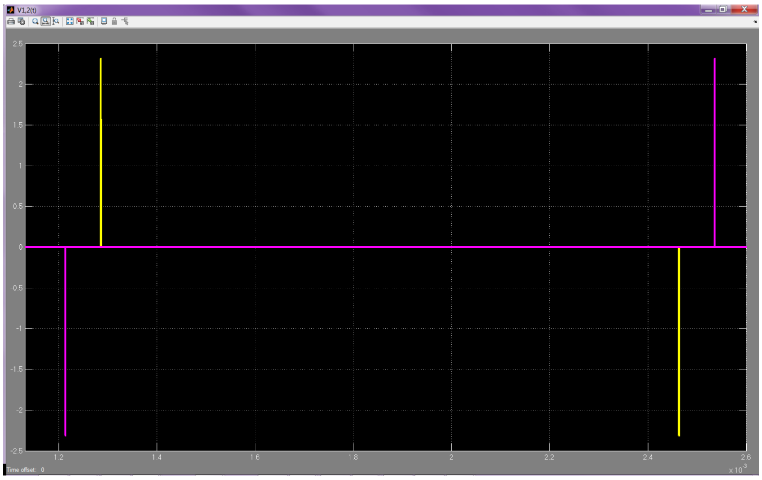

Figure 4.10: *Output voltage for each toroid, the voltage output is the sum of those signals*

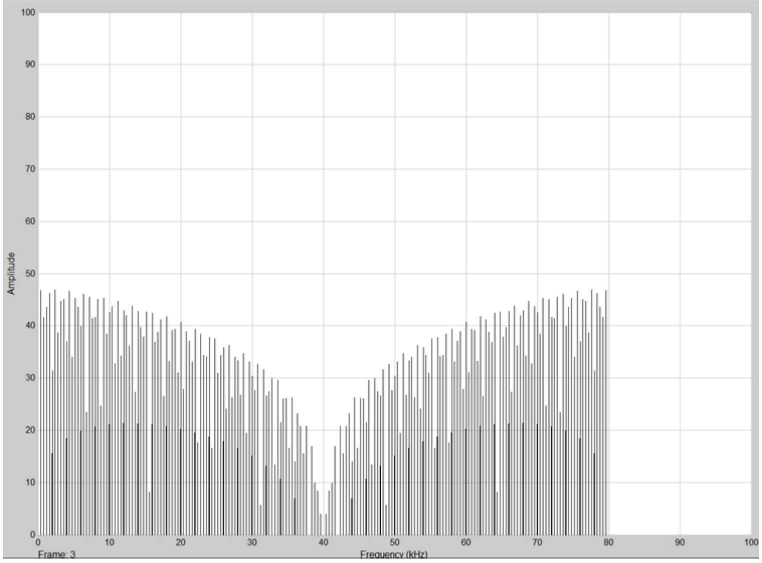

Figure 4.11: *Spectrum of the signal in Fig. 4.10*

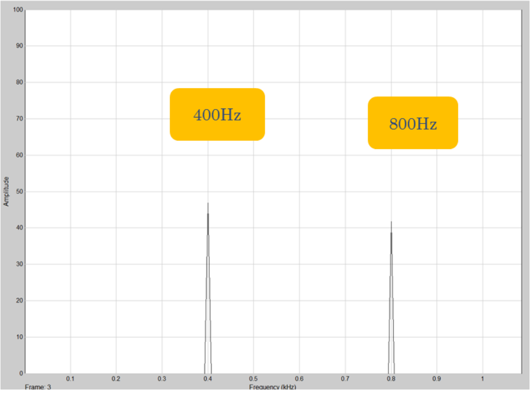

Figure 4.12: *Zoom of the Spectrum in Fig. 4.11*

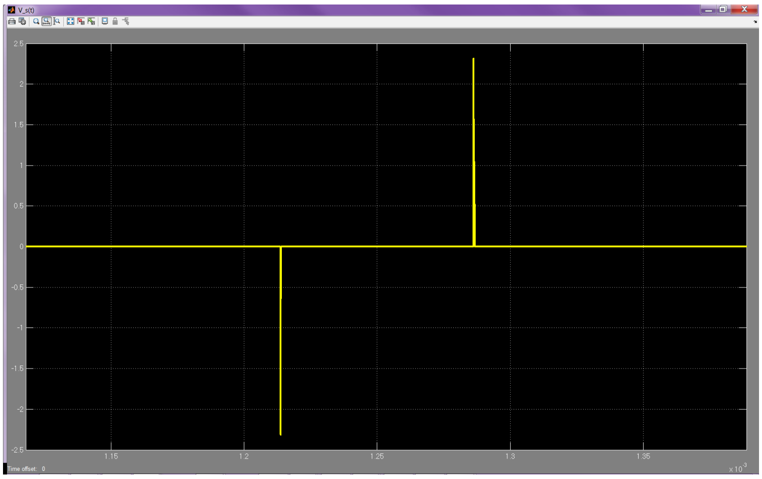

Figure 4.13: *Sum of the outputs from each toroid.*

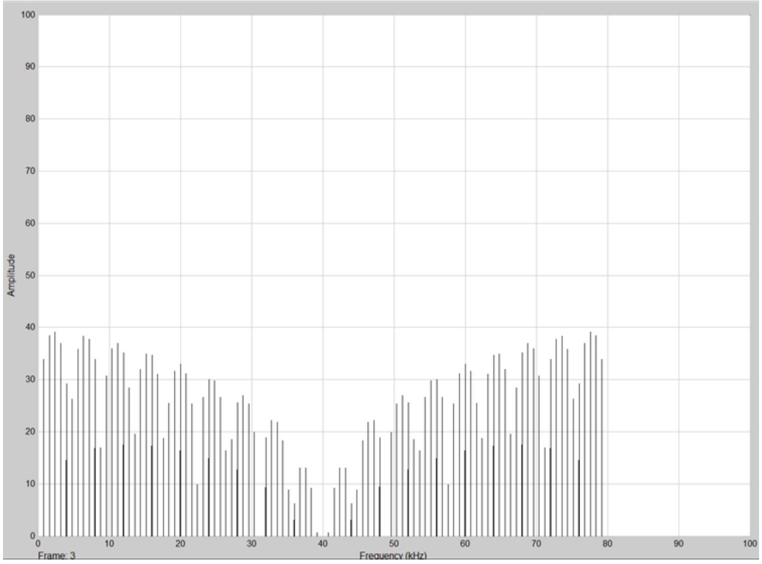

Figure 4.14: *Spectrum of the signal in Fig. 4.13.*

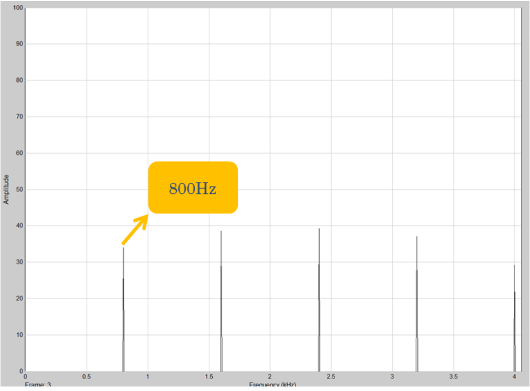

Figure 4.15: *Zoom of the Spectrum in Fig. 4.14*

4.2 DC Section

The signal processing in the DC section consists in the detection of the amplitude of the second harmonic. This signal can be converted in the baseband using a digital down converter (DDC). The function of the DDC is to determinate the phase (I) and quadrature (Q) of the signal downconverted in baseband as shown in the block diagram in *Fig.* 4.16.

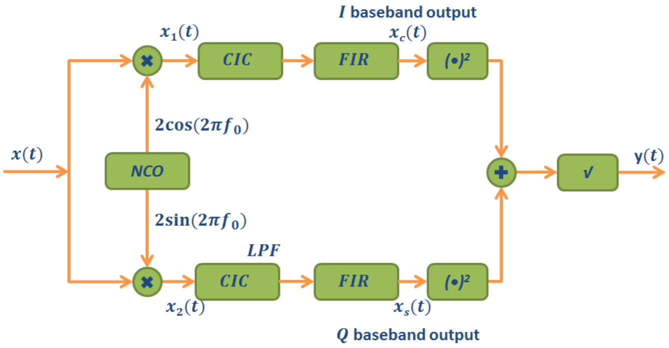

Figure 4.16: *Demodulator block diagram*

If the input signal is at the f_0 frequency, the digital oscillator has to generate a sinusoids in phase and quadrature at the same frequency. After the multiplication between the input signal and the sinusoids from the oscillator there is a low pass filter, to isolate the signal downconverted.

The input signal is $x(t)$ and is expressed in the following way:

$$x(t) = m(t)\cos(2\pi f_0 + \Theta) \tag{4.1}$$

Where $m(t)$ is the modulated signal, f_0 is the modulating frequency and Θ is the phase of the modulating signal.

After the multiplication for a sine wave and a cosine wave at the same frequency f_0:

$$x_1(t) = x(t)2\cos(2\pi f_0 t) = 2m(t)\cos(2\pi f_0 t{+}\Theta)\cos(2\pi f_0 t) = m(t)(\cos(\Theta){+}\cos(4\pi f_0 t{+}\Theta)) \tag{4.2}$$

$$x_2(t) = x(t)2\sin(2\pi f_0 t) = 2m(t)\cos(2\pi f_0 t)\sin(2\pi f_0 t) = m(t)(\sin(4\pi f_0 + \Theta) - sin(\Theta)) \tag{4.3}$$

The low pass filters (LPF) is designed to cut the higher frequencies, if particular the component at $2f_0$. After the LPF, the results are:

$$x_c = m(t)\cos(\Theta) \tag{4.4}$$

$$x_s = -m(t)\sin(\Theta) \tag{4.5}$$

Summing the previous components and taking the square root, the output is:

$$y(t) = \sqrt{x_c(t)^2 + x_s(t)^2} = |m(t)|\sqrt{\cos^2(\Theta) + \sin^2(\Theta)} = |m(t)| \tag{4.6}$$

In the VHDL implementation, this stage is not just a LPF, but instead it is a cascade of CIC filter and low pass FIR filter. The CIC filter is used to downsample the signal. After this, the FIR filter with a strong attenuation outside the pass band is used.

To complete rebuild the signal of both polarities a signum detector is used, in stead of a phase detector, taking advantage from the fact that the signal is slow. This signum can be detected on the input signal or after the filter on the phase chain (from the equation 4.4 it is clear that the output of the filter is in phase with the input signal). Considering that the filtering stage can add delays, this block has been added after the filter to avoid distortion.

To realize this design, the specifications of the system have to be considered. The bandwidth of the signal we want to detect is from the dc to $100Hz$. The clock frequency is $62.5MHz$. This sampling rate is too high to have good digital filters. So a first downsample stage has been added in input. This first CIC downsamples to $500kHz$. This will be the same sampling frequency used to generate the sinusoid in the NCO. After the multiplication there is a second CIC to downsample to $2kHz$, this sampling frequency allows to build a more efficient FIR low pass filter. At this point there is the low pass filter with $f_c = 100Hz$. Afterwards the mathematical blocks rebuild the signal.

The complete block diagram is shown in *Fig.* 4.17.

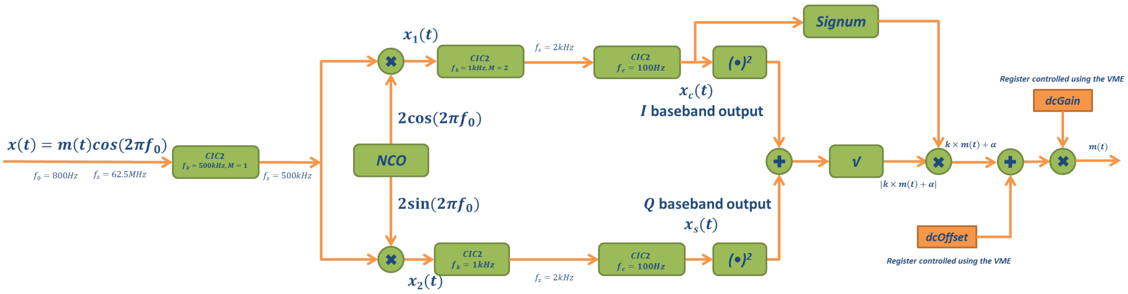

Figure 4.17: *Complete demodulator block diagram*

4.2.1 Numerically Controlled Oscillator

The Numerically Controlled Oscillator (NCO) is necessary to generate the modulator signal to the toroids. It is also necessary to generate multiplication signal, to downconvert the input signal.

The simplest way to realize a digital oscillator is use a programmable read only memory (PROM), an address counter, and a precision reference clock. At every clock cycle, the system access as the memory location pointed by the counter. The final stage is the DAC. In general this technique is called direct digital synthesis (DDS). An example of the simplest system is in *Fig.* 4.18

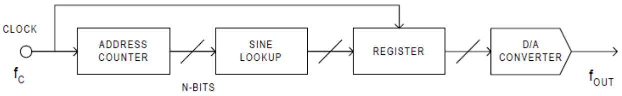

Figure 4.18: *Simple Direct Digital Synthesis*

To control the frequency of the output signal of the Numerically Controlled Oscillator (NCO), a phase accumulator can be introduced. This phase accumulator is controlled by the input tuning word (*Fig.* 4.19).

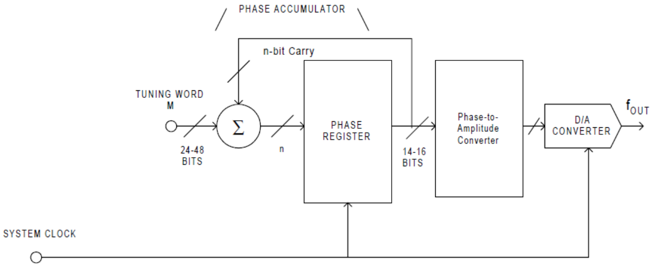

Figure 4.19: *Direct Digital Synthesis with the phase accumulator and the tune word.*

To better understand the NCO, the output sinewave can be seen as a vector that rotates around a phase circle (*Fig.* 4.20). A complete cycle around this wheel is equivalent to one cycle of the desirable sinewave by changing the tune word (M), the speed with which the complete cycle is done, changes, as well as the frequency of the output sinewave.

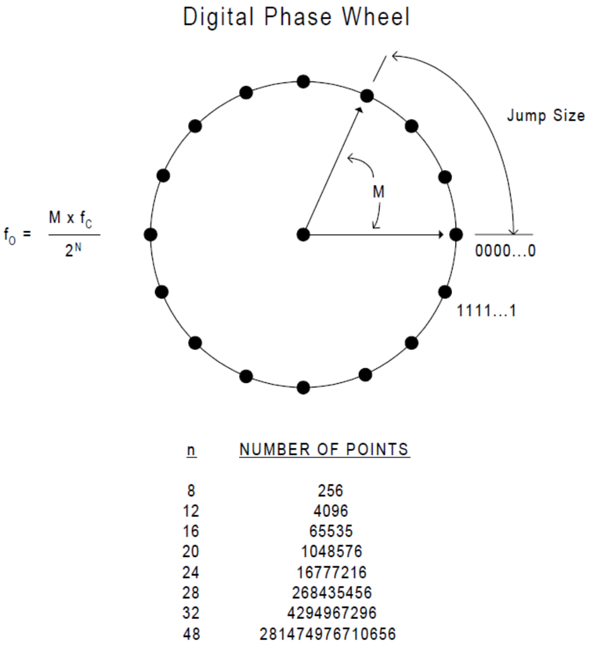

$$f_O = \frac{M \times f_C}{2^N}$$

n	NUMBER OF POINTS
8	256
12	4096
16	65535
20	1048576
24	16777216
28	268435456
32	4294967296
48	281474976710656

Figure 4.20: *Digital Phase wheel*

The output frequency is calculated by:

$$f_0 = \frac{Mf_c}{2^N} \tag{4.7}$$

Where f_c is the clocking frequency and N is the number of points on the wheel and also the length in bits of the tuning word.

Making an NCO using the PROM can occupy too many resources on the FPGA. A good solution can be to use instead an algorithm, that generates the corresponding value of the sinewave at that phase, starting from the signal generated by the accumulator.

4.2.2 Cascade Integrator and Comb Filter

The Cascade Integrator and Comb Filters (CIC) are based on the FIR technique. There are two version for a CIC Filter. One is a decimation filter, the other one is an interpolation filter. In the decimation filter, an integrator section *Fig.* 4.21, operating at the high sampling frequency, is followed by a comb section *Fig.* 4.22, operating at a lower sampling frequency. The interpolation filter has these two sections switched.

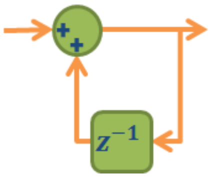

Figure 4.21: *Block Diagram of the integrator section*

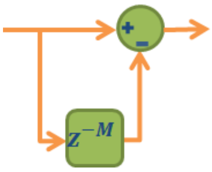

Figure 4.22: *Block Diagram of the comb section*

In *Fig.* 4.23 there ia a basic implementation of a decimation CIC filter is shown.

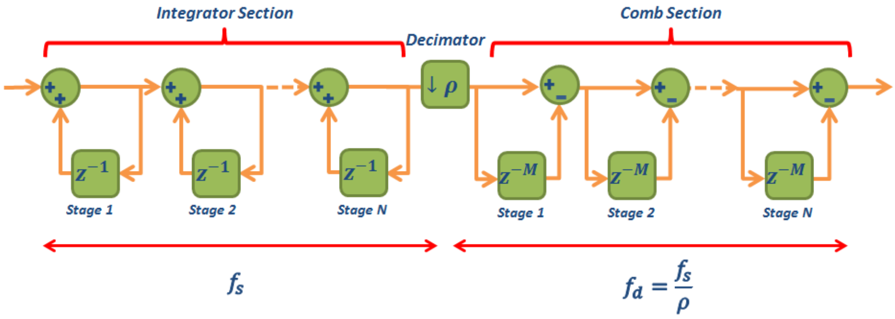

Figure 4.23: *CIC Filter Block Diagram*

The transfer function for the generic CIC Filter using the z variable can be calculated.

In the integrator section there are N elementary digital integrators, operating at f_s. The transfer function for each integrator is:

$$H_i(z) = \frac{1}{1 - z^{-1}} \tag{4.8}$$

The transfer function for a cascade of the N integrators is:

$$H_I(z) = [H_i(z)]^N = \left(\frac{1}{1 - z^{-1}}\right)^N \tag{4.9}$$

Afterwards the signal obtained is decimated at the frequency $f_d = f_s/\rho$. The corresponding period is $T_d = \rho T_s$, where ρ is called rate change factor.

The comb section is made up by N elementary comb stages and work at f_d. Each block has e delay of M. This parameter is called differential delay. The transfer function for each comb stage is:

$$H_{c_{f_d}}(z) = (1 - z^{-M}) \tag{4.10}$$

For the cascade of the N comb stages:

$$H_{C_{f_d}}(z) = [H_c(z)]^N = (1 - z^{-M})^N \tag{4.11}$$

Using the frequency f_s:

$$H_C(z) = (1 - z^{-\rho M})^N \tag{4.12}$$

Combining the 4.9 and the 4.12, the global transfer function for the filter is as follows:

$$H(z) = H_I(z) H_C(z) = \left(\frac{1 - z^{-\rho M}}{1 - z^{-1}} \right)^N \tag{4.13}$$

The equation in 4.13 is the result of a convergent series :

$$\sum_{k=0}^{n} q^n = \frac{1 - q^{n+1}}{1 - q} \tag{4.14}$$

Applying the 4.14 to the 4.13:

$$H(z) = \left(\frac{1 - z^{-\rho M}}{1 - z^{-1}} \right)^N = \left[\sum_{k=0}^{\rho M - 1} z^{-k} \right]^N \tag{4.15}$$

In summary, the CIC filter is a cascade of N FIR operating at f_s, accompanied by decimation stage at the frequency of f_d.

Applying the transformation from the z variable to the frequency ($z = e^{j2\pi f/f_s}$), the frequency response is as follow:

$$H(f) = \left(\frac{1 - e^{-j2\pi\rho M\frac{f}{f_s}}}{1 - e^{-i2\pi\frac{f}{f_s}}} \right)^N = e^{-j\pi\frac{f}{f_s}(\rho M - 1)N} \left[\frac{\sin(\pi\frac{f}{f_s}\rho M)}{sin(\pi\frac{f}{f_s})} \right]^N \tag{4.16}$$

The amplitude response is:

$$|H(f)| = \left| \frac{\left(\pi\rho M\frac{f}{f_s}\right)}{sin\left(\pi\frac{f}{f_s}\right)} \right|^N \tag{4.17}$$

To calculate $|H(f)|$ when $f \to 0$, the theory of limits has to be applied. It results:

$$|H(0)| = (\rho M)^N \tag{4.18}$$

The normalized frequency response is:

$$H_n(f) = \frac{H(f)}{H(0)} = e^{-j\pi\frac{f}{f_s}(\rho M-1)N}\left[\frac{1}{\rho M}\frac{sin\left(\pi\frac{f}{f_s}\rho M\right)}{sin\left(\pi\frac{f}{f_s}\right)}\right]^N \tag{4.19}$$

The CIC filter is used not only to downsample a signal, but can also be used to notch frequency components. The frequency response of the CIC has a notch at the frequencies f_k. These frequencies are calculated for $H(f) = 0$:

$$H(f) = 0 \to \sin\left(\pi\rho M\frac{f}{f_s}\right) = 0 \to \pi\rho M\frac{f}{f_s} = k\pi \tag{4.20}$$

The result is the following:

$$f_k = \frac{kf_s}{M\rho} \tag{4.21}$$

This is true only for $k \neq 0$. If $k = 0$ and $f = 0$, the function is $|H(f)| = (\rho M)^N \neq 0$.

When designing a CIC, the parameters to be considered are the order N, the differential delay M, and the rate change factor ρ. They act on the frequency response as shown in *Fig.* 4.24 .

4.2.2.1 Simulink Implementation

The two CIC filters to realize the demodulator have been simulated in Simulink. The classical scheme has been implemented, as shown in *Fig.* 4.25.

The sampling time is the most important parameter in this model, because the frequency response depends heavily on it. It can be set using the block *zero order hold* or

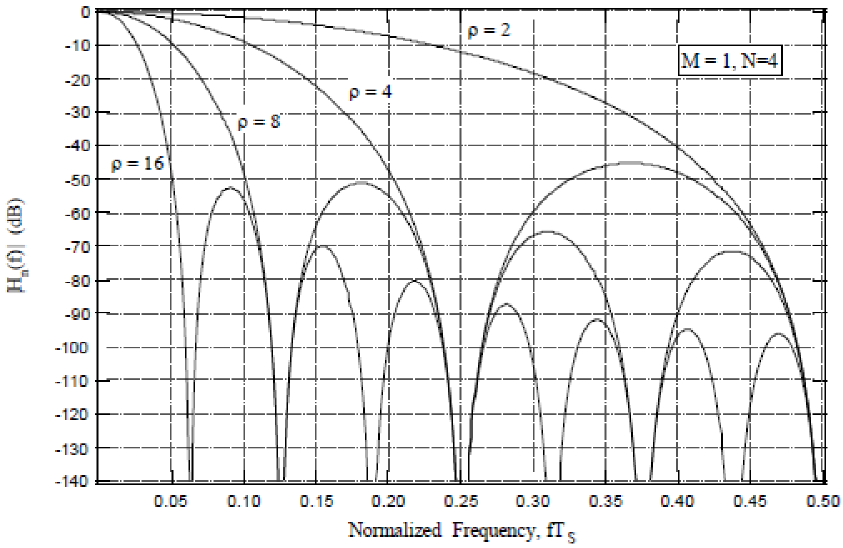

Figure 4.24: *Normalized frequency response for a CIC Filter, varying the parameter* ρ

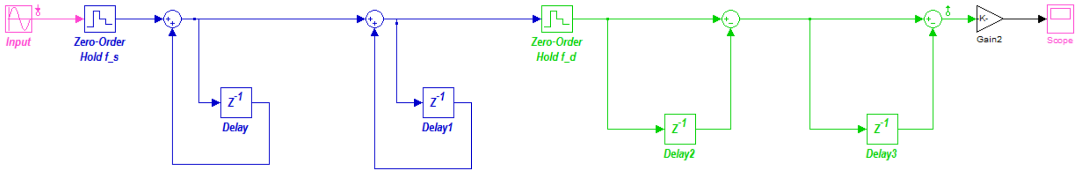

Figure 4.25: *CIC Filter in Simulink. In blue the integrator section, in green the comb section*

changing the parameter *delay length* inside the block *delay*.

The signal at the first CIC has a sampling frequency of $f_s = 62.5MHz$, and it has to be downsampled to $f_d = 500kHz$. The resulting parameters are: $\rho = 125$, $M = 1$, and $N = 2$. It will cut the frequencies at $f_k = k\frac{f_s}{M\rho}$; the first notch will be at $f_1 = 500kHz$. The gain will be $G = (M\rho)^2 = 15625$.

At the second CIC the signal has a sampling frequency $f_s = 500kHz$ and has to be downconverted to $f_d = 2kHz$. The parameters used are: $\rho = 250$, $M = 2$, and $N = 2$. It will cut the frequencies at $f_k = k\frac{f_s}{M\rho}$; the first notch will be at $f_1 = 1kHz$. The gain will be $G = (M\rho)^2 = 250000$.

The frequency response for the second CIC has been calculated with the Control Design Tool available in Matlab, and it is shown in *Fig.* 4.26

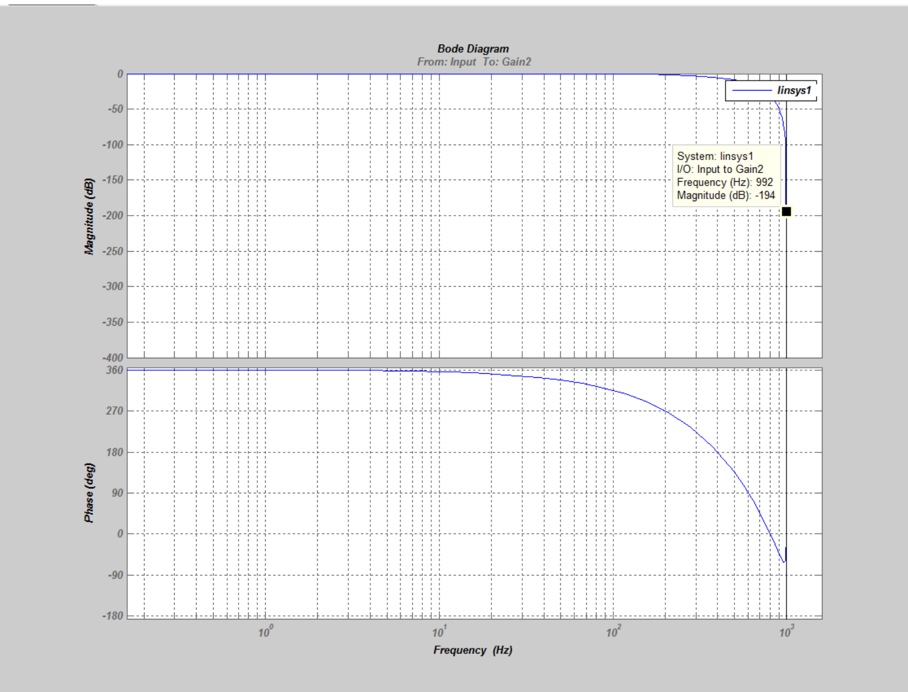

Figure 4.26: *Frequency repose for the second CIC filter using the Control Design Tool of Simulink*

4.2.3 Finite Impulse Response Filter

The Finite Impulse Response (FIR) digital filters operate on discrete time signals. They are called 'finite impulse response', because its impulse response (finite length input) sets to zero in a finite time. The output is the result of the convolution between the input signal is an impulse sequence where each impulse is weighted for a coefficient. In general the impulse response can be expressed as in the following equation

$$h[n] = \sum_{k=0}^{M} b_k \delta[n-k] \tag{4.22}$$

Where M is a finite number. If $x[n]$ is the input the resulting output is:

$$y[n] = \sum_{k=0}^{M} h[k]x[n-k] \tag{4.23}$$

The function $h[k]$ is a series of unitary impulses multiplied for different coefficients, so that previous equation can be written as:

$$y[n] = \sum_{k=0}^{M} b_k x[n-k] \tag{4.24}$$

The block diagram of an FIR Filter is in *Fig.* 4.27

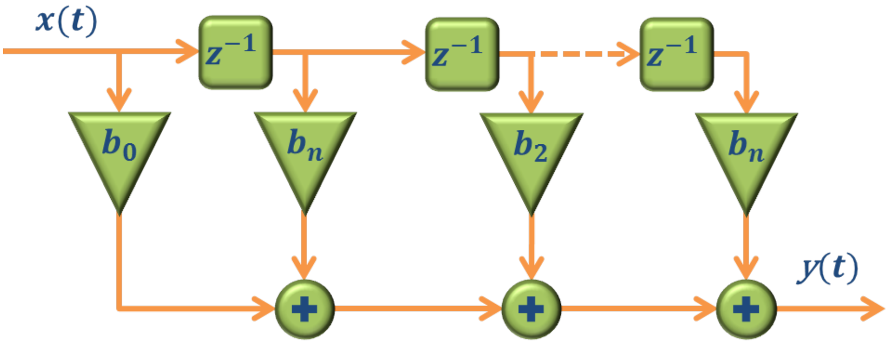

Figure 4.27: *Block Diagram for the FIR Filter Implementation*

4.2.3.1 Simulink Implementation

The FIR used has $f_c = 100Hz$. The passband is nearly $1dB$ ripple, and the stopband ia at least 80dB.

The FDA Tool of Matlab has been used to design the filter, establishing the coefficients (*Fig.* 4.28).

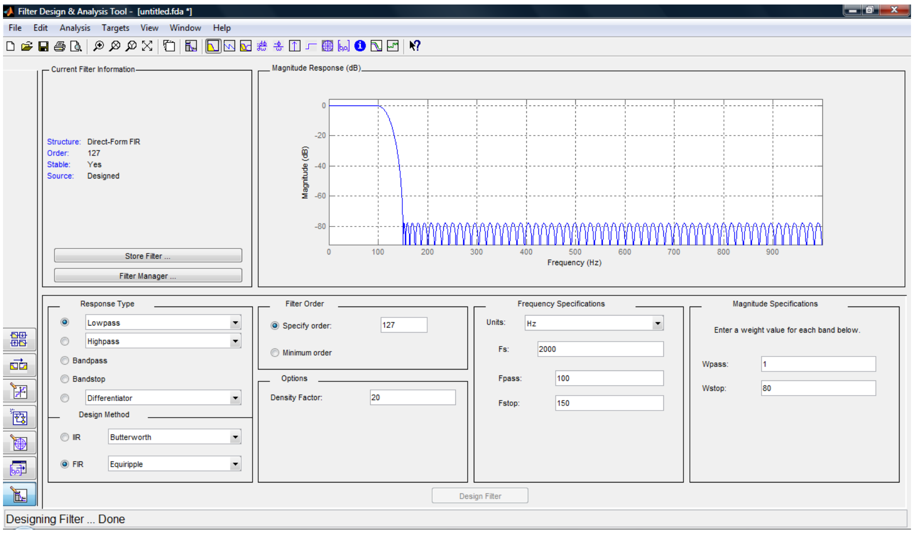

Filter Design & Analysis Tool - [untitled.fda *]

Current Filter Information

Structure: Direct-Form FIR
Order: 127
Stable: Yes
Source: Designed

Response Type: ● Lowpass
Design Method: ● FIR Equiripple
Filter Order: ● Specify order: 127
Options: Density Factor: 20
Frequency Specifications: Units: Hz; Fs: 2000; Fpass: 100; Fstop: 150
Magnitude Specifications: Enter a weight value for each band below. Wpass: 1; Wstop: 80

Designing Filter ... Done

Figure 4.28: FDA Tool in Matlab and Simulink to design an FIR FIlter

4.2.4 Demodulator

Both in Simulink and in VHDL the system has been built combining all the blocks explained before. The block diagram is defined in *Fig.* 4.17.

The implementation in Simulink is in *Fig.* 4.29

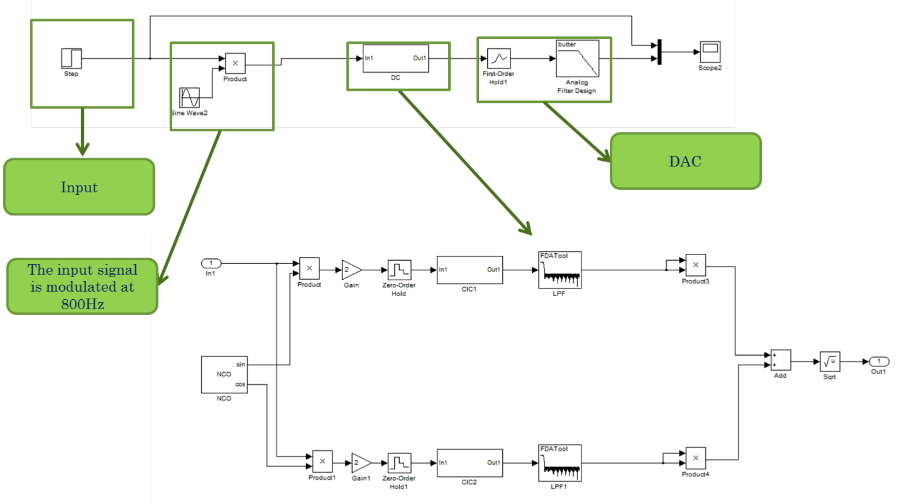

Figure 4.29: Demodulator block diagram in Simulink

In *Fig.* 4.30 the time response to a step in input in shown.

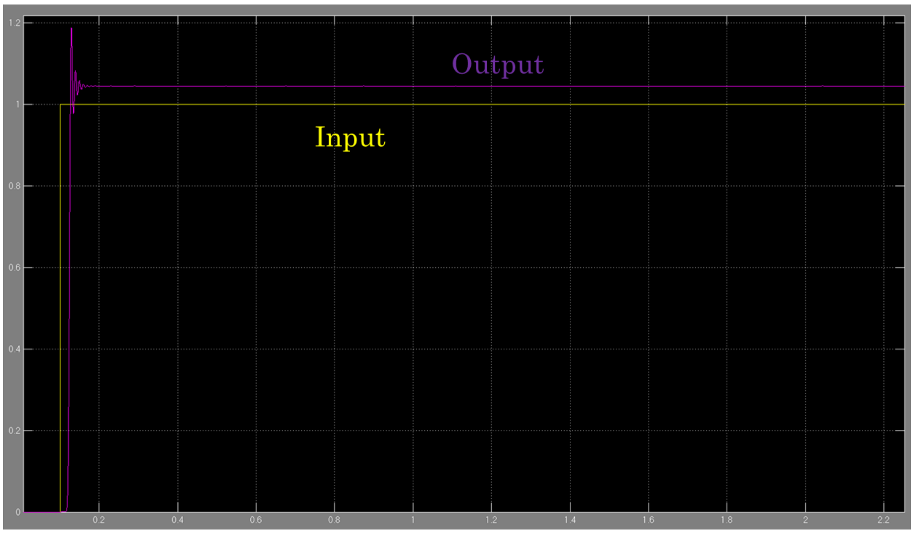

Figure 4.30: *Step response for the demodulator in Simulink*

Adding the signum detection and putting in input a signal at the low frequencies, modulated at $800Hz$, we have a complete rebuilding of the signal in phase and magnitude, as shown in *Fig.* 4.31

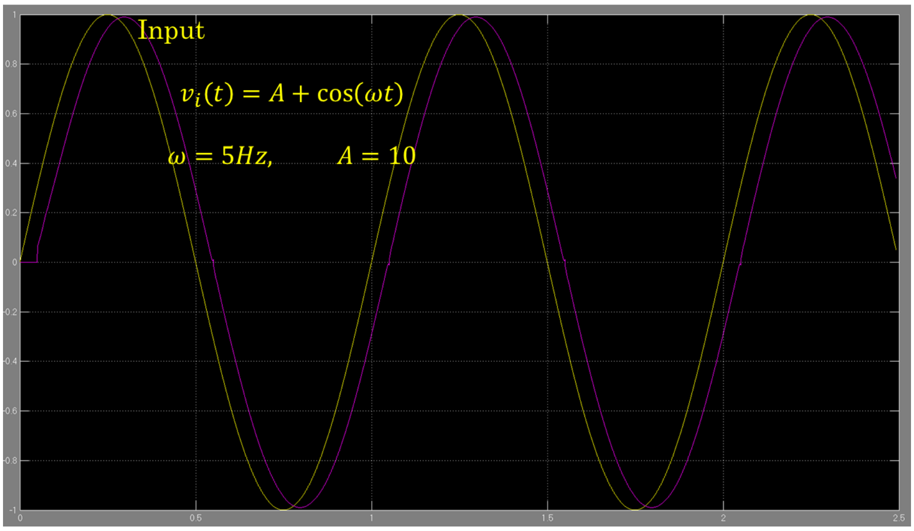

Figure 4.31: *Rebuilt of a signal in magnitude and phase*

4.3 Simulink Model

Once that the each module is separately tested and simulated using Simulink the complete model can be built.

In *Fig.* 4.32 the block diagram realized with Simulink.

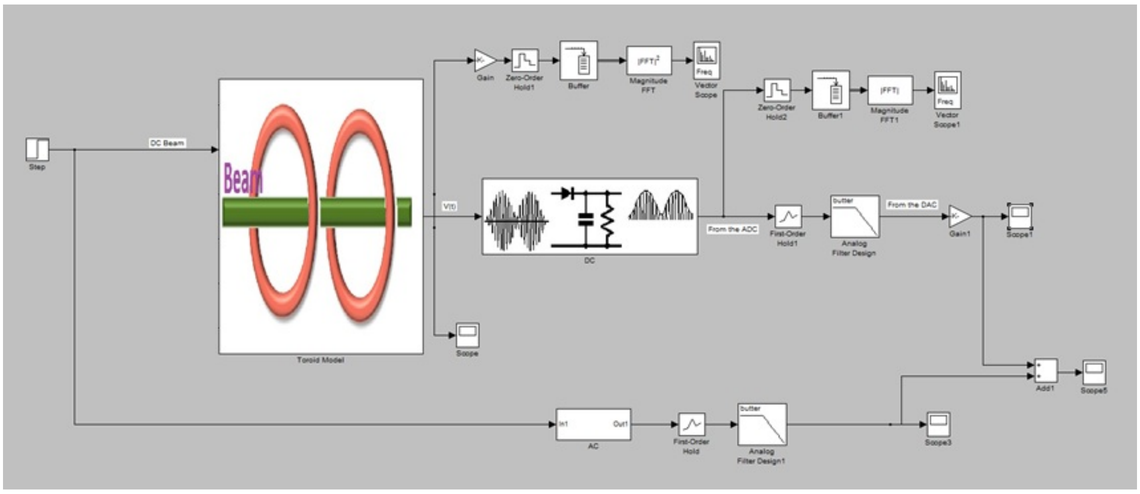

Figure 4.32: *Block diagram of the DCCT and the AC Section in Simulink.*

The block of the toroids has been used to relate the amplitude of the second harmonic to the input signal. In this model there is not only the block simulating the detection for the DC parts, but also for the AC part. The AC detection is a bandpass FIR filter with a band from $100Hz$ to $1MHz$.

To complete the model, there is a simulation of the DAC to rebuilt the processed signal. This DAC is composed by a block that interpolates the samples and a low pass filter.

The open loop response to a step input is shown in *Fig.* 4.33.

The closed loop response to a step in input, is shown in *Fig.* 4.34

The last simulation is done putting in input a signal at low frequencies and high frequencies (*Fig.* 4.35)

The spectrum of the input signal is shown in *Fig.* 4.36. It has a component in DC, a

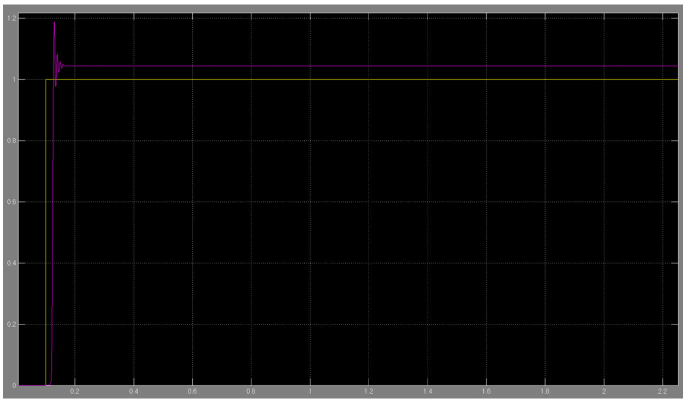

Figure 4.33: *Open loop response to a step input in Simulink*

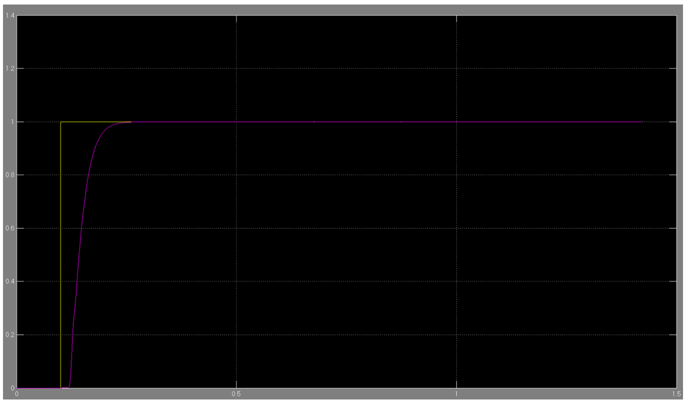

Figure 4.34: *Closed loop response to a step input in Simulink*

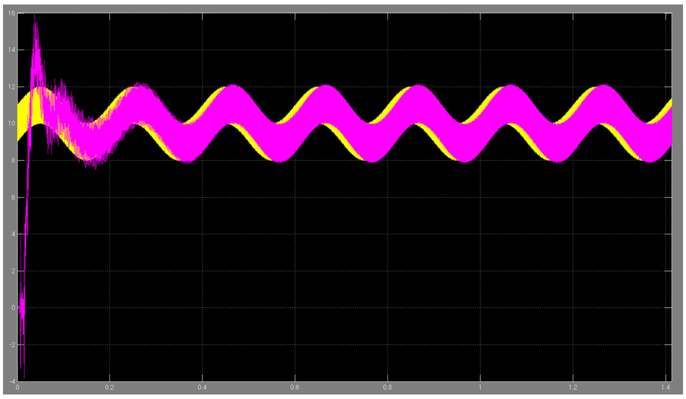

Figure 4.35: *Closed loop response to a signal with DC and AC components in Simulink*

component at $5Hz$, and a component at $1kHz$.

While the spectrum of the output signal is shown in *Fig.* 4.37. A zoom of the low frequencies components is shown in *Fig.* 4.38.

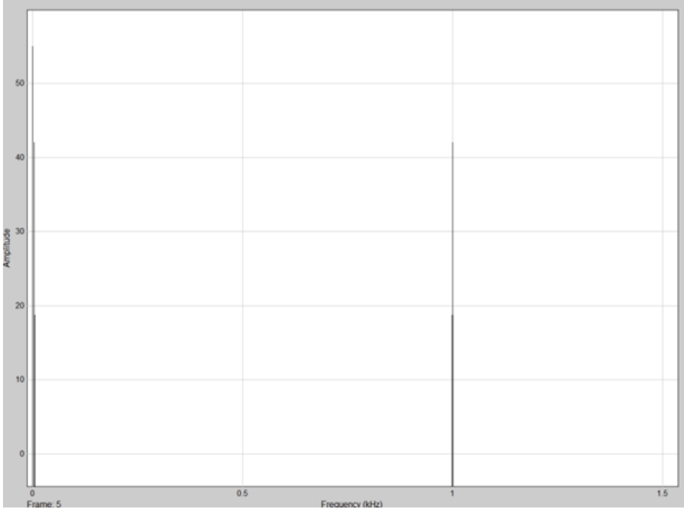

Figure 4.36: *Spectrum of the input signal*

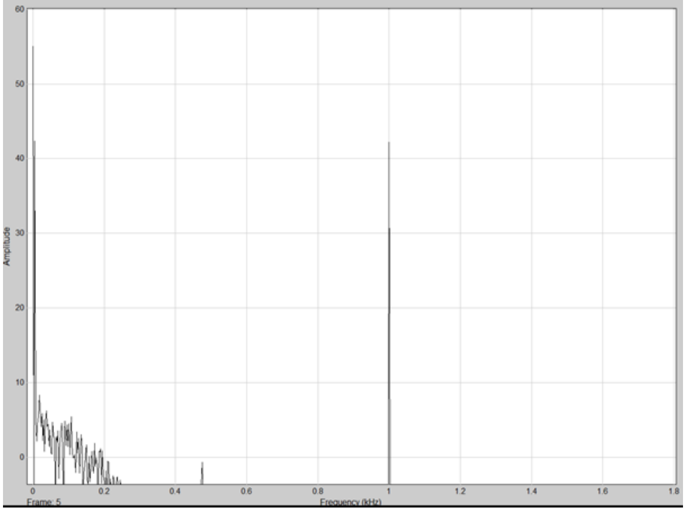

Figure 4.37: *Spectrum of the output signal*

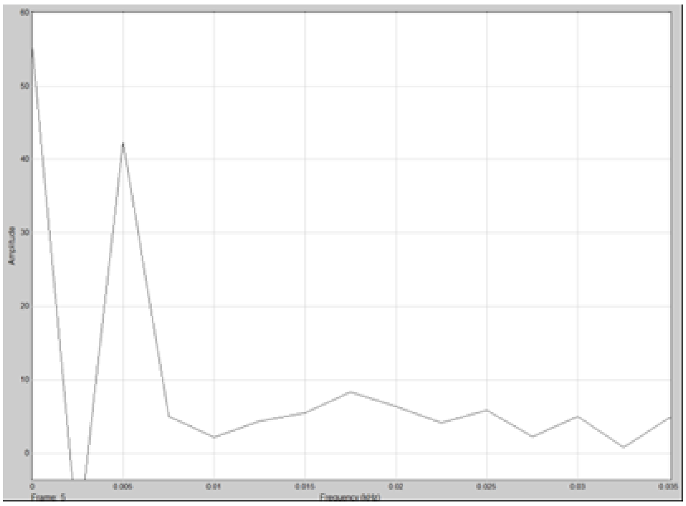

Figure 4.38: *Zoom of the spectrum in Fig. 4.37*

Chapter 5

System Tests and Results

All the systems components have been explained in the *Chapter 3*, the simulation of the function to be realized has been discussed in the *Chapter 4*. In this chapter we are going to test each elementary block, and builds the complete system to make the definitive tests, measurement and evaluate the performances.

5.1 VHDL Implementation

We are now going to test the firmware implemented. The VHDL code is available in the Appendix.

5.1.1 NCO

In VHDL, there are two NCO systems: one for the modulator, and one for the downconvertor. The modulator loop has to be $400Hz$, while for the downconvertor has to be $800Hz$.

They were both realized using the NCO Altera Macrofunction. In *Fig.* 5.1 and *Fig.* 5.2 there are two block diagrams of this function. Each for one NCO type. The clock is generated by a PLL, that receives in input the clock of the system at $62.5MHz$ and generates on output clock at $500kHz$. The phase modulation input, to determinate the frequency of the output, is controlled using the available memory registers.

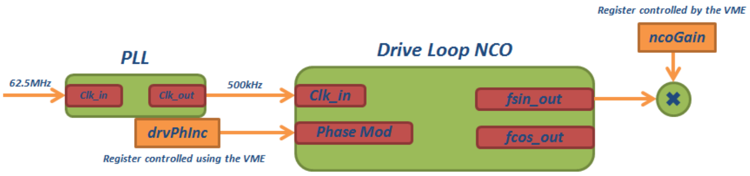

Figure 5.1: *Block Diagram for the Drive Loop NCO*

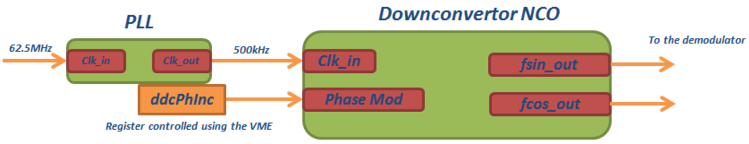

Figure 5.2: *Block Diagram for the Downconverter NCO*

The Altera Macrofunction allows to change different paramenters, as in *Fig.* 5.3. In this case, $f_c = 500kHz$, $N = 32$, and the output is on 16 bits.

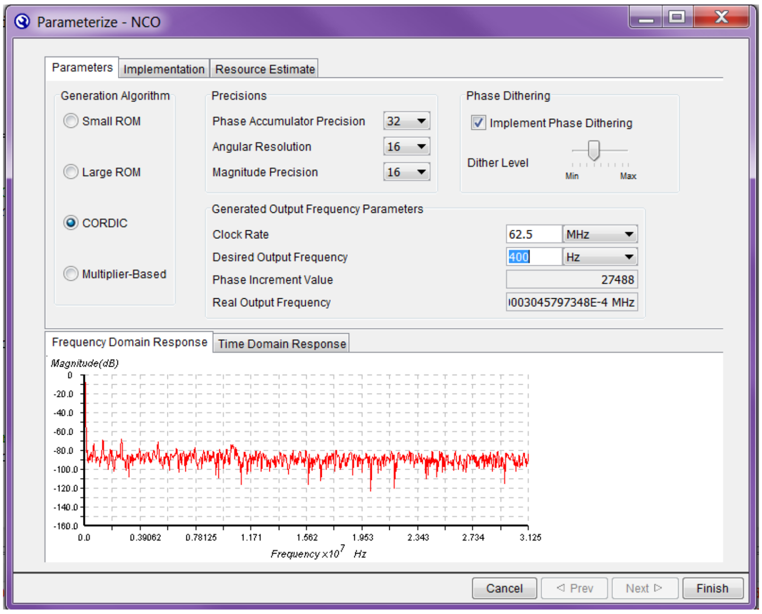

Generation Algorithm
○ Small ROM
○ Large ROM
● CORDIC
○ Multiplier-Based

Precisions
Phase Accumulator Precision 32
Angular Resolution 16
Magnitude Precision 16

Phase Dithering
☑ Implement Phase Dithering
Dither Level

Generated Output Frequency Parameters
Clock Rate 62.5 MHz
Desired Output Frequency 400 Hz
Phase Increment Value 27488
Real Output Frequency ı003045797348E-4 MHz

Figure 5.3: *NCO realized with the Altera Macrofunction*

5.1.1.1 Tests and measurements

To check the NCO, the setup in *Fig.* 5.4 has been used.

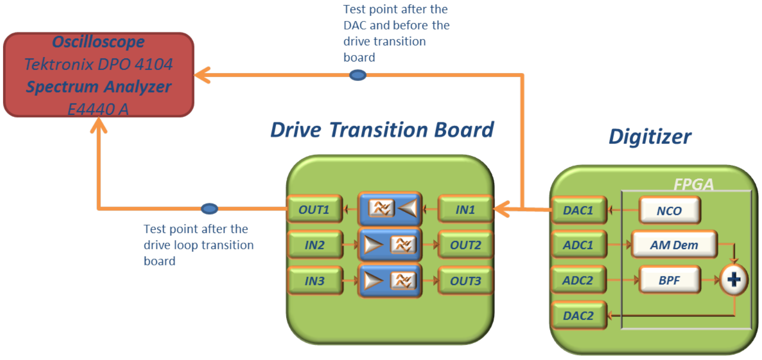

Figure 5.4: *Measure setup to test the NCO*

The gain, controlled with the LabView interface, has been fixed in way that the output of the DAC is $624mVpp$.

The output directly from the DAC is shown in *Fig.* 5.5, while the spectrum is in *Fig.* 5.6.

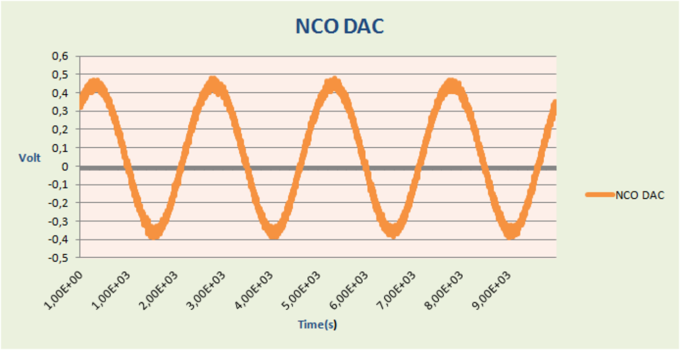

Figure 5.5: *Output voltage from the DAC*

There are others frequency components, because of the asymmetry of DAC output.

The time response from the transition board in *Fig.* 5.7, and its spectrum in *Fig.* 5.8.

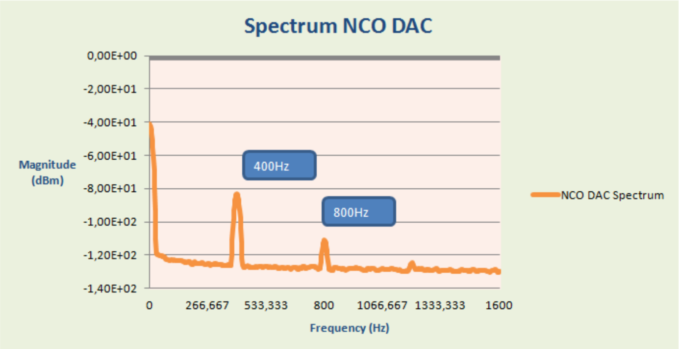

Figure 5.6: *Spectrum of the output voltage from the DAC*

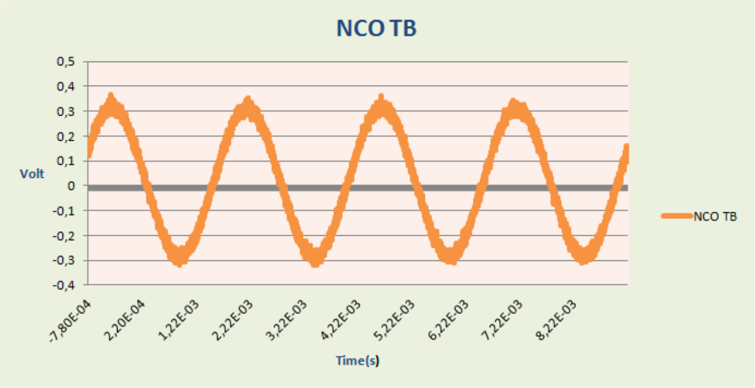

Figure 5.7: *Output voltage from the drive loop transition board*

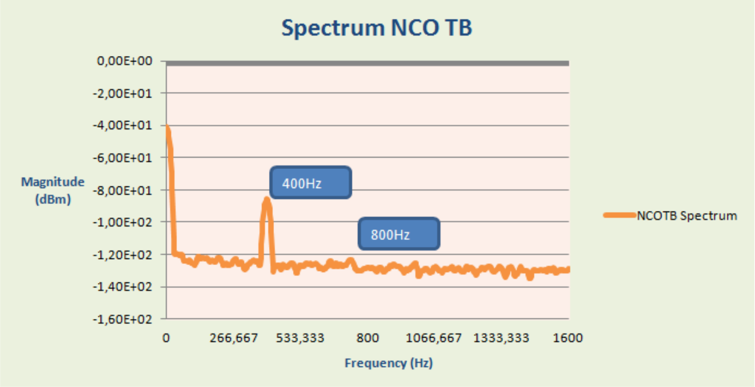

Figure 5.8: *Spectrum of the voltage output from the drive loop transition board*

5.1.2 CIC

To drive the stages at different sampling frequencies, in the VHDL implementation, clock dividers have been used, instead of PLL. They don't generate clock signals but impulses at the desired frequency. Those impulses drive the enable of the flip flops.

To the CIC operations the length in bits of the signal has been increased. This is later restricted when the gain is adjusted.

A block diagram of the VHDL implementation is in *Fig.* 5.9

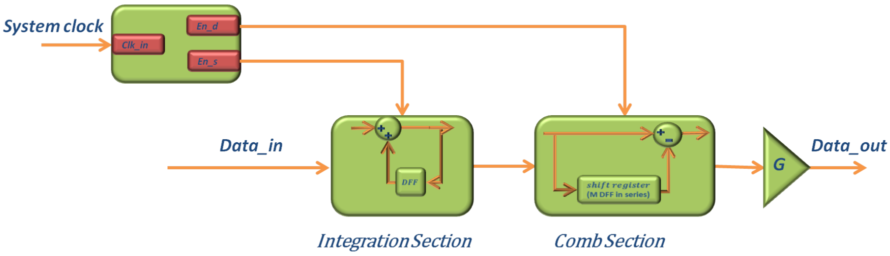

Figure 5.9: *Block Diagram of the generic CIC in VHDL*

5.1.2.1 Tests and Measurements

The frequency response of the filters have been measured. The measuring setup in *Fig.* 5.10 has been used.

The frequency response for the first CIC is in *Fig.* 5.11. There are notches at $500kHz$ and multiples. The phase frequency response in *Fig.* 5.12 is linear as aspected.

The frequency response of the second CIC is in *Fig.* 5.13. There are notches at $1kHz$ and multiples. Also in this case the phase (*Fig.* 5.13) is linear.

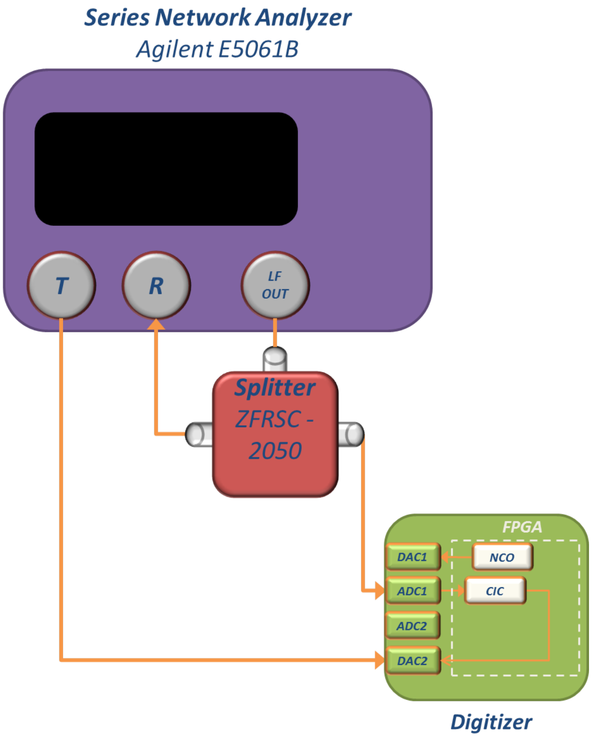

Figure 5.10: *Measure setup to test the CIC Filter*

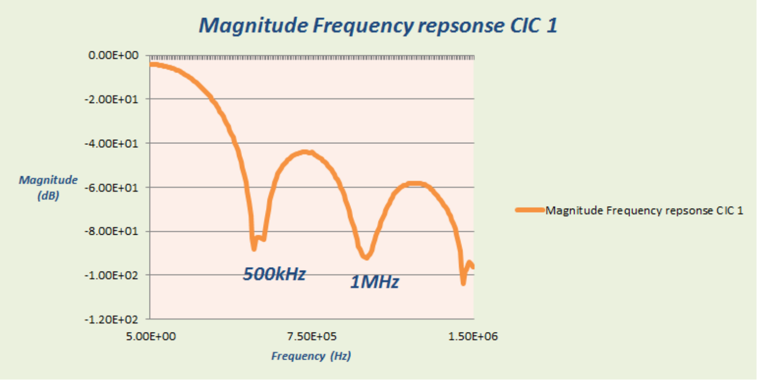

Figure 5.11: *Magnitude frequency response for the first CIC*

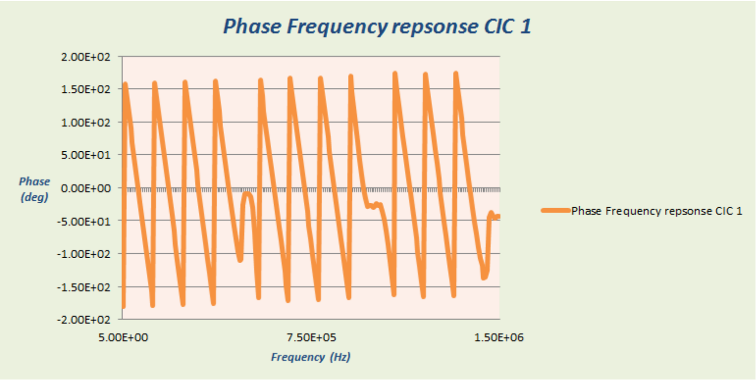

Figure 5.12: *Phase frequency response for the first CIC*

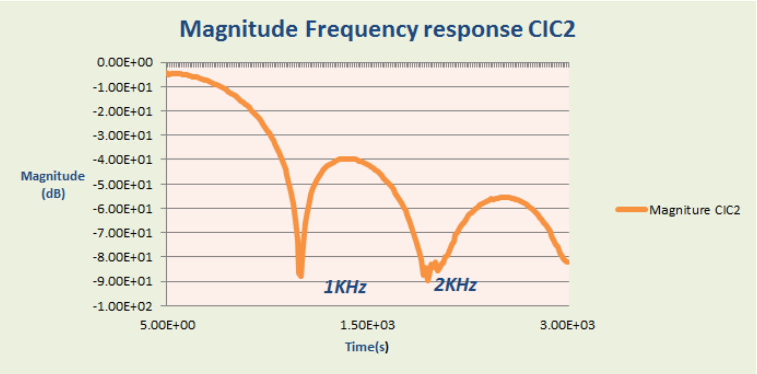

Figure 5.13: *Magnitude frequency response for the second CIC*

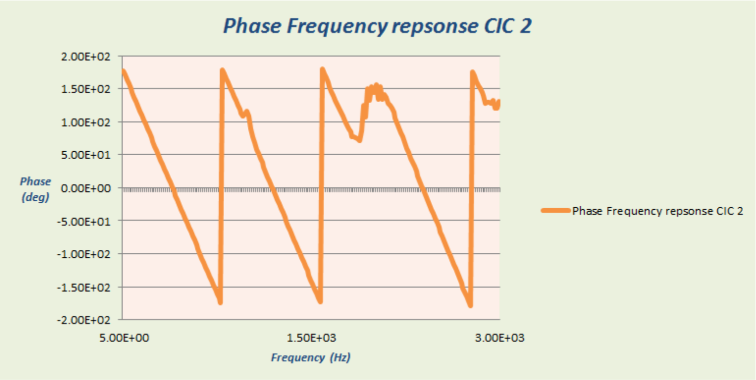

Figure 5.14: *Phase frequency response for the second CIC*

5.1.3 FIR Filter

The same procedure for the CIC filters has been used in the FIR's VHDL implementation. There are no PLLs, but clock dividers synchronize the stages. The output is generated at the data rate $f_s = 2kHz$. There is also another internal frequency that is higher than $N * f_c$, $f_d = 10MHz$was chosen so that in one sampling period, it is possible to make 127 multiplications and additions. This is possible because the filter works in a sequential mode. All the operations are synchronized by the system clock $f_{clk} = 62.5MHz$.

The filter works in a sequential mode. Making parallel operations required a number of multiplicative modules equal to the order of the filter. In this case it is 127 and its synthesis requires more resources than available on the FPGA.

The coefficients calculated with the FDA Tool of Matlab are stored in a ROM memory. The address of the ROM is generated by a counter that two enables signals. The first one counts from zero to 127 that works at f_d, while the other enable reset the counter, at f_s.

A block diagram of the VHDL implementation is in *Fig.* 5.15

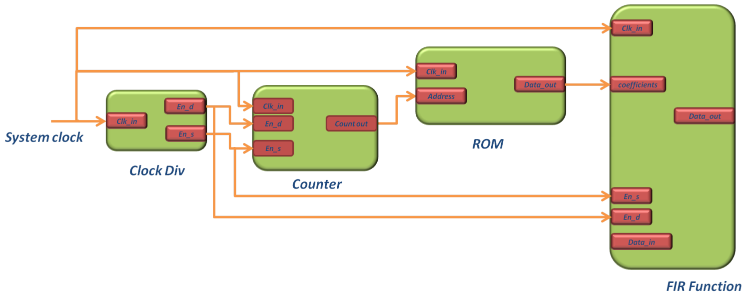

Figure 5.15: *Block diagram of the VHDL implementation for an FIR Filter*

5.1.3.1 Tests and measurements

To measure the frequency response of the two CICs and of the FIR filter, the same setup for CIC was used (*Fig.* 5.10).

The magnitude frequency response is in *Fig.* 5.16, while the phase of the frequency response is in *Fig.* 5.17. The magnitude is exactly as designed with the FDA Tool, the phase is linear in the bandpass.

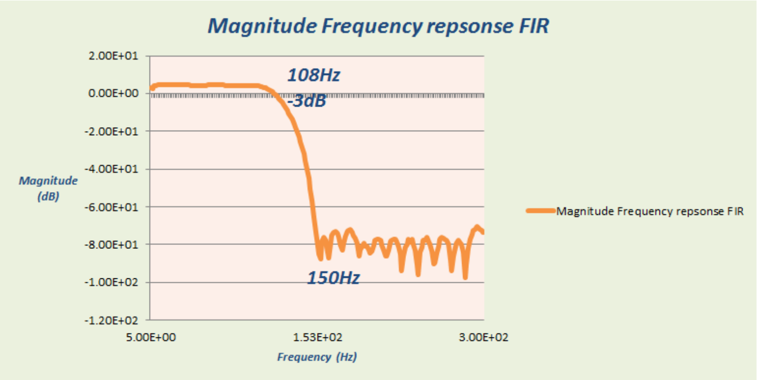

Figure 5.16: *Magnitude frequency response, FIR Filter*

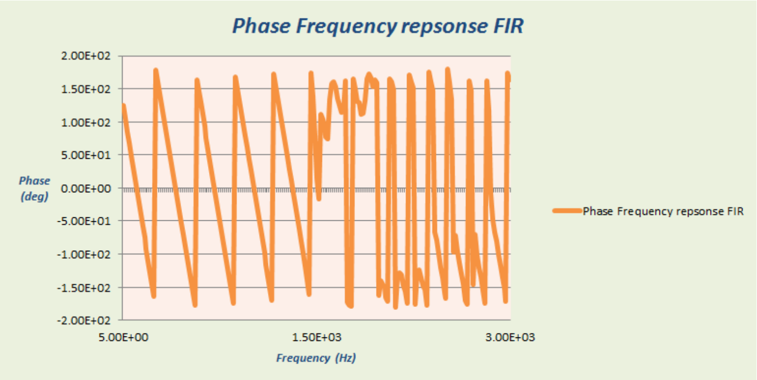

Figure 5.17: *Phase frequency response, FIR Filter*

5.1.4 AM demdulator

The system designed as explained in the previour chapter has been developed in VHDL. It has been tested in the time domain and in the frequency domain. For the block diagram see *Fig.* 4.17.

To make the tests we refer to block diagram in *Fig.* 5.18.

As an input, a signal at the low frequencies modulated at $800Hz$ has been applied. It

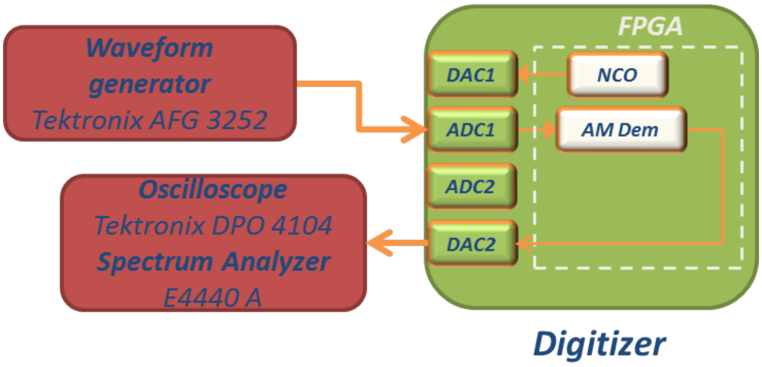

Figure 5.18: *Block diagram to test the AM demodulator implemented in VHDL*

is described by the following equations:

$$v_in(t) = m(t)cos(2\pi\omega_0 t)Acos(2\pi\omega_c t)cos(2\pi f_0 t) \tag{5.1}$$

The signal $m(t) = Acos(2\pi f_c t)$ has to be detected, f_c is lower then $100Hz$. In this case $f_c = 20Hz$ and $A = 400mVpp$

The response in the time domain is shown in *Fig.* 5.19, compared with the input signal.

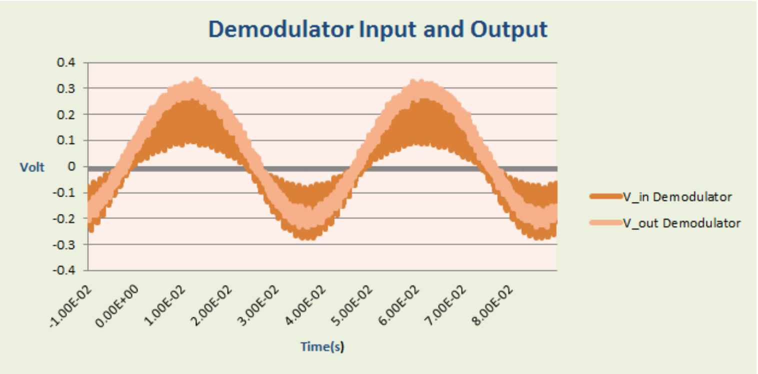

Figure 5.19: *Demodulated signal in output and modulated signal in input*

The signals are in phase. An offset ad gain adjustment is necessary, but it will be applied at the open loop response.

5.2 Open Loop response

The open loop response is monitored by the $Output3$ of the feedback loop transition board and on the output od the power amplifier terminated on 5Ω. Connections realized are shown in *Fig.* 5.20, the test points are underlined.

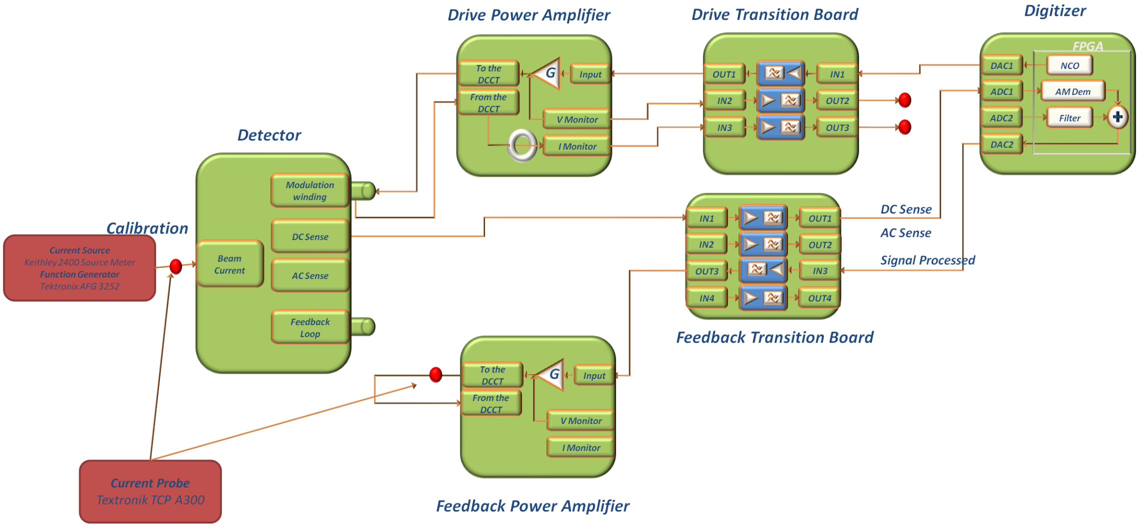

Figure 5.20: *Test points and block diagram for the open loop measurements*

The first test to do is to check the monitoring points on the drive cores. An input current of $0.4A$ is applied.

The *Fig.* 5.21 shows the signal from the DC section. From the spectrum in *Fig.* 5.22, the first harmonic should be cancelled, it is present because of some leakages. In addition there are some others frequencies components, that are cleaned passing through the transition board, as in *Fig.* 5.23. The *Fig.* 5.24 shows the spectrum of this signal after the transition board, there is only the second harmonic.

The output voltage observed in the open loop measurements has to go into the feedback power amplifier. The gain of the power amplifier is $G = 100$, and is terminated on an impedance $R_s = 5\Omega$. That means that the output current is given by the following

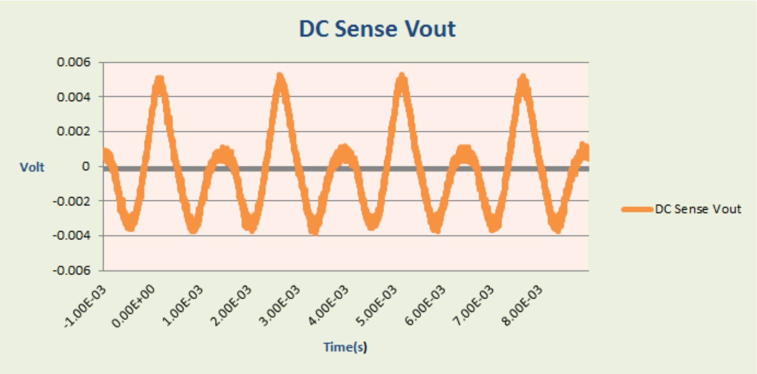

Figure 5.21: *Signal from the DC detector, before the transition board.*

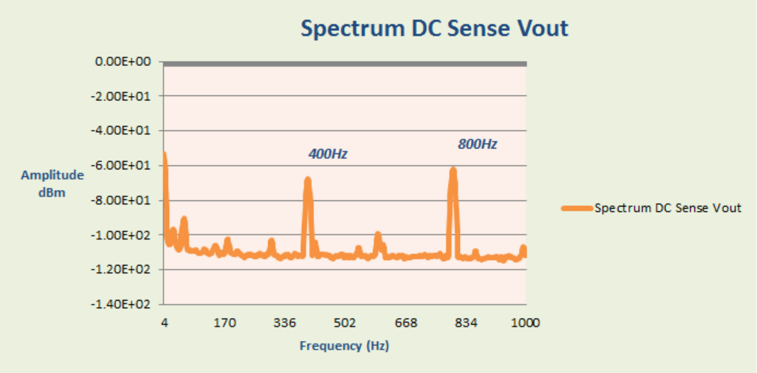

Figure 5.22: *Spectrum of the signal from the DC detector, before the transition board.*

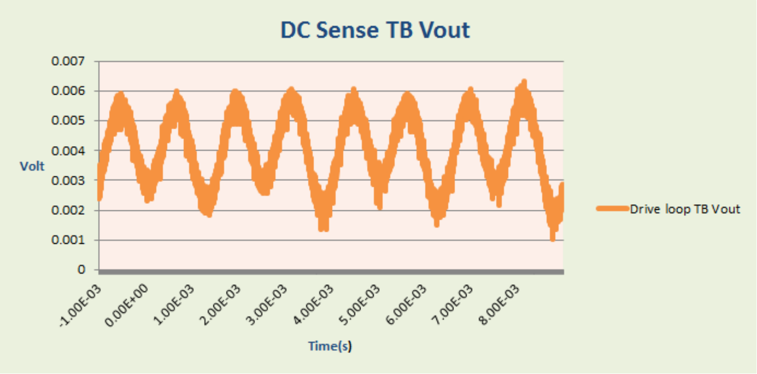

Figure 5.23: *Signal from the DC detector, before the transition board.*

equation:

$$I_{out} = G\frac{V_{in}}{R_s} \tag{5.2}$$

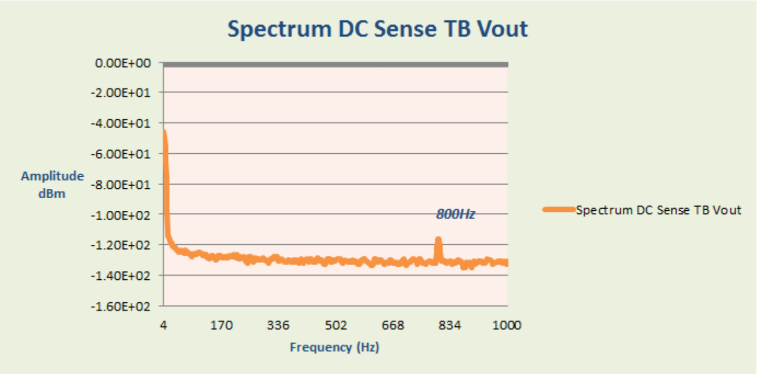

Figure 5.24: *Spectrum of the signal from the DC detector, after the transition board.*

At this point the signal is processed, passes through the feedback loop transition board (Channel 3). The measure is done connecting the output of the feedback loop power amplifier called 'to the DCCT' to the scope, terminated at $1M\Omega$, it is shown in *Fig.* 5.25. The most important component is the DC and the frequency component at $800Hz$ is cancelled, that means that the firmware has well demodulated the signal.

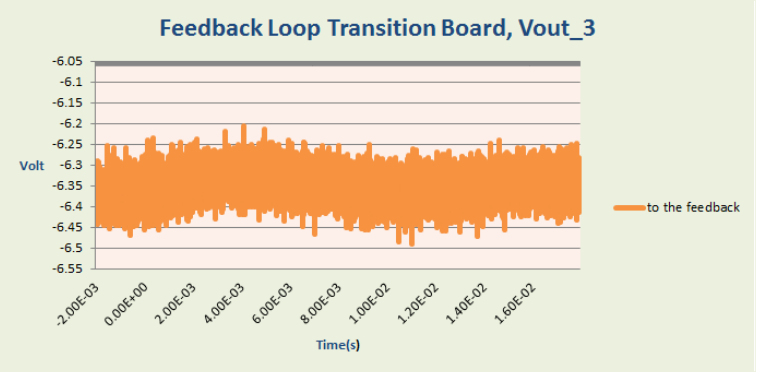

Figure 5.25: *Signal in time domain, output of the feedback loop power amplifier that receives in input the signal demodulated*

It is possible to regulate the gain with the LabView Interface so that the output voltage is the voltage that we need.

With the current probe the result is show in *Fig.* 5.26

Finally also the open loop step response has been monitored (*Fig.* 5.27)

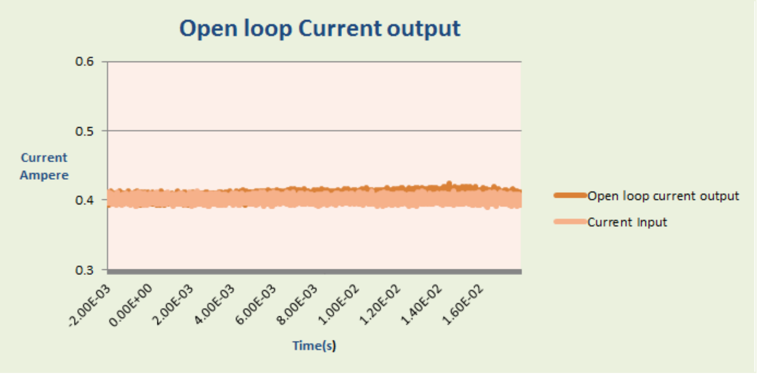

Figure 5.26: *Open loop measurement on the input and output of the system, current output*

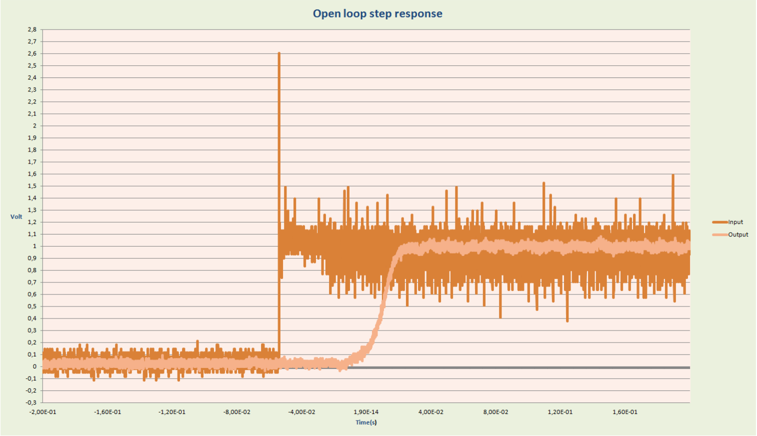

Figure 5.27: *Open loop measurement on the input and output of the system, step response*

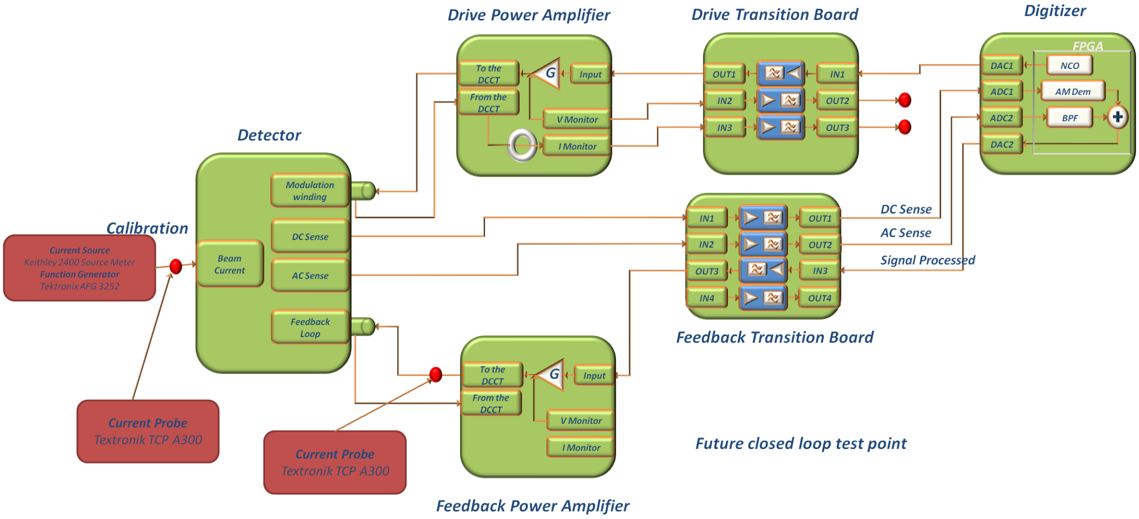

Figure 5.28: *Test setup for the closed loop measurements*

5.3 Closed Loop

The test setup for the closed loop is in *Fig.* 5.28.

The current monitor on the feedback loop power amplifier will be the real output of the system. It has not been yet implemented. Currently to test the system a current probe has been used.

The control implemented is only a P control, using a gain register inside the firmware, that is controlled with the LabView interface.

The first test has been done putting in input a current of $I_{in} = 0.4A$, controlling the gain and measuring the input and output with the current probe, the result is shown in *Fig.* 5.29. The two signal are quite the same, that means that the error is zero.

The step response (*Fig.* 5.30) will give some informations about the rise time.

The rise time is the time to go from the 10% to the 90% of the output voltage. In this case is about $\tau = 0.05s$. Of course it can be increased using a PI control, this will fall in the future work to do on this instrument.

Finally to test the response, and how the output track the input current a signal at $1Hz$

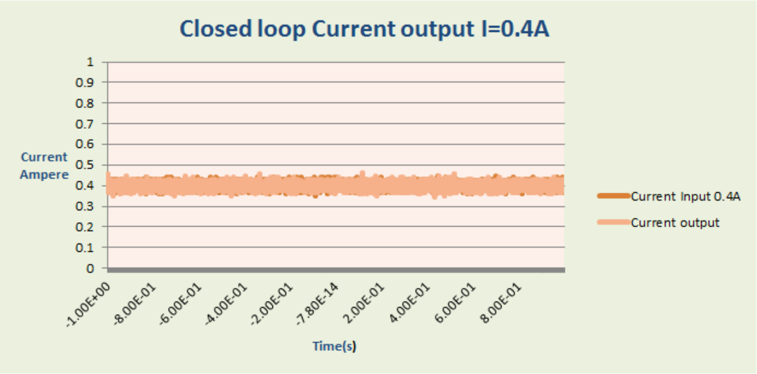

Figure 5.29: *Closed loop response with 0.4A in input*

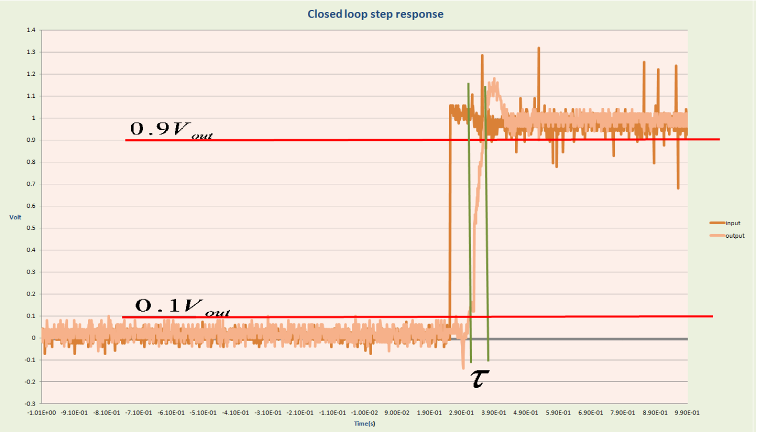

Figure 5.30: *Closed loop measurement on the input and output of the system*

has been putted in input with the waveform generator, at an amplitude of $5Vpp$, to give to the signal enough power.

The result is in *Fig.* 5.31.

The input current is very low, but with a little distortion the signal is well tracked. This give also an information about the resolution, that is higher than $0.01A$.

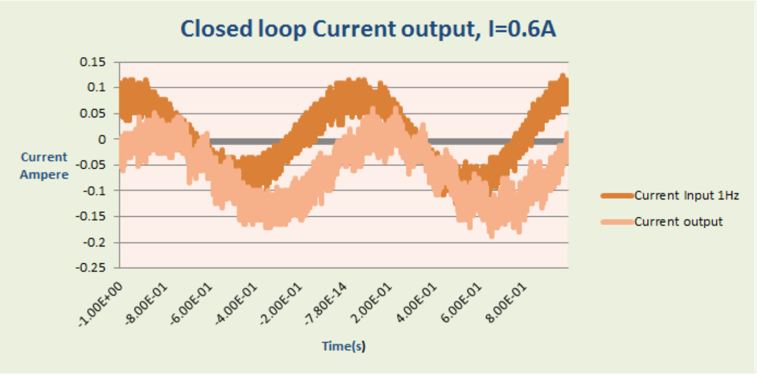

Figure 5.31: *Closed loop measurement, whit an AC signal in input*

Conclusion

The goal of the thesis activity was to study and develop a DC Current Transformer.

This system has been studied making an accurate model, considering both the AC and the DC sections, with Simulink and his tools. It was also characterized. The specifications were fixed basing from the study of the physical behaviour of the toroids (i.e. number of turns and bandwidth of the DC and AC section). Finally the available hardware has been tested and corrected when needed.

The main goal was to detect and follow the low frequency components of the input current, in particular the DC. This result has been reached as explained. The DC component is well tracked open and closed loop, and also low frequencies are detected.

To fully implement the control system a PI controller will be needed to achieve the necessary system bandwidth as well as perform the AC detection. Only combining the two sections, with a particular attention at the cross between the two open loop bandwidths, the state-of-art for a DCCT will be reached.

Bibliography

[1] Enrico Bravin, Transverse Profiles, CERN, CAS - Dourdan, France 28 May - 6 June 2008

[2] F. W. Crane and NI. P. Baker, Neutron Detectors, in Passive Nondestructive Assay of Nuclear Material T. D. Reilly, N. Enssl n, and H. A. Smith, Eds., U.S. Nuclear Regulatory Commission contractor report NUREG CR 5550 (March 1991)

[3] James Crisp *et al.*, Operation of the DC Current Transformer Intensity Monitors at FNAL during Run II, Journal of Instrumentation, Volume 7, Issue 01, pp. T01002 (2012)

[4] Guenther Rehm, Accelerator Diagnostics, Cockcroft Institute Postgraduate Lectures, Autumn 2008

[5] H.Koziol,Beam Diagnostic For Accelerator, CERN, Geneva, Swizterland

[6] Michiko G. Minty, Frank Zimmermann,Measurement and Control of Charged Particle Beams, Springer

[7] Peter Fork, Lectures Notes on Beam Instrumentation and Diagnostics, Joint University Accelerator School, January - March 2007

[8] Ulrich Raich, Beam Diagnostics, CERN Accelerato School 2010

[9] Robert E. Shafer, Beam Position Monitoring, Los Alamos National Laboratory, 1992 American Institute of Physicist.

[10] Peter Strehl, Beam instrumentation and diagnostic, Springer

[11] Robert C. Webber, Charged Particle Beam Current Monitoring Tutorial, Beam Instrumentation Workshop, Vancouver, Canada, October 3-6,1994

[12] Robert C. Webber, A Tutorial on Non-Intercepting Electromagnetic Monitors for Carghed Particle Beams

[13] Helmut Wiedemann, Particle Accelerator Physics, Springer

Acknowledgements

It is a great pleasure to thank my professor Luca Fanucci, who supported me to make this experience at Fermilab. Further thanks to my supervisor and mentor Manfred Wendt, who gave me the opportunity to work in this laboratory. Manfred took care of me, he was very patient, and I really appreciated his time and availability.

I am also very grateful to the entire team of the Instrumentation Department everyone was very helpful. Each time I asked, the colleagues provided support for my thesis with their know-how and resources. In particular I am very thankful to Nathan Eddy, Aisha Ibrahim, Ning Liu, Alexei Semenov, Pierpaolo Stabile, and Dallas Heikkinen, everyone was very present and responsive during the critical periods of this work. Special thanks to Peter Prieto and Andrea Saewert, their experience and smart ideas were very useful to fix some practical problems. Outside the Accelerator Division, thanks to Eliana Gianfelice, for editing the first part in this thesis, and also for the advices she gave me.

Finally a big hug to the little, big Italian family at Fermilab! Everyone gave me a piece of Italy; everyone helped me to feel at home, also with 5000 miles distance. Thanks to Pierpaolo, not only as colleague, thanks to Gallo, Margherita, Alessandra, Paolo, Gianfranco, Marco, Giannino, and Giani for the good time we spent together, the laughs, and the dinners. Thanks to Donato, every time I needed he was there to help and to support me, I am sorry if sometimes I forgot to say "thank you"!

Let’s leave the English language in favour of the Italian, to better express my greetings to my family and friends.

Il primo grande ringraziamento va alla mia famiglia, a mamma e papá per tutto quello che hanno fatto per me, percheé non sempre gli ho fatto capire quanto apprezzato il fatto che abbiano sempre accettato le mie scelte.

Grazie a mia sorella Mila e ad un fratello acquisito Raffaele, mi hanno sempre fatto sentire la loro vicinanza.

Grazie alle mia famiglia tutta, alle mie zie ed ai miei zii, a zia Maria e a zia Teresa che mi hanno cresciuto, a zio Eduardo e zia Laura che mi hanno accolto quando ho deciso di trasferirmi in Toscana.

Ringrazio di cuore tutti i miei amici ’pisani’. Questi anni di Universitá non sarebbero stati gli stessi senza le paranoie della mia amata Martona, le chiacchiere con il Mark, i frignoli del Don (Antonio), le lasagne della col (Francesca), i caffé con Giada e i thé con Paolona, le risate con Mariagrazia, le pazzie di Psico (Daniela) e gli scherzi con la mia amanta Antonella. Sappiate che vi (ci) voglio bene. In questo periodo di lontanza ogni volta che ci siamo sentiti, anche se a distanza di mesi, era sempre come se non fosse cambiato niente e questo credo che sia il regalo piú bello che dei veri amici possano fare!

Grazie a Claudio e Mattia, per la splendida ed unica esperienza che abbiamo vissuto insieme e che ha reso il nostro rapporto unico.

Grazie a Francesca, che mi sopporta ormai da 13 anni.

Grazie ad Orazzini per la sua pazienza, per il bene che mi ha dimostrato sempre ed incondizionatamente e per avermi aspettato senza mai chiedermi niente.

Grazie a Fiorella, Dario, Alessio ed Ica che mi hanno accolto come una persona di famiglia e per l’aiuto che mi hanno dato.